ISSN 1590-2595

quaderni di geofisica

n. 56

ETNA 2003 FIELD CAMPAIGN: CALIBRATION AND VALIDATION OF SPACEBORNE AND AIRBORNE INSTRUMENTS FOR VOLCANIC APPLICATIONS

ASI Projects: I/R/157/02, I/R/203/02

Fabrizia Buongiorno et alii

Istituto Nazionale di Geofisica e Vulcanologia

2008

Segreteria di Redazione
Francesca Di Stefano (responsabile)
Tel. +39 06 51860068
Fax +39 06 36915617
Rossella Celi
Tel. +39 06 51860055
Fax +39 06 36915617
redazionecen@ingv.it

quaderni di geofisica

ETNA 2003 FIELD CAMPAIGN: CALIBRATION AND VALIDATION OF SPACEBORNE AND AIRBORNE INSTRUMENTS FOR VOLCANIC APPLICATIONS

ASI Projects: I/R/157/02, I/R/203/02

CAMPAGNA ETNA 2003: CALIBRAZIONE E VALIDAZIONE DI SENSORI SU PIATTAFORME SATELLITARI ED AEREE PER APPLICAZIONI VULCANICHE

Progetto ASI: I/R/157/02, I/R/203/02

Maria Fabrizia Buongiorno[1], Stefania Amici[1], Laura Colini[1], Giuseppe Di Stefano[1], Fawzi Doumaz[1], Valerio Lombardo[1], Massimo Musacchio[1], Luca Merucci[1], Maria Ilaria Pannaccione Apa[1], Claudia Spinetti[1], Tommaso Caltabiano[1], Boris Behncke[1], Mike Burton[1], Nicola Bruno[1], Salvatore Giammanco[1], Vincenza Longo[1], Filippo Murè[1], Marco Neri[1], Giuseppe Salerno[1], Benedetto Badalamenti[1], Iole Serena Diliberto[1], Marcello Liotta[1], Paolo Madonna[1], Malvina Silvestri[1], Sergio Pugnaghi[2], Stefano Corradini[2], Lorenzo Guerrieri[2], Luca Lombroso[2], Sergio Teggi[3], Matteo Remitti[3]; Gian Paolo Gobbi[4], Francesca Barnaba[4], Maria Sgavetti[5], Loredana Pompilio[5], Valerio Tramutoli[6], Vito Lanorte[6], Nicola Pergola[6], Francesco Marchese[6], Gerardo Di Bello[6], Oronzo Candela[6], Erwin Lindermeier[7], Peter Haschberger[7], Volker Tank[7], Dieter Oertel[7], Herman Kick[7], Nicola Santantonio[8], Michele Mannarella[8], Maria Paola Bogliolo[9]

[1]INGV (Istituto Nazionale di Geofisica e Vulcanologia, Depts: CNT, CT, PA)
[2]UNIMORE-DIMA (Università di Modena - Dipartimento di Ingegneria dei Materiali e dell'Ambiente)
[3]DIMeC (Dipartimento di Ingegneria Meccanica e Civile)
[4]ISAC-CNR (Istituto di Scienze dell'Atmosfera e del Clima)
[5]UP (Università di Parma - Dip. Scienze della Terra)
[6]IMAA-CNR (Istituto di Metodologie per l'Analisi Ambientale) DIFA-UNIBAS (Dipartimento di Ingegneria e Fisica dell'Ambiente)
[7]DLR (Deutsche Zentrum für Luft- und Raumfahrt)
[8]TELESPAZIO s.p.a.
[9]ISPESL (Istituto Superiore Prevenzione e Sicurezza sul Lavoro)

Indice

Abstract

The field measurements campaign made in July 2003 on Etna, Vulcano Island and Campi Flegrei was dedicated to the calibration and validation of airborne and spaceborne data. The campaign activities were relevant part of two ASI funded projects:

1) FASA, dedicated to airborne system and data validation/calibration
2) HypSEO, dedicated to multispectral an hyperspectral spaceborne data validation/calibration on specific test areas.

The airborne campaign was organized in the frame of a three-year project funded by ASI and DLR as it represented the flight test of the FASA system, which combines a Fourier interferometer in the MIR-TIR region and an imager (ABAS).

The main objectives of this proposal are:
1. Design and implementation of an airborne system for the Fourier Spectrometer MIROR and ABAS (Bird Airborne Simulator);
2. Airborne Operational tests of the FASA system over the main Italian volcanic areas (i.e. Etna, Stromboli and Vulcano) and possibly on controlled forest fires (Germany);
3. Organization of the necessary ground campaign for calibration and validation of the acquired data;
4. Development of the algorithms for the selection of the "spectral windows" and for the determination of the presence of some gasses: in particular SO_2, CO_2, H_2S and other gasses of volcanic origin.

Riassunto

Il progetto FASA, organizzato in diversi campi di ricerca, ha focalizzato gli studi su: calibrazione e procedure di correzione atmosferiche per i dati ASTER ed HYPERION; analisi e comparazione delle procedure SO_2 retrieval applicate ai dati ASTER e MODIS: analisi delle caratteristiche del plume dell'Etna con dati a bassa ed alta risoluzione; spettroscopia delle superfici rocciose per le analisi minerali con HYPERION e spettri di laboratorio.

Le misure di campagna effettuate nel Luglio 2003 sul Monte Etna, l'isola di Vulcano ed i Campi Flegrei sono state mirate alla calibrazione ed alla validazione dei dati ricevuti dai sensori su supporti satellitari ed aerei. Le attività di campagna sono state parte rilevante di due progetti sovvenzionati da ASI:

1) FASA dedicato ai sistemi avio-trasportati ed alla calibrazione e validazione dei dati;
2) HYPSEO, dedicato alla calibrazione e validazione dei dati satellitari multispettrali ed iperspettrali in specifiche aree di test.

La campagna aerea è stata organizzata nell'ambito di un progetto triennale sovvenzionato da ASI e DLR, ed e rappresentato dal volo test del sistema FASA, che combina un interferometro di Fourier nella regione MIR-TIR ed un sistema per il rilevamento delle immagini (ABAS: Bird Airborne Simulator).

I principali obiettivi di questa ricerca sono stati:
1. Disegno ed implementazione di un sistema avio-trasportato per lo Spettrometro di Fourier MIROR ed ABAS;
2. Tests operativi di volo del sistema FASA sulle principali aree vulcaniche italiane (Etna, Stromboli, Vulcano) ed su possibili controlli di fuochi forestali (Germania);
3. Organizzazione della campagna di misura per la calibrazione e la validazione dei dati acquisiti;
4. Sviluppo degli algoritmi per la selezione delle "finestre spettrali" e per la determinazione della presenza di gas, in particolare SO_2, CO_2, H_2S ed altri gas di origine vulcanica.

Introduction

Firstly, the ASI (contract n.I/R/203/02) project was aimed to built an airborne simulator for the Focus mission on ISS (ESA proposed Externally Mounted payload).

In early 2001, the Focus project didn't continue its development, nevertheless the ASI project, dedicated to the construction of an airborne version of a system based on the simultaneous acquisition of a Fourier interferometer (MIR-TIR) and image sensor (VIS/MIR/TIR), did not loose its scientific and technological value. In fact, the system was built by the INGV/DLR cooperation represented the only airborne simulator for space missions combining the very high spectral resolution of the FTIR and the information of a multispectral imager.

During 2002, the project name was changed in Fire Airborne Spectral Analyser – (FASA).

FASA became an airborne system com-

bining a modified-Michelson Fourier interferometer (MIROR) with and imager (ABAS, VIS/MIR/TIR cameras system). This sensor system (operating in the nominal spectral range 3-13 m m) aims at investigating and monitoring the emissions from natural sources such as volcanoes or wild fires.

Concernig the temperatures and (burned) areas FASA can provide concentration profiles of gaseous effluents. These data are needed to improve the knowledge of the local effects of such emissions as well as on the global ecosystem.

Otherwise, airborne system FASA also permits the access to potentially dangerous areas, like the active craters of volcanoes and the burning forests.

The project was carried out in collaboration with DLR and INGV, CNR-IROE (recently renamed CNR-IFAC).

The test flights, scheduled for summer 2002, were realized in summer 2003 on Campi Flegrei, Etna and Stromboli island.

The airborne campaign was organized in the frame of the ASI project HYPSEO (contract n. I/R/157/02) which wanted to establish a number of test sites for the validation.

The validation campaign was carried out on Italian test-site reprensenting the permanent areas for spaceborne (multispectral and hyperspectral imagers) and airborne data calibration and validation.

On July 2003 the field measurements campaign was carried out on Mt. Etna.

The data acquisition was scheduled contemporaneously (LANDSAT ETM, HYPERION/ALI, ASTER/MODIS, MERIS). The ground campaing was coordinated by INGV and carried out by the following scientific teams: INGV: Roma, Napoli, Catania and Palermo sections, with the collaboration of Dr. B. Behncke, DIMA, DIMeC, UP: Dipartimento di Scienze della Terra, CNR-ISAC, CNR- IMAA.

Moreover a logistic support, relevant only the Solfatara of Pozzuoli radiosounding, was provided by Telespazio S.p.A..

The FASA project, organized in different tasks, was dedicated to: calibration and atmospheirc correction procedures for ASTER and HYPERION data; analysis and comparison of SO_2 retrieval procedures applied to ASTER and MODIS data; anlaysis of the Etna plume characteristics with high and low resolution data; spectroscopy of rock surfaces for mineral analysis on HYPERION and laboratory spectra.

The FASA campaign results were published on a web site available to ASI as demonstration of the hyperspectral data applications.

1. Geological and geophysical setting of selected test-site

The test-sites selected in the frame of the Project are: Mt. Etna, Solfatara, Stromboli and Vulcano.

Mount Etna, the tallest volcano in Europe, lies close to the subduction-related Aeolian magmatic arc but shows little trace of subducted material in its magmas. Mount Etna is also situated on continental crust yet shows oceanic basalt affinities, suggesting that the same type of mantle source feeds it as mid-ocean ridge basalts ones [Tanguy, 1978]. The volcanic complex of Mt. Etna is located on the suture between two main structural units: the Iblean Foreland, and the European Plate. It is characterized by open conduit degassing and periods of quiescence (~few years) interrupted by quite strong eruptions with emission of large quantities of lava [Romano et al. 1986; Barberi, 1990; Armienti et al. 1994; Bencke et al. 2003; Andronico et al. submitted]. Volcanism in the Eolian island arc [Barberi et al. 1974] is thought to be related to the subduction of the Ionian lithosphere. Stromboli has rhythmic explosive activity (periodicity of ~20 minutes) and has given rise to the term “Strombolian activity”. It has also episodic activity of minor lava flows. La Fossa crater of Vulcano Island (Eolian Archipelago) has a closed conduit and low gas emissions from a wide field of fumaroles inside crater area. The last eruption on Vulcano occurred in 1888-1889 [Keller, 1980; Mercalli et al. 1981].

1.1 Mt. Etna test-site

1.1.1 Eruptive activity of Mount Etna: general features

Mount Etna is the largest and most active of Europe’s volcanoes, with a present summit elevation of 3315 m, and eruptive activity occurring nearly every year. Eruptions occur both at the summit, where there are four craters (Northeast Crater, Voragine, Bocca Nuova, Southeast Crater) and on the flanks, of which more than 300 individual craters bear testimony. Summit activity may be continuous over many years or even decades, while flank eruptions occur every few years, with a clear trend towards an increase in the frequency of flank eruptions and in the long-term output rate being observed in the past 50 years or so.

Since the late 1970s, summit eruptions have shown a clear increase in their intensity, and one hallmark of this activity has been the

extremely high rate of short-lived, extremely violent paroxysmal eruptive episodes, which culminated in more than 120 paroxysms during the 6 years between 1995 and 2001, most of which occurred at the youngest of the summit craters, the Southeast Crater. Such events commonly produce lava fountains that reach heights of many hundred meters, in some cases exceeding 1000 m. Etna can even boast having produced the tallest lava fountain ever measured on any volcano, >2000 m, on 4 September 1999. Most lava fountains are accompanied by the generation of abundant tephra that consists of highly inflated scoriae and can fall tens of kilometers away from the volcano on the downwind side.

In contrast to these impressive but brief (rarely more than 30 minutes) episodes, summit eruptive activity at other times occurs in a continuous but notably milder manner, sometimes for years without interruption. This is what once was believed to be the most characteristic activity at Etna in times between flank eruptions, called "persistent" by Rittmann [1958]. It consists of relatively small Strombolian bursts accompanied, generally at distinct vents, by slow lava effusion (<1 m^3 s^{-1}). Before it started its exceptional series of lava fountains in 1998-2001, the Southeast Crater was the site of such "persistent" activity, and similar activity, accompanied by sporadic intracrater lava effusions, also occurred at the Bocca Nuova and the Voragine between 1995 and 1999. The Bocca Nuova itself produced a spectacular eruption in October-November 1999 with exceptionally strong Strombolian activity alternating with Hawaiian-style lava fountaining and copious overflows of lava onto the western flank of the volcano. Summit eruptions do not represent any significant threat to human property although episodic tephra falls generated by paroysmal events may cause damage to cultivated land and represent a nuisance to local residents.

Flank eruptions, on the other hand, are distinct events that have occurred on an average of 4 years during the 20th century. Since they occur lower on the slopes, they represent a major hazard to human property and infrastructures, and out of the 25 flank eruptions of the 20th century, 10 have caused significant material damage, including the destruction of an entire village (Mascali) in 1928. These eruptions tend to occur preferably in certain sectors of the volcano, along more or less radially arranged fissure swarms, of which the most active are the South Rift and the Northeast Rift, with their respective fan-shaped fissure zones extending to the NNE and SE flanks [Acocella and Neri, 2003]. Out of the 15 flank eruptions that have occurred since 1971, 13 have occurred in these areas.

Flank eruptions were until recently believed to be mainly effusive, with only mild Strombolian activity at the source vents. The eruptions of 2001 [Behncke and Neri, 2003a; Billi et al., 2003; Lanzafame et al., 2003] and 2002-2003 [Neri et al., 2003] have shown that flank eruptions can be highly explosive: the latter of the two produced even more tephra than lava, which is extremely rare at Etna. In the long term flank eruptions are seen to occur in a cyclic manner [Behncke and Neri, 2003b]: rather than at random intervals, they occur in conspicuous clusters, or series, so that it can be assumed that in certain periods the volcano is more unstable than in others. Stable periods are marked by exclusively summit eruptions (and little seismic activity along the numerous faults criscrossing the eastern and southern flanks, which are affected by gravitational instability), whereas flank eruptions are frequent when there is also heightened evidence for flank instability. The latest flank eruptions, which occurred after a period of long-lived summit eruptions, coincide with a new period of flank instability, as was clearly seen during the 2002-2003 eruption [Neri et al., 2003].

It is now believed that the dynamics of Etna's volcanism are strongly controlled by the accumulation of magma below the volcanic edifice and flank instability [Acocella et al., in press]. Recent observations by Lundgren et al. [2003] indicate that flank instability is triggered by the rapid inflation of the volcano during sub-edifice magma accumulation, which, in turn, might be influenced by regional tectonics [Acocella and Neri, 2003]. It is likely that the voluminous accumulation of magma in sub-edifice reservoirs, the enhanced instability observed since 2001 and the unusually short interval between the flank eruptions of 2001 and 2002-2003 mark the beginning of a new eruptive cycle [Behncke and Neri, 2003a,b]. This implies that more flank eruptions will occur at brief intervals as long as the volcano remains unstable.

1.2 Geological setting and general features

1.2.1 Solfatara test-site

Solfatara is a volcanic crater located in the central area of the Phlegraean Fields caldera complex, west of the city of Naples (Italy). It represents the most active zone of Phlegraean Fields, and sits inside the sprawling urban area of Pozzuoli (Figure 1.1) Activity in the

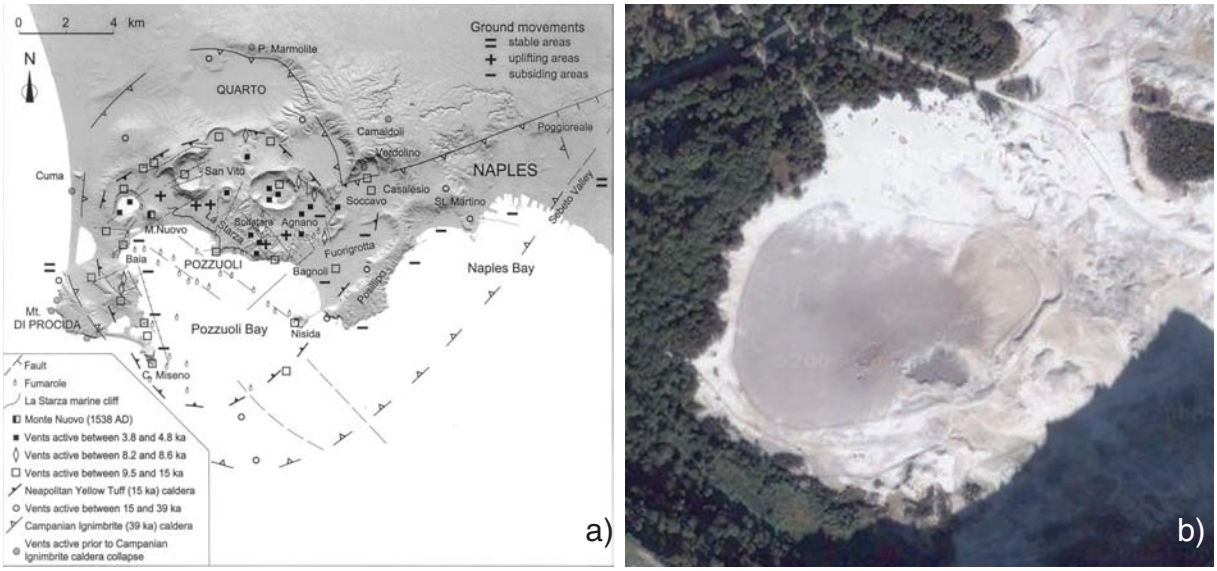

Figure 1.1 (a) Structural sketch map of the Campi Flegrei Caldera (Orsi et al., 2004); (b). Phlegraean Fields (Courtesy of Google Maps).
Figura 1.1 (a) Mappa strutturale della Caldera dei Campi Flegrei (Orsi et al., 2004); (b). Campi Flegrei (Cortesia Google Maps).

Phlegraean area has been dominated by two large-volume, caldera forming eruptions: the Campanian Ignimbrite and the smaller Neapolitan Yellow Tuff (Orsi et al., 2003 and references therein). The eruption producing the Campanian Ignimbrite occurred 39.000 years b.p. and resulted in the collapse of a large area including Campi Flegrei and part of the gulf of Naples. The eruption of Neapolitan Yellow Tuff occurred 15.000 years b.p, had a very complex history that led to the formation of a caldera of smaller dimensions inside that of the Campanian Ignimbrite. In the last 15.000 years, the Neapolitan Yellow Tuff caldera floor has been seat of intense volcanic activity and ground deformation (Di Vito et al., 1999). Volcanism was concentrated in three epochs: 12.000 and 9.500 years b.p., 8.600 and 8.200 years b.p., and 4.800 and 3.800 years b.p. (e.g. at Cigliano, Agnano - Monte Spina, Astroni, Averno, Solfatara), followed by the last eruption in 1538 that brought to the formation of the Monte Nuovo (Di Vito et al., 1987).

Since 1800, sea-level measurements made at ancient roman ruins have indicated a slow sinking of the area. This slow sinking of the ground continued until 1968. In the periods 1969-1972 and 1982-1984 two important brady-seismic events (ground uplift) occurred in the Pozzuoli area (Corrado et al., 1976; Berrino et al., 1984), (maximum uplift of 1.7 and 1.8 m respectively) accompanied by shallow seismicity. More recently, two minor sudden ground uplifts and seismic swarms were recorded in 1989-90 and in 1994.

The Solfatara volcano is one of the most recent (about 4.000 years b.p.) of the Phlegraean Fields caldera. It has a dimension of 0.5 x 0.6 km, with steep walls on the north, east, and south sides. To the west the crater wall is missing. Its rectangular shape is mostly due to the presence of faults at NW-SE and S W- N E . The volcanic cone is made of pyroclastic rocks, with the exception of Mt. Olibano that is a trachytic lava dome.

The flat-floored crater (Piano Sterile) is characterized by strong fumarolic activity which causes both single vent emissions, with temperature up to 160°C, and diffuse degassing. The gases emitted are mostly composed by H2O, CO_2, H_2S and smaller quantities of H2, CH4, He, HCl, Ar (Valentino et al., 1999).

One of the most recent hydrothermal models (Chiodini et al., 1997) describes a system divided in three parts: 1) a heat source which is made up of a relatively shallow magmatic chamber; 2) one or more aquifers located above the chamber; the degassing magma supplies fluids and heat to them; 3) an intensely fractured zone, sited above the uppermost aquifer and occupied by a pure vapor phase, which is produced through boiling of the underlying aquifers.

The intense fumarolic activity has given

origin to strong hydrothermal alteration of the original rocks (De Gennaro et al., 1980) and to secondary deposits. In fact, the trachytic rocks of the floor and of the flanks of the volcano are bleached and corroded by the effluent vapours, with formation of gypsum, alum, kaolin and alunite (Valentino et al., 1999). Moreover, sublimation of the emitted gas causes deposition of sulphur, arsenic sulphide (realgar), ammonium chloride (sal ammoniac), mercury sulphide, antimony sulphide.

1.2.2 Stromboli and volcano test-site

Stromboli is a basaltic composite volcano that forms an island of about 3 km diameter and 926 m above sea level, north of Sicily (38.8 N, 15.2 E) (Figure 1.2).

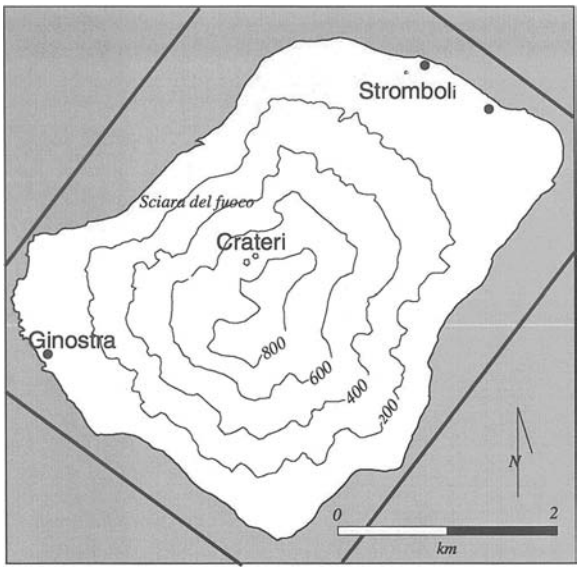

Figure 1.2 Map of Stromboli island, Aeolian Arc.
Figura 1.2 Arco Eoliano, mappa dell'isola di Stromboli.

Stromboli has been in a state of near continual eruption through history. Most of the eruptions are small gas explosive events at intervals of few minutes to hours that hurl incandescent blobs of magma above the crater rim. Occasional large explosion has happened.

Vulcano is one of the most important Aeolian island in the south of Italy (38° 24' 13'' N 14° 57' 42''E). It is stratovolcano resultingby two overlapping calderas named Caldera del Piano (south West) and Caldera della Fossa (north West). The last explosive eruption occurred on 1890 but presently active fumaroles fields are present (Figure 1.3).

Figure 1.3 Aerial view of Vulcano island, Aeolian Arc (courtesy of Google maps).
Figura 1.3 Arco Eoliano,vista aerea dell'isola di Vulcano (da Google maps).

2. FASA project : description of airborne campaigns

2.1 FASA system characteristics

2.1.1 Characteristics of the airborne system FASA

FASA, the Fire Airborne Spectral Analyser, is a combination of a Fourier Transform Spectrometer and a three channels imaging system. This sensor, was developed to provide a system investigating and monitoring emissions from natural sources such as volcanoes or wild fires. Furthermore, FASA is able to get concentration profiles of gaseous effluents.

The data knowledge improvement is necessary at meantime for the effects of such local emissions and for the global ecosystem. Moreover, airborne system FASA allows riskless access to potentially dangerous areas (volcano craters).

The spectrometer and the camera are detaily described in following sections.

2.1.2 Fourier transform spectrometer MIROR

The Michelson Interferometer with Rotating Retroreflector (MIROR) is a Fourier transform spectrometer, with a special optical layout realized by DLR to achieve a stable and robust spectrometer for application in harsh environment. Previously, it was tested for in-flight measurements of aircraft exhausts.

The spectrometer consists of an INSB/MCT sandwich detector permitting spectral coverage from 600 to 3000 cm^{-1}, with a spectral resolution of 0.2 cm^{-1}. These detectors

are cooled to 77 K by liquid nitrogen.

Therefore, it is possible to resolve the emission/absorption lines of gases. At high resolutions MIROR acquires one interferograms data-set in 220 ms. This short time is necessary to avoid the smear effects. The radiometric calibration of the instrument is performed in-flight by using three black bodies. The sphere black bodies, with low power consumption were realised by using cavity sources with small apertures (diameter 10 mm). The spectrometer is operated automatically. The software performs on command full calibration At the end of the calibration cycle the collimator is removed, and the spectrometer receives radiation from the ground again. Calibration requires about 2 minutes and can therefore be performed while approaching the target area or often even while moving from one flight line to the next.

The technical data of MIROR are summarized in Table 2.1. For the FASA experiment MIROR was operated in a NADIR configuration.

Table 2.2 provides the footprint diameter on the ground and the smear for some flight altitudes. Typically these are in the range 3000 to 4000 m.

2.1.3 Camera system ABAS

ABAS consists of the MIR/TIR Hot Spot Recognition Sensor (HSRS) and VIS/NIR Wide-Angle Airborne Camera (WAAC).

HSRS is a bi-spectral push-broom scanner with spectral bands in the MWIR at 3.9 µm and TIR at 8.8 µm. The sensitive devices are 2 MCT photodiode lines. The lines – with identical layout in the MWIR and TIR – comprise 2 x 512 elements each in a staggered structure.

These arrays have to be cooled to 100 K in the MWIR and to 80 K in the TIR. The maximum achievable TIR photodiode cut-off wavelength of about 10 µm at 80 K and the atmospheric ozone band at 9.6 µm make it necessary to use the 8.5 – 9.3 µm band for TIR channel of the HSRS instead of the commonly used 10.5 – 11.7 µm band. The cooling is realized by means of small Stirling cooling engines. HSRS sensor head components of both spectral channels are based on identical technologies to provide good pixel co-alignment. Both spectral channels have the same optical layout but with different wavelength-adapted lens coatings.

The HSRS sensor data are read out continuously with a clock time which is exactly one half of the pixel dwell time. This time controlled "double sampling" and the staggered line array structure allow a geometric resolution enhancement compared to a classic line array.

Radiometric fire measurements require a large dynamic range. To fulfil this requirement, a second scene sampling is performed with reduced exposure time (within the same sampling clock time interval!), if hot areas are identified during the real-time processing of the data from the first scene sampling. This second sam-

Technical description	Values
Spectral range	600 – 3000 cm^{-1}, (3.3 – 16.6 µm)
Spectral resolution	0.2 cm^{-1}
Registration time per interferogram	0.22 s
Measurement rate	3 Hz
Field of View	20 mrad
NESR (single scan)	6.2 x 10^{-8} W/(cm^2 sr cm^{-1})

Table 2.1 Technical data of the MIROR Fourier Transform Spectrometer.
Tabella 2.1 Dati tecnici dello Spettrometro di Fourier MIROR.

Flight altitude over ground (m)	MIROR footprint diameter (m)	Footprint smear for 75 m/s speed over ground (%)
2000	40	27.5
3000	60	14
4000	80	7

Table 2.2 Footprint diameter and smear for various flight altitudes over ground by the FASA experiment (MIROR was operated in a NADIR configuration).
Tabella 2.2 Diametro del campo di vista e "smear" a varie quote di volo del FASA (MIROR opera in configurazione nadirale).

pling is performed only if the real-time processing of the first sampling set indicates that detector elements are saturated or close to saturation. These supplementary sampled pixels are added to the normal thermal scene measurement data as the so called "Hot Area (HA)" data sub-set. All these sampled data are transmitted to the HSRS data acquisition controller via a special serial interface. Altogether, the HSRS has an adaptive radiometric dynamic range which permits recognition of High Temperature Events (HTE) such as wildfires, volcanic activities, or coal seam fires without sensor saturation.

In addition to the cameras there are a GPS receiver and a gyro processing unit which aid in geo-referencing the recorded images. ABAS is also connected to the aircraft's ARINC bus which provides additional (house keeping) data from the aircraft

Table 2.3 shows the main technical data of ABAS, and Table 2.4 lists the swath widths and pixel sizes on the ground for various flight altitudes.

2.1.4 Co-alignment and Synchronisation

ABAS and MIROR are installed as mechanically independent instruments in the aircraft. It is therefore necessary to align their measurement spots (co-alignment). Furthermore, synchronisation of the recorded spectra and images in time is required.

The latter task is solved by establishing a common time base, i.e. the GPS time of ABAS. In addition, MIROR is provided with an electrical signal that permits counting of the currently recorded image line of ABAS' VIS/NIR channel. This line counter is stored together with the images and the interferograms. Thus the correct assignment of the data from both systems is guaranteed.

Co-alignment is established by using the ABAS VIS/NIR channel: An additional small video camera is fixed at the optical block of the spectrometer. Its line of sight is directed in parallel to the spectrometer's line of sight. The camera's FOV is about 10 times larger than the spectrometer's FOV. Therefore the area observed by the spectrometer can be determined within the video camera images. This is done before flight in the laboratory.

During flight the video images are recorded simultaneously with the interferograms and the ABAS images. By applying well known techniques (e.g. correlation) during data evaluation the spectrometer FOV is located in the ABAS images.

The following figures show the aircraft installation. Figure 2.1 depicts the racks with the spectrometer electronics.

Figure 2.2 shows the optical part of the spectrometer and the calibration unit.

Technical data	Values	
Spectral range	VIS/NIR: MIR: TIR :	0.4 - 0.6 µm 3.4 – 4.1 µm 8.5 – 9.3 µm
Field of View	VIS/NIR: MIR/TIR:	80° 19°
Detector elements number (N° of pixels/line)	VIS/NIR: MIR/TIR:	5184 2 x 512 (staggered)
Instantaneous Field of View	VIS/NIR: MIR/TIR:	0.27 mrad 0.66 mrad

Table 2.3 ABAS Technical Data.
Tabella 2.3 Dati tecnici dell'ABAS.

Flight altitude over ground (m)	Swath width (m)		Linear pixel size (m)	
	VIS/NIR	MIR/TIR	VIS/NIR	MIR/TIR
2000	~ 3300	~ 660	~ 0.7	~ 1.4
3000	~ 5000	~ 1000	~ 1.0	~ 2.0
4000	~ 6600	~ 1320	~ 1.4	~ 2.8

Table 2.4 ABAS-Swath width and pixel sizes for various flight altitudes over ground.
Tabella 2.4 Dimensioni del pixel e campo di vista totale di ABAS per diverse altezze di volo.

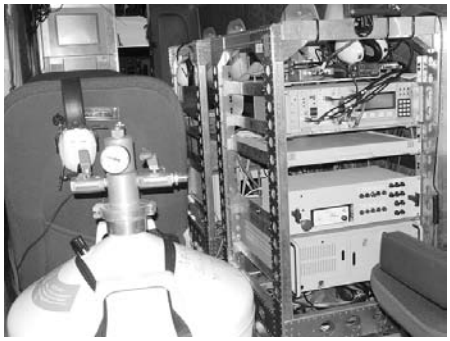

Figure 2.1 The spectrometer electronics installed in the aircraft and its rack (right).
Figura 2.1 Componenti elettrici dello spettrometro istallati sull'aereo (destra).

Figure 2.2 View of the calibration unit (left) and the spectrometer optics (right) and thermal boxes on the aircraft back side.
Figura 2.2 Vista dell'unità di calibrazione (sinistra), degli spettrometri ottici (desta) e delle scatole termiche, montati nella parte posteriore dell'aereo.

2.2 FASA configuration

The blocks schematic of the new FASA system is showed in the Figure 2.3 The M-PC (MIROR_PC) controls the spectrometer electronic during the acquire process of the interferograms. To have a automatic calibration and acquisition process of the spectrometer on board on the aircraft during the campaign, new parts are developed and integrated at the MIROR developing a specific optic and mechanical interface. A video M-camera, co-aligned at the spectrometer, grabs the images during in flight observation (in order to correlate the interferograms with the bi-spectral images from cameras of ABAS device); MIROR and M-camera look down through a folding mirror M1 fixed in front of MIROR aperture; tree Black Bodies with different temperatures (100, 150 and 190 Celsius degree) generate the reference radiation; a system of two mirrors, M2 and M3, directs the reference radiation in to the spectrometer window; two stepper motors (Motor1 and Motor2) move

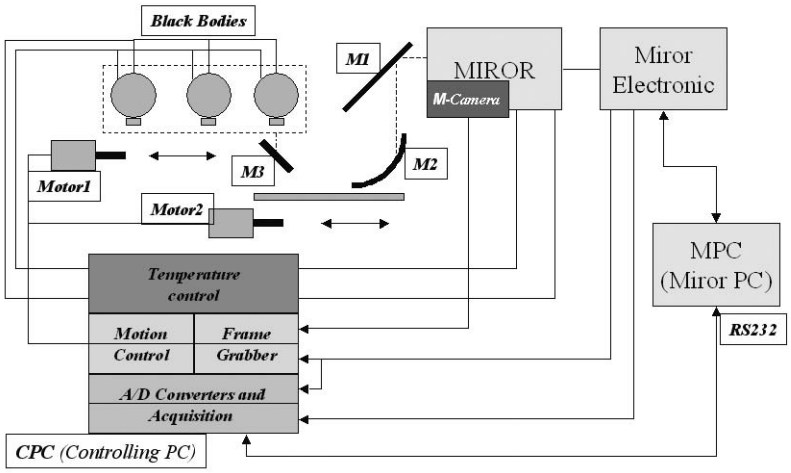

Figure 2.3 Configuration and integration of the FASA system. M-PC (MIROR_PC) controls the spectrometer electronic and manages the acquisition process of the interferograms; A video M-camera, co-aligned at the spectrometer, grabs the images during in flight observation; MIROR and M-camera look down through a folding mirror M1 fixed in front of MIROR window; three Black Bodies with different temperatures (100, 150 and 190 Celsius degree) generate the reference radiation; two mirrors, M2 and M3, directs the reference radiation in to the spectrometer window; two stepper motors (Motor1 and Motor2) move the black bodies and mirrors for automatic calibration of the spectrometer during the flight; Controlling PC (C-PC) controls the black bodies and spectromet temperatures.
Figura 2.3 Configurazione ed integrazione del sistema FASA.

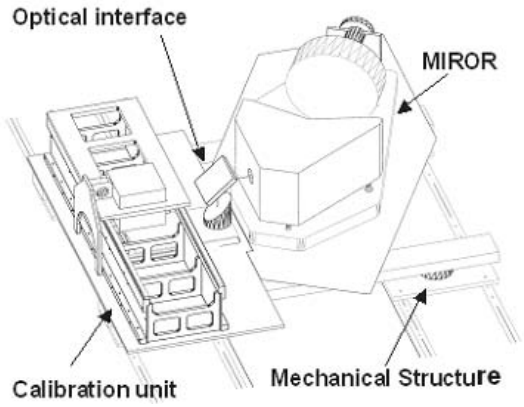

Figure 2.4 A preliminary 3D model of the MIROR, optical interface and calibration unit alignment. The model was developed to analyze the global size, optical path, weight and to design optic and mechanical parts . A flat folding mirror is fixed in front of the spectrometer window.
Figura 2.4 Modello preliminare 3D del MIROR, allineamento dell'interfaccia ottica ed unità di calibrazione.

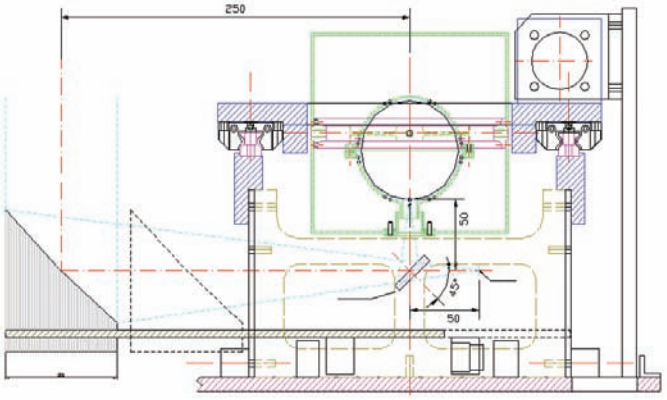

Figure 2.5 A section of the calibration unit. The reference radiation from the black bodies is redirect two wise: first by a small flat mirror M3 and afterward by a off axis parabolic mirror M2. The focal path is 300mm.
Figura 2.5 Sezione dell'unità di calibrazione.

the black bodies and mirrors for automatic calibration of the spectrometer during the flight; a Controlling PC (C-PC) controls the black bodies and spectrometer temperatures, the black bodies and mirrors motion and acquires the spectrometer interferograms and camera images.

2.3 Development of fasa system: mechanics

The FASA FTIR and calibration systems were installed and the aircraft (Dornier 228) using a mechanical interface like aluminium truss structure fixed on the seat railway using four dampers. The spectrometer and the calibration unit (included their thermal boxes) were fixed on this structure and their align was kept by reference pins. A structural analysis was performed simulating the dynamic loads, transmitted by airplane during the flight, to evaluate the strength on the mechanical interface.

The Figure 2.4 shows the model of the mechanical system mounted on the truss structure and the alignment between one black body and the spectrometer. A carriage moves the black bodies in the flight direction to change the reference radiation during the calibration; a second carriage moves a parabolic and small flat mirrors under the B.B. in the spectrometer direction. The two mirrors redirect twice the B.B. radiation as showed in the Figure 2.5: a folding small mirror (first) and a off-axis parabolic mirror (second).

A flanged aluminum bracket keeps the folding mirror in front of the MIROR aperture and the video camera co-aligned with the spectrometer beam (Figure 2.6). The spectrometer and camera can look together on the ground by means of window under the aircraft fuselage.

2.3.1 Control system: C-PC

To control the calibration system, instruments thermal stabilization and to acquire images and interferogram backup from spectrometer, a second industrial Controller PC (C-PC) was developed. It uses modular hardware with high flexibility configuration and object oriented software in order to modify and to adapt the programs during laboratory and on board test very fast.

The Figure 2.7 shows the blocks representation of the C-PC internal configuration and the electronic interfaces. Six NI-boards implement different functions. Frame grabber board acquires the images from video camera during the observation process. A very fast I/O board read the digital date driving the sampling of two 14 bits A/D converters (mounted on external board) that acquire the analog signals (interferogram) coming from the MIROR detector. The MIROR electronic provides two digital signal for synchronizing both interferogram and image acquisition with the revolution of the retro-reflector mirror. The thermal stabilization is operated by two systems: two board reads the

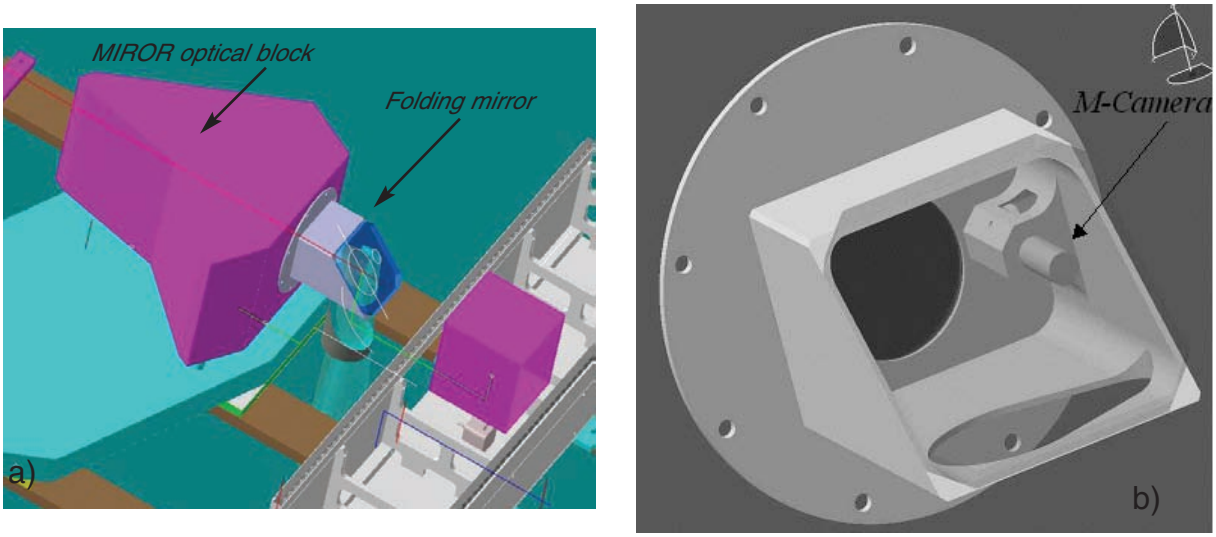

Figure 2.6 (a) A 3D model of the MIROR optical interface. A flat folding mirror is fixed in front of the spectrometer aperture, using a flanged aluminum support (picture on the right).(b) A small black and white video camera is fixed inside the flange (courtesy Galileo Avionica).
Figura 2.6 (a) Modello 3D dell'interfaccia ottica del MIROR. (b) Posizionamento della video camera in bianco e nero.

temperature sensors of the black bodies and spectrometer with a accuracy of ± 0.01 °C; each board has sixteen input channels and sixteen 24bits sigma-delta A/D converters. The temperatures information is processed by four close loop PID regulators implemented on the C-PC. The output data of the regulators drive e PWM signals generators board that regulate, trough a power switch devices, the current duty cycle of the heating elements on the black bodies and MIROR optical block. The last block is a motion controller board, which moves the motors during the calibration and check the black bodies position.

The software of the CPC has been developed on LabVIEW platform and consists in procedures in according to different function. It contains two main program that operate sepa-

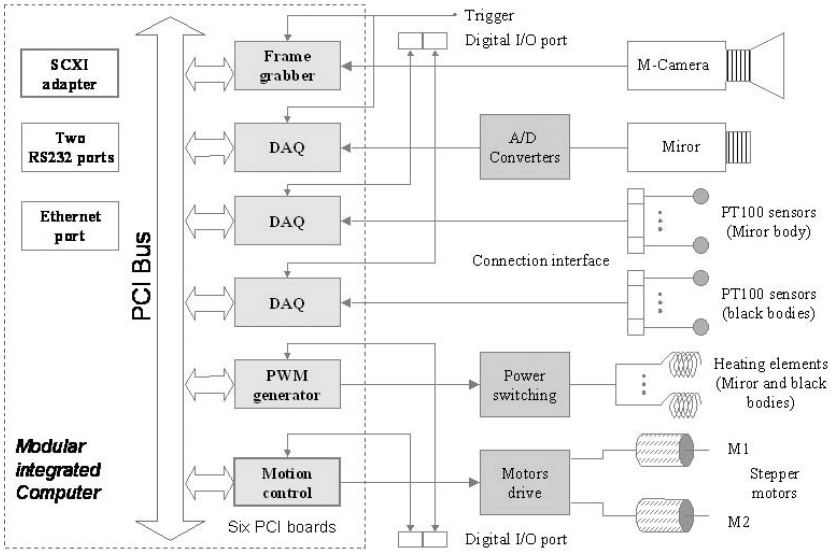

Figure 2.7 Functional blocks scheme of Controller-PC (C-PC) and interfaces with Calibration unit and Spectrometer.
Figura 2.7 Schema a blocchi funzionale del Controller-PC (C-PC) e interfacce con unità di calibrazione e spettrometro.

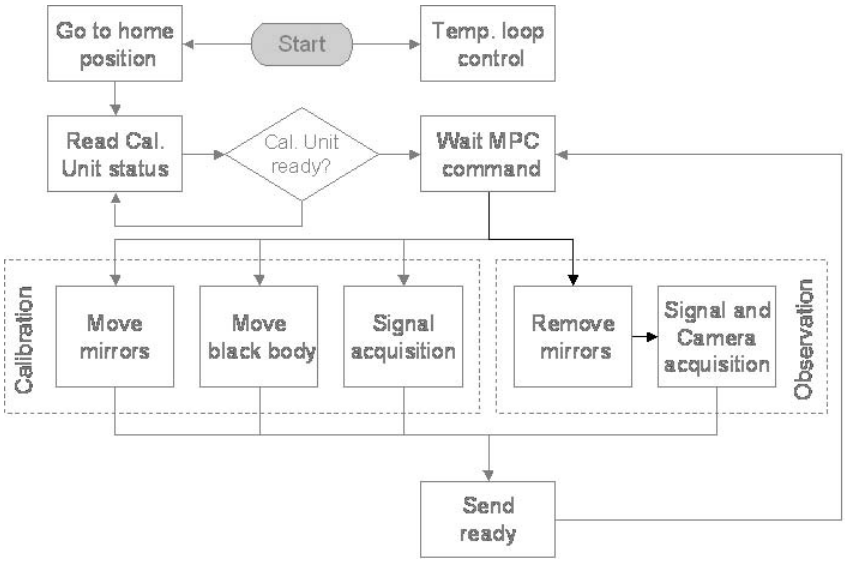

Figure 2.8 Flow diagram of the spectrometer calibration and images grabber program. When the program starts the C-PC move the black bodies in home position and begin the thermal control of the system. When the temperatures information are in range and the calibration status is ready the C-PC waits for command from the MIROR-PC. The calibration and observation process are performed separately. Receiving few calibration commands the C-PC can operate a sequence of three procedures: positioning the mirrors, moving one or more black bodies, acquiring the reference interferograms. Before the observation process the C-PC removes the black bodies mirrors and goes at the acquisition procedure.
Figura 2.8 Diagramma di flusso della calibrazione dello spettrometro.

rately sharing some commands: the first one implements a thermal control process (a background process) for stabilizing the BB and spectrometer optical block temperatures; the second one program contains the calibration and observation acquisition process and operates by command from MPC.

The second program operates in this way: when the program starts, the first operation is to move the calibration unit in home position for the take-off of the aircraft. When the mechanical is in home status and the thermal stabilization is done (less 10 minutes), the program sends a ready message to the M-PC and waits next command. During the calibration process, the M-PC computer sends a sequence of commands to the CPC, which actives some sub-procedures respectively: moves one BB, moves the mirrors, arms the A/D converter, opens the date file and sends a ready message (Figure 2.8). Then the MIROR actives two digital signals and the acquisition starts until the MPC stops the process. The observation process is similar to the calibration: the M-PC sends one command followed by start time; then the CPC program removes the mirrors and runs the acquisition unit and a second file will be generated for the images sequence.

2.4 FASA: laboratory pre-flight test

A pre-flight laboratory test were performed for characterizing and testing the flight set-up.

To certify the measurement instrument before a avionic use a simulated structural analysis was necessary for the estimation of the mechanical strength of the integrated system, including the spectrometer-aircraft mechanical interface, under static and dynamics loads. The acceleration transmitted by airplane holder has been applied on three axes using two different model simulation. A analysis model consisting of dynamic check: gravitational loading, vibrations and mass-inertial properties; a static stress analysis was performed in the three directions X, Y, Z for checking the damper and the ultimate strength. The result was conform to the Aeronautic constrain showing only a deformation of the system at 13G acceleration (Figure 2.9).

On September 2002, a first mechanics integration test was realized at the DLR in Oberpfaffenhoffer. The calibration unit and spectrometer alignment was checked using the reference points on booth structures; the black bodies radiation path was tested operating on the mirrors position of the optical interfaces.

The second test (INGV Laboratory) was PID parameters characterization for heating the

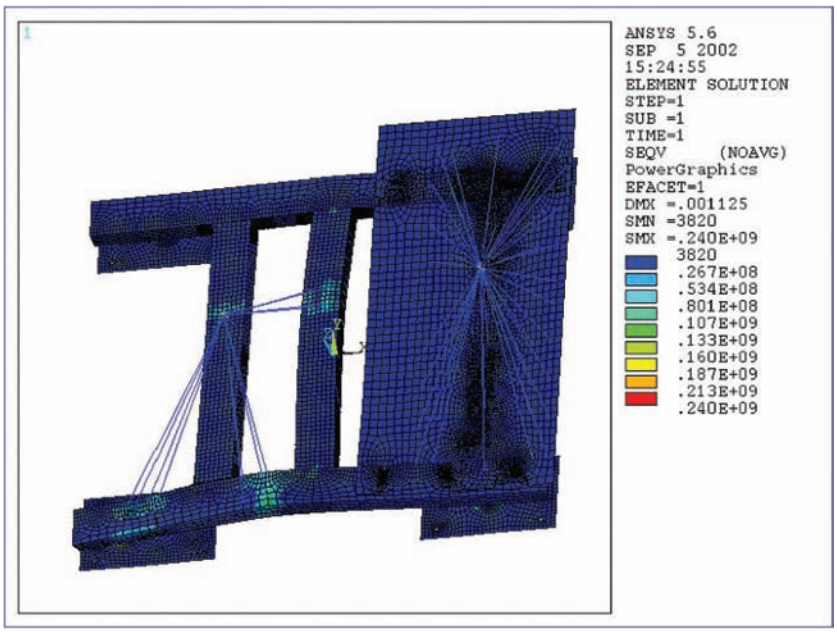

Figure 2.9 Results of the Analysis of the structural deformation using a Finite Elements Method and applying a 13G load (*Galileo Avionica*).
Figura 2.9 Risultati delle analisi della deformazione strutturale (*Galileo Avionica*).

black bodies and to perform ripple stabilization's. Many date were acquire to analyze the rising and falling time of the temperatures waveform at different final set point temperature: 100, 150, 180 °C. In this case when the temperature reach the set point, the PWM generator turns off automatically. (Figure 2.10).

Before the final system integration at DLR in Germany, many test were take at INGV: in particular, the movement of the Black Body has been calibrated (Figure 2.11).

In spring 2003 were tested the Calibration Unit hardware and controlling software and the Black Body heating temperature process in the DLR laboratory. A measure of the internal temperature of the BB. (four thermometer) was

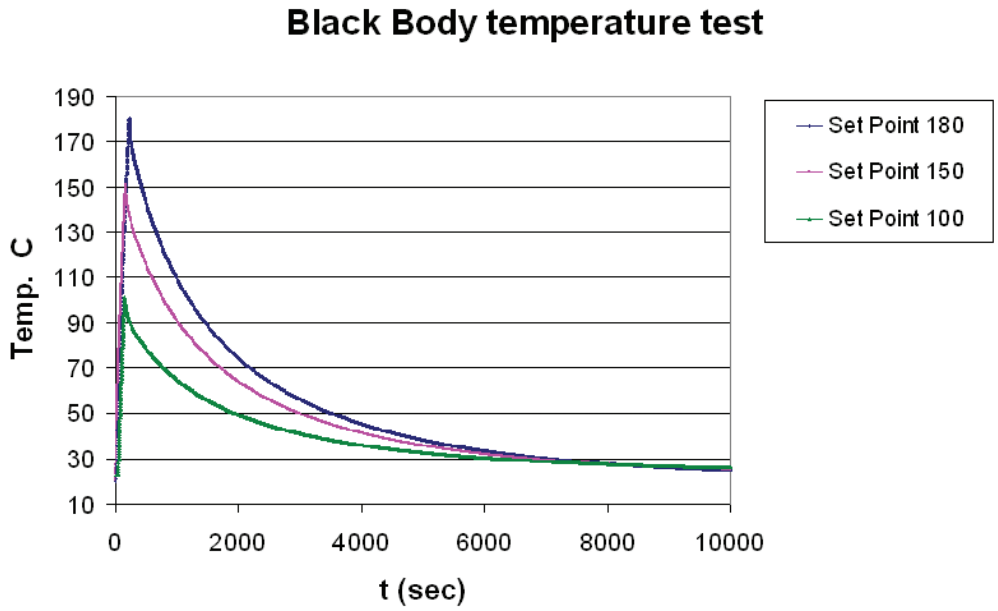

Figure 2.10 Black Body heating test. Temperature.
Figura 2.10 Test di temperatura del corpo nero.

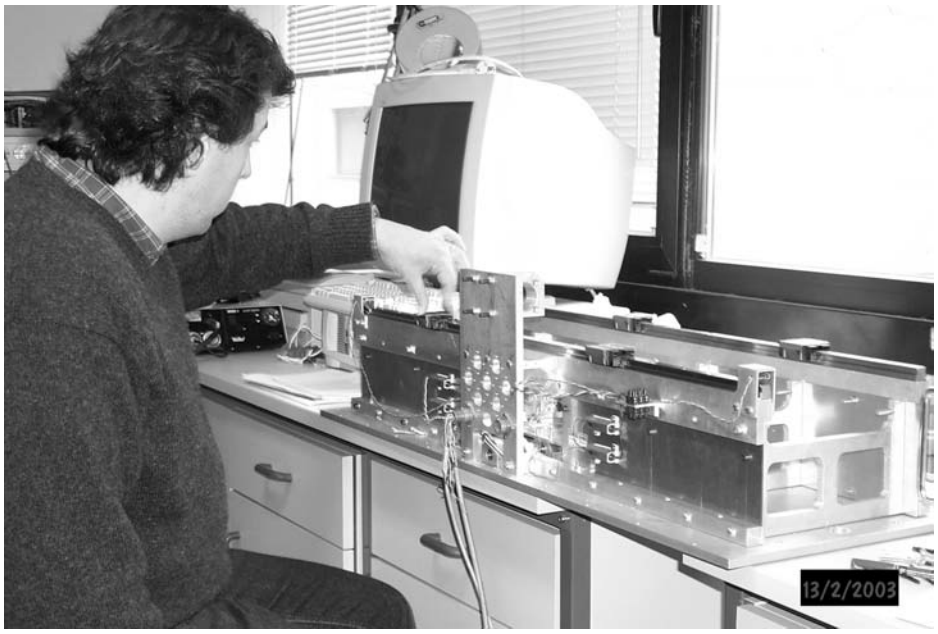

Figure 2.11 Test of the mechanic for moving of the calibration unit. The black bodies carriage will run on two "railway" using four ball bearing (visible on the picture).
Figura 2.11 Test di meccanica per l'azionamento dell'unità di calibrazione.

acquired in different measurements cycle to verify the stability and the rising time. Mechanics and electromagnetic compatibility test were took after the arrangement of the instruments on board and running the aircraft engines.

2.5 FASA test flight

2.5.1 Measurements

Course of events

The following table (Table 2.5) shows the course of events.

2.5.2 Details

The installation of the FASA experiment proceeded with the "usual" minor problems which are common to all first time installations. All checks and tests to get the flight approval were passed without any difficulty. The flight permission was granted until 31.08.2003.

During the test flight (15.07.) the single instruments performed very well. As it had been the case on ground also the communication and synchronisation between the different systems ABAS/MIROR, CPC/MPC worked well.

Date	Actions	Flight hours used
07.07.	Transfer Braunschweig – Oberpfaffenhofen	1:40 h
08.07. – 15.07	Installation and ground tests to pass flight worthiness approval	
15.07.	Test flight	1:05 h
16.07.	Transfer Oberpfaffenhofen – Catania including measurements over Solfatara	5:05 h
17.07.	Measurements over Etna	2:20 h
19.07.	Measurements over Etna	2:45 h
20.07	Measurements over Etna	2:20 h
23.07.	Transfer Catania – Oberpfaffenhofen	4:50 h
31.07.	Transfer Oberpfaffenhofen – Braunschweig	1:45 h

Table 2.5 FASA test-fligts: course of events.
Tabella 2.5 Test di volo del FASA: cronologia degli eventi.

During the first three flights (16.07, 17.07, and 19.07) over target areas all instruments successfully acquired data. On 19.07 the flight took place about 1 h after an over-flight of the satellite ASTER.

At the last flight over Etna (20.07) the Fourier spectrometer could not acquire data due to a broken beamsplitter. Condensation of water on the hygroscopic plates had destroyed it. Condensation occurred during landing when the "cold" instrument was brought back to the hot and highly humid air on ground.

2.5.3 Flight lines

Before the flights INGV and DLR agreed on flight lines over the respective target areas. There were 6 flight lines over Etna and one line over Solfatara. These covered the volcano craters as well as other areas of interest as defined by INGV.

2.5.4 Flights over Solfatara

Data were acquired along the flight line specified in the table (Table 2.6) below. The flight directions were north to south and also south to north. Two flights in each of these directions were performed. Data were recorded from 13:00 to 13:35 UTC.

Data were recorded on the 17th and 19th July 2003. The times were 8:00 to 9:45 UTC and 10:50 to 12:35 UTC, respectively.

The table below lists the coordinates of the flight lines (Table 2.7).

The actual flights were performed in the following order (Table 2.8)

2.6 Summary of acquired datasets

Entire dataset is summarized in the following table (Table 2.9).

Each data-set consists of one InSb and one MCT interferogram plus a VIS image. Due to the way ABAS operates not each data-set has a corresponding ABAS image. However, the flights were organized such that at Solfatara the flight line was completely covered by ABAS images. Over Etna the timing ensured that the interesting parts of the flight lines (craters, Valle del Bove) were completely covered. For the other parts coverage depended on the ABAS timing.

3. Satellite data acquired during the Etna 2003 campaign

A great effort was made to plan and to acquire the contemporaneous overpass of the available NASA and ESA satellite over the main test site represented by Mt. Etna during the FASA system flights.

In particular the Hyperion and ASTER data were used to validate the retrieval algorithms for atmospheric and surface parameters developed during the Hypseo ASI project.

3.1 Satellite acquisitions

In the period 17 – 26 July 2003 various satellite sensors acquired data over the Sicilian volcanoes. Depending on the ground swath of the sensor the target test sites is ranged from Mt. Etna to the whole Sicily, including the Eolian Islands. Remote sensing images were acquired in the spectral range from Visible to Thermal Infrared by the following satellites:

- Advanced Land Imager (ALI) on EO-1;
- Advanced Spaceborne Thermal Emission and Reflection Radiometer (ASTER) on Terra;
- Advanced Very High Resolution Radiometer (AVHRR) on NOAA constellation satellites;
- EROS-A;
- Hyperion on EO-1;
- Micro-satellite on Bi-spectral Infrared Detection (BIRD);
- Moderate Resolution Imaging Spectroradiometer (MODIS) on Terra and Aqua.

Unfortunately during the time period of

Flightline	LAT 1) start 2) end	LONG 1) start 2) end	Altitude (ft)	DATE - Velocity (knots)	Sensor type
1	40N46.4917' 40N52.4917'	14E8.2083' 14E8.2083'	11,000	16.07.2003-130	MIROR and ABAS
2	40N52.4917' 40N46.4917'	14E8.2083' 14E8.2083'	11,000	16.07.2003-130	MIROR and ABAS

Table 2.6 FASA test-fligts: Solfatara test site flight lines.
Tabella 2.6 Test di volo del FASA: linee di volo sulla Solfatara.

the measurements campaign the Landsat 7 satellite had technical problems, so any ETM+ data was acquired. Instead of Landsat 7, ALI data were acquired, but are not available in time for this publication.

In Table 3.1 the satellite data and the acquisition times are reported. In the following paragraphs a single satellite sensor, is described.

3.2 ASTER

The satellite platform TERRA launched by NASA as a part of the EOS (Earth Observing System) is equipped with ASTER (Advanced Spaceborne Thermal Emission and Reflection Radiometer), an instrument developed by a cooperation of NASA, the Japan's Ministry of Economy, Trade and Industry, and ERSDAC (Earth Remote Sensing Data Analysis Center).

ASTER is constituted by three different subsystems, operating in the visible an near infrared (VNIR), the short wave infrared (SWIR) and the thermal infrared (TIR) region of

Flightline	LAT 1) start 2) end	LONG 1) start 2) end	Altitude (ft)	DATE - Velocity (knots)	Sensor type
A–B	37N39.1000' 37N46.3667'	15E8.0667' 15E58.1167'	20,000	17.07.2003- 150 19.07.2003-: 170	MIROR and ABAS
C–D	37N43.3000' 37N45.3500'	15E8.7000' 14E57.0667'	20,000	17.07.2003-: 150 19.07.2003-: 170	MIROR and ABAS
E–F	37N43.4833' 37N49.8167'	14E58.5167' 15E3.0333'	20,000	17.07.2003-: 150 19.07.2003-: 170	MIROR and ABAS
G–H	37N37.1500' 37N46.6000'	15E0.2000' 15E0.0667'	20,000	17.07.2003-: 150 19.07.2003-: 170	MIROR and ABAS
J–K	37N39.9167' 37N48.3000'	14E52.9167' 15E8.1667'	20,000	17.07.2003-: 150 19.07.2003-: 170	MIROR and ABAS
I–L	37N37.2667' 37N45.6333'	14E55.1167' 15E10.3667'	20,000	17.07.2003-: 150 19.07.2003-: 170	MIROR and ABAS

Table 2.7 FASA test-fligts: Etna test site flight lines.
Tabella 2.7 Test di volo del FASA: linee di volo sull'Etna.

17.07.2003	19.07.2003
A–B	B–A
C–D	D–C
K–J	J–K
J–K	E–F
I–L	F–E
F–E	I–L
H–G	H–G
I–L	D–C
	B–A

Table 2.8 FASA test-fligts: flight order.
Tabella 2.8 Test di volo del FASA: piani di volo.

Date	Target area	Number of acquired data-sets
16.07.2003	Solfatara	1208
17.07.2003	Etna	3900
19.07.2003	Etna	4210

Table 2.9 Summary of acquired datasets.
Tabella 2.9 Sommario delle serie di dati acquisite.

Date	Satellite	Acquisition Time (GMT)
17.07.2003	ASTER	21:08
	AVHRR	01:30, 04:50, 06:29, 09:44, 11:17, 12:57, 16:10, 17:50, 21:05
	MODIS	01:30, 10:00, 10:05, 11:40, 20:25
18.07.2003	BIRD	21:40–21:41
	AVHRR	01:19, 06:06, 09:22, 12:45, 17:26, 20:43
19.07.2003	ASTER	09:52
	AVHRR	01:08, 05:42, 07:23, 08:59, 10:40, 12:34, 17:03,20:20
	HYPERION	09:25
	MERIS	09:36
	MODIS	00:20, 00:25, 09:50, 11:25, 20:55
20.07.2003	AVHRR	00:56, 02:38, 05:19, 06:59, 08:37, 10:17, 12:23, 16:39, 18:20, 19:58, 21:38
	BIRD	10:44–10:45
	MODIS	01:05, 10:35, 12:10, 21:35
21.07.2003	AVHRR	00:45, 02:26, 04:56, 06:35, 09:54, 12:11, 16:16, 17:56, 19:36, 21:15
	MODIS	00:10, 09:40, 12:50, 20:40
22.07.2003	AVHRR	00:34, 02:15, 06:12, 09:31, 12:00, 13:42, 15:53, 17:32, 20:52
	EROS	09:22, 09:24
	MODIS	00:55, 10:20, 11:55, 21:25
23.07.2003	AVHRR	02:23, 04:04, 07:48, 11:09, 12:49, 13:49, 15:31, 17:31, 19:09, 22:30
24.07.2003	AVHRR	02:12, 03:52, 07:25, 09:05, 10:47, 12:27, 13:38, 15:19, 18:45, 20:26, 22:07, 23:48
25.07.2003	AVHRR	03:41, 07:02, 08:41, 10:24, 12:04, 13:27, 18:22, 20:02, 21:45, 23:25
26.07.2003	ASTER	21:02
	AVHRR	01:30, 06:18, 09:41, 11:16, 12:56, 15:59, 17:38, 19:23, 21:02
	EROS	09:23
	HYPERION	09:31
	MODIS	00:30, 09:55, 11:30, 11:35, 21:00

Table 3.1 The table shows the satellite sensors acquisitions (period: 17 – 26 July 2003).
Tabella 3.1 La Tabella mostra le acquisizioni dei sensori satellitari (periodo: 17-26 Luglio 2003).

Characteristic	VNIR	SWIR	TIR
Spectral Range	Band 1: 0.52-0.60 μm Nadir looking	Band 4: 1.600-1.700 μm	Band 10: 8.125-8.475 μm
	Band 2: 0.63-0.69 μm Nadir looking	Band 5: 2.145-2.185 μm	Band 11: 8.475-8.825 μm
	Band 3: 0.76-0.86 μm Nadir looking	Band 6: 2.185-2.225 μm	Band 12: 8.925-9.275 μm
	Band 4: 0.76-0.86 μm Backward looking	Band 7: 2.235-2.285 μm	Band 13: 10.25-10.95 μm
		Band 8: 2.295-2365 μm	Band 14: 10.95-11.65 μm
		Band 9: 2.360-2.430 μm	
Ground Resolution	15 m	30 m	90 m
Data Rate(Mbit/s)	62	23	4.2
Cross-track Pointing (deg)	±24	±8.55	±8.55
Cross-track Pointing (Km)	±318	±116	±116
Swath Width (Km)	60	60	60
Detector Type	Si	PtSi-Si	HgCdTe
Quantization (bits)	8	8	12

Table 3.2 Characteristic of the ASTER sensor.
Tabella 3.2 Caratteristiche del sensore ASTER.

the electromagnetic spectrum. Every subsystem is provided with a different telescope. The main instrument characteristics are summarized in Table 3.2 ASTER data were collected upon request on specific scenes.

During the July, 2003 campaign on Sicilian Volcanoes were possible four ASTER data acquisitions on July 17 (nighttime), 19 (daytime), and two (nighttime and daytime) on July, 26. All of these were timely requested and scheduled in order to have simultaneous ground data acquisitions for satellite data validation. The July, 26 daytime acquisition was cancelled while the field campaign was not, and thus it is failed a rare opportunity to have a double ASTER daytime and nighttime acquisition provided with an extensive ground data acquisition on an important target like Mount Etna. The list of all the different satellite borne sensors data collected during the July, 2003 Sicily campaign comprehensive of the ASTER data acquisition is reported on Table 3.1.

3.3 MODIS

MODIS (Moderate Resolution Imaging Spectroradiometer) [NASA, 2003a] is a key instrument aboard the Terra (EOS AM) [NASA, 2003b] and Aqua (EOS PM) [NASA, 2003c] satellites. Orbit of Terra around the Earth is timed so that it passes from north to south across the equator in the morning, while Aqua passes south to north over the equator in the afternoon. Terra MODIS and Aqua MODIS are viewing the entire Earth's surface every 1 to 2 days, acquiring data in 36 spectral bands, or groups of wavelengths, with variable spatial resolution (Table 3.3).

Starting from the raw MODIS acquisitions and ancillary information data are elaborated to obtain 44 final products that are listed in Table 3.4. Each of these products can be freely downloaded for scientific purposes [NASA, 2003a].

For the period of the ground-based measurements 28 MODIS images acquired over the Mount Etna area are available (Table 3.5).

Primary Use	Band	Bandwidth (nm)	Spatial resolution
Land/Cloud/Aerosols Boundaries	1	620 - 670	250 m
	2	841 - 876	250 m
Land/Cloud/Aerosols Properties	3	459 - 479	500 m
	4	545 - 565	500 m
	5	1230-1250	500 m
	6	1628-1652	500 m
	7	2105-2155	500 m
Ocean Color/Phytoplankton/ Biogeochemistry	8	405-420	1000 m
	9	438-448	1000 m
	10	483-493	1000 m
	11	526-536	1000 m
	12	546-556	1000 m
	13	662-672	1000 m
	14	673-683	1000 m
	15	743-753	1000 m
	16	862-877	1000 m
Atmospheric Water Vapour	17	890-920	1000 m
	18	931-941	1000 m
	19	915-965	1000 m
Surface/Cloud Temperature	20	3660-3840	1000 m
	21	3929-3989	1000 m
	22	3929-3989	1000 m
	23	4020-4080	1000 m
Atmospheric Temperature	24	4433-4498	1000 m
	25	4482-4549	1000 m
Cirrus Clouds Water Vapour	26	1360-1390	1000 m
	27	6535-6895	1000 m
	28	7175-7475	1000 m
Cloud Properties	29	8400-8700	1000 m
Ozone	30	9580-9880	1000 m
Surface/Cloud Temperature	31	10780-11280	1000 m
	32	11770-12270	1000 m
Cloud Top Altitude	33	13185-13485	1000 m
	34	13485-13785	1000 m
	35	13785-14085	1000 m
	36	14085-14385	1000 m

Table 3.3 Characteristic of the MODIS sensor.
Tabella 3.3 Caratteristiche del sensore MODIS.

Only 11 images out off 28 were acquired in near-nadiral direction and cloud-free conditions, five of which during daytime. All the products listed in Table 3.4, for each days reported in Table 3.5 can be downloaded and made available for the purposes of this project. As an example, in Figure 3.1 is reported the columnar water vapour content map retrieved for July 19.

3.4 BIRD

BIRD was successfully piggy-back launched by an Indian Polar Satellite Launch Vehicle (PSLV-C3) in a circular sun-synchronous orbit on 22 October 2001.

The BIRD small satellite mission is a technology demonstrator including new infrared push-broom sensors dedicated to recognition and quantitative characterisation of thermal anomalies on the Earth surface [Briess et al., 2003]. BIRD primary mission objectives are:
test of small satellite technologies, such as an attitude control system using new star sensors and new actuators, an on-board navigation system based on a new orbit predictor,

- test of the latest generation of infrared array sensors with an adaptive radiometric dynamic range
- detection and scientific investigation of High Temperature Events (HTE) such as forest fires, volcanic activity, and coal seam fires.

The BIRD main sensor payload consists of:

- a two-channel infrared Hot Spot Recognition Sensor system (HSRS),
- a Wide-Angle Optoelectronic Stereo Scanner (WAOSS-B).

Their characteristics are given in Table 3.6.

WAOSS-B is a modified version of a scanner that was originally developed for the Mars-96 mission. It is a three-line stereo scanner working in the push-broom mode. All three detector lines are located in the focal plane of a single wide angle lens. The forward- and backward-looking lines have a visible (VIS) and near-infrared (NIR) filters, respectively, while the nadir-looking line has a NIR filter.

Level 1A Radiance Counts	Chlorophyll a Pigment Concentration
Level 1B Calibrated, Geolocated Radiances	Photosynthetically Active Radiation (PAR)
Geolocation Data Set	Suspended Solids Concentration in Ocean Water
Aerosol Product	Organic Matter Concentration
Total Precipitable Water (near-IR method)	Coccolith Concentration
Cloud Products	Ocean Water Attenuation Coefficient
Atmospheric Profiles	Ocean Primary Productivity
Gridded Atmosphere Products-Level 3	Sea Surface Temperature
Atmospherically Corrected Surface Reflectance	Sea Ice Cover
Snowcover	Temperature and Moisture Profiles
Land Surface Temperature and Emissivity	Phycoerythrin Concentration
Land Cover/Land Cover Change	Ocean Processing Framework and Matchup DB
Vegetation Indices	Gridded Snowcover
Thermal Anomalies, Fires, Biomass Burning	Gridded Vegetation Indices
Leaf Area Index and FPAR	Cloud Mask
Surface Resistance and Evapotranspiration	Total Absorption Coefficient
Vegetation Production , Net Primary Productivity	Ocean Aerosol Properties
Normalized Water Leaving Radiance	Clear Water Epsilon
Pigment Concentration	Albedo 16-Day Level 3
Chlorophyll II Fluorescence	Vegetaion Cover Conversion and Continuous Fields

Table 3.4 MODIS product list.
Tabella 3.4 Lista dei prodotti MODIS.

DATE	TERRA		AQUA	
16.07.2003	09:20	Good	01:30	On the side
	20:25	Good	12:35	On the side
17.07.2003	10:00+10:05	Good	00:35	On the side
	21:05	Good	11:40	On the side
19.07.2003	09:50	Good	00:20+00:25	On the side
	20:55	Good	11:25	Very much on the side
20.07.2003	10:35	On the side; clouds	01:05	Good
	21:35	On the side	12:10	Good, clouds
July 21	09:40	Some clouds	00:10	Very much on the side
	20:40	A little on the side	12:50	Very much on the side
July 22	10:20	A little on the side	00:55	Good
	21:25	A little on the side	11:55	Good
July 26	09:55	Good	00:30	A little on the side
	21:00	Good	11:30+11:35	On the side

Table 3.5 MODIS passages over Mount Etna during the campaign.
Tabella 3.5 Passaggi MODIS sul Monte Etna durante la campagna.

HSRS is a two-channel push-broom scanner with spectral bands in the mid-infrared (MIR) and thermal infrared (TIR) spectral ranges. The detectors are two Cadmium Mercury Telluride (CdHgTe) linear photodiode arrays. The lines - with identical layout in the MIR and TIR - comprise 2 x 512 elements each in a staggered structure where two linear detector arrays are arranged parallel to each other with an along-line shift of a half element size. The HSRS sensor head components of both spectral channels are based on identical technologies to provide accurate pixel co-alignment. Both spectral channels have the same optical layout but with different wavelength-adapted lens coatings.

The detector arrays are cooled to 100 K in the MIR and to 80 K in the TIR. The cooling is achieved by small Stirling cooling engines. The maximal TIR photodiode cut-off wavelength of about 10.5 µm, which can be achieved at 80 K, on one hand and the atmospheric ozone band at 9.6 µm on the other hand require use of the 8.5 – 9.3 µm band for the TIR channel of the HSRS instead of the usual 10.5 – 11.7 µm band. The HSRS sensor data are read out continuously with a sampling interval that is exactly one half of the pixel dwell time. This time-controlled "double sampling" and the staggered line array structure provide the sampling step that is a factor of 2 smaller than the HRSR pixel size, coinciding with the sampling step of the WAOSS NIR nadir channel [Skrbek and Lorenz, 1998].

Radiometric investigations of thermal anomalies require (a) a large dynamic range not to be saturated by HTE occupying the major part of a pixel and (b) a large signal to noise ratio to be able to observe small thermal anomalies at normal temperatures and detect small sub-pixel HTE. To fulfil these requirements, a

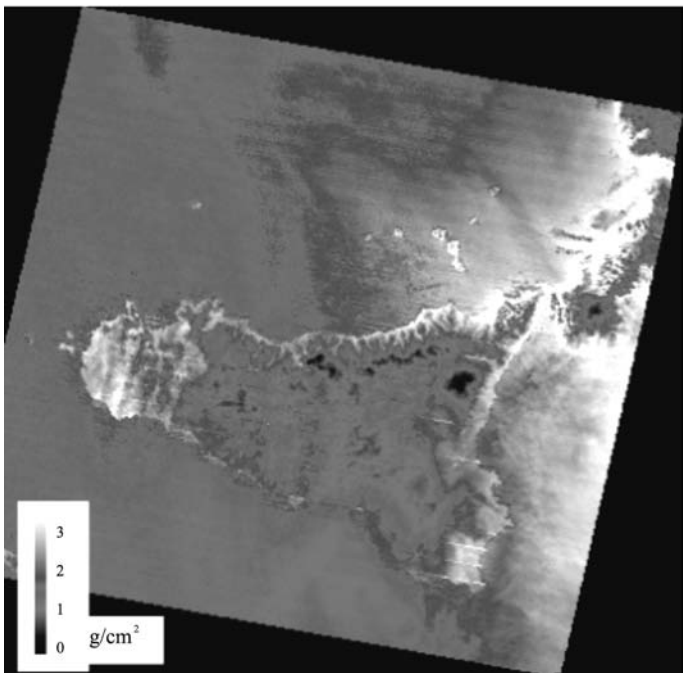

Figure 3.1 Columnar water vapor content map over Sicily estimated from the MODIS acquisition on July 19, 2003, 09:50 GMT.
Figura 3.1 Mappa di contenuto colonnare di vapor acqueo sulla Sicilia stimato dall'acquisizione MODIS del 19 Luglio 2003 alle 09:50 GMT.

	WAOSS-B	HSRS
Spectral bands	VIS: 600-670nm NIR: 840-900nm	MIR: 3.4-4.2µm TIR: 8.5-9.3µm
Focal length	21.65mm	46.39mm
Field of view	50°	19°
f-number	2.8	2.0
Detector	CCD lines	CdHgTe Arrays
Detector cooling	Passive, 20°C	Stirling, 80-100 K
Pixel size	7µm x 7µm	30µm x 30µm
Pixel number	2880	2x512 staggered
Quantisation	11bit	14bit* exposureexposure)
Ground pixel size	185m	370m
Sampling step	185m	185m
Swath width	533km	190km

Table 3.6 BIRD main sensor parameters.
Tabella 3.6 Principali paramentri del sensore BIRD.

second scene exposure is performed with a reduced integration time (within the same sampling interval) if the real-time processing of the first exposure indicates that detector elements are saturated or close to saturation. As a result, the effective HSRS radiometric dynamic range is significantly expanded preserving a fine temperature resolution of 0.1-0.2 K at normal temperatures [Lorenz and Skrbek, 2001].

3.4.1 Short summary of the BIRD hot spot data processing approach

The following processing is applied to the BIRD data:

- absolute radiometric correction and inter-channel geometric co-registration using on-ground calibration files that are periodically updated by in-flight calibration,
- geo-referencing using ground control points from detailed maps of the region, providing an accuracy of a few hundred meters,
- detection and estimation of hot spot characteristics (effective fire temperature, effective fire area, fire radiative energy release) as described in [Zhukov et al. 2003].

The detection and estimation of hot spot characteristics is conducted on sub-pixel level, providing spatially and radiometrically high-resolution remote sensing of high temperature events with a push broom IR sensor which has (1) a moderate spatial resolution of about 200 m for "normal" temperature targets and (2) an adaptive radiometric dynamic which avoids saturation.

3.4.2 BIRD observations during the Etna campaign 2003

BIRD imaged the area of Stromboli (Figure 3.2) and Etna (Figure 3.3) acquired during night (20 July 2003) and during daytime (18 July 2003).

In the night-time MIR image of

Hotspots on Stromboli	Effective fire temperature, K	Effective fire area, Ha	Radiative fire energy release, MW
18.07.2003:			
hotspot 1	510	0.16	5.3
hotspot 2	650	0.04	3.9
20.07.2003:			
hotspot 3	>580	<0.04	1.3

Table 3.7 Estimation of the hotspots characteristics on Stromboli.
Tabella 3.7 Stima delle caratteristiche degli "hotspots" su Stromboli.

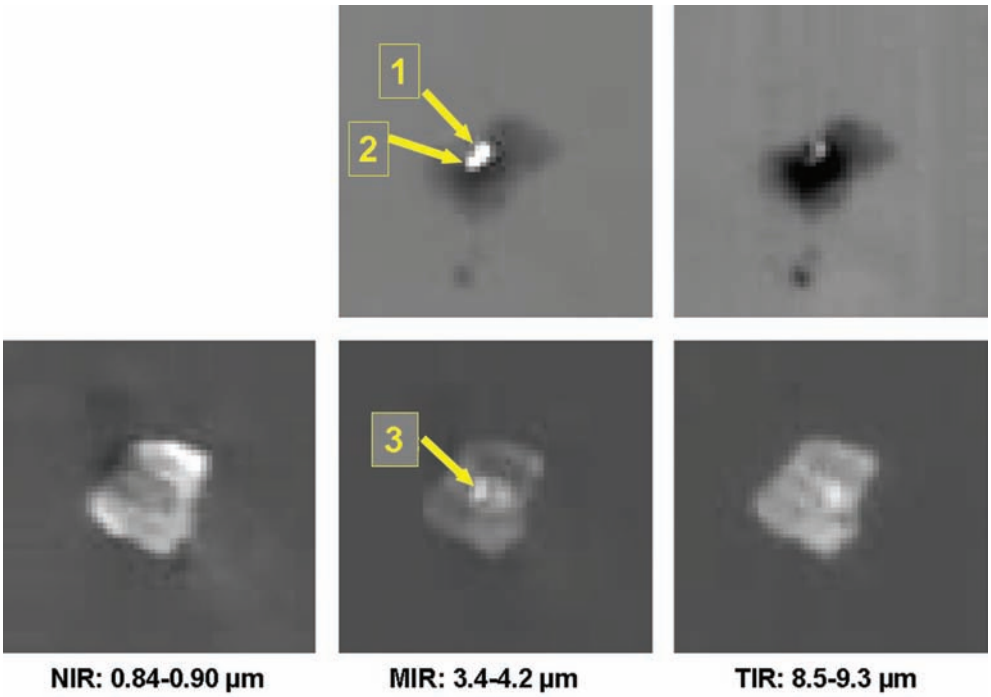

Figure 3.2 Images fragments with Stromboli obtained by BIRD in the NIR, MIR and TIR spectral channels. Upper row: night-time images obtained on 18 July 2003; lower row: daytime images obtained on 20 July 2003.
Figura 3.2 Immagini di Stromboli ottenute con BIRD nei canali spettrali NIR, MIR e TIR. Riga in alto: immagine notturna acquisita il 18 Luglio 2003; riga in basso: immagine diurna acquisita il 20 Luglio 2003.

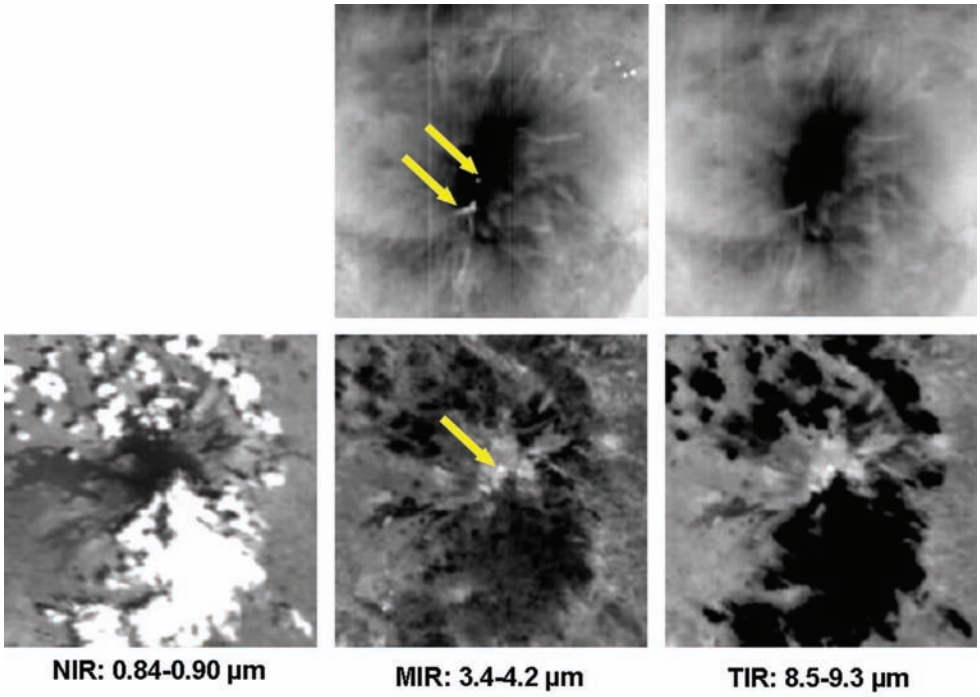

Figure 3.3 Images fragments with Etna obtained by BIRD in the NIR, MIR and TIR spectral channels: upper row: night-time images obtained on July 18th 2003; lower row: daytime images obtained on July 20th 2003.
Figura 3.3 Immagini dell'Etna ottenute con BIRD nei canali spettrali NIR, MIR e TIR. Riga in alto: immagine notturna acquisita il 18 Luglio 2003; riga in basso: immagine diurna acquisita il 20 Luglio 2003.

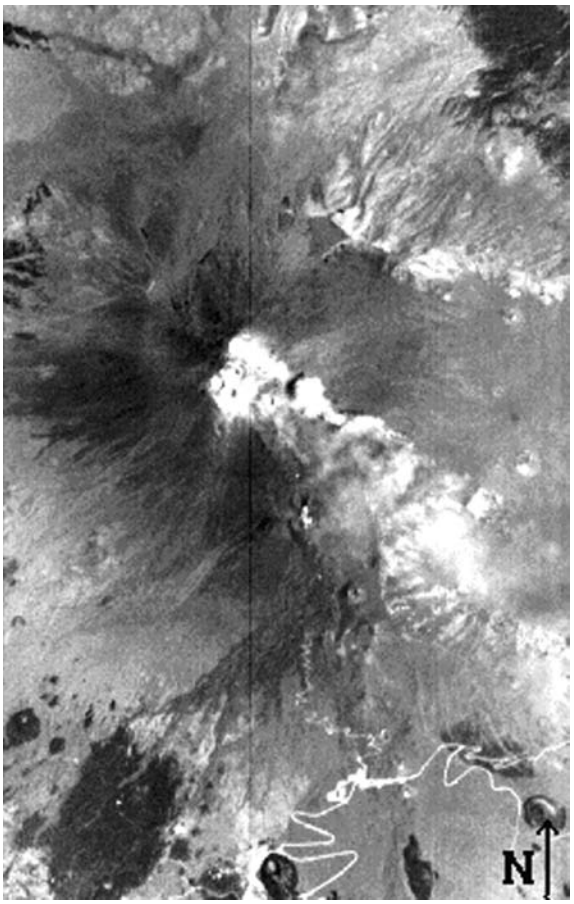

Figure 3.4 Etna HYPERION image acquired July 19th 2003.
Figura 3.4 Immagine dell'Etna acquisita con HYPERION il 19 Luglio 2003.

Stromboli, closely located hotspots 1 and 2 are clearly seen. In the daytime MIR image of Stromboli, one hotspot (hotspot 3) can be noticed. Of these three hotspots, only hotspot 1 has a relatively strong TIR signal significantly exceeding background variations, making Dozier estimations of the effective fire temperature and area relatively accurate (Table 3.7). For hotspot 2, these estimations are not reliable. For hotspot 3, only the lower bound for the effective fire temperature and correspondingly the upper bound for the effective fire area could be estimated. Nevertheless, it is certain that all three hotspots correspond to hot sources.

The radiative fire energy release (FRE) was estimated using the Bi-spectral technique for hotspot 1 and the MIR radiance method [Wooster et al, 2003] for hotspots 2 and 3. The MIR radiance method is more accurate for small hotspots where the Bi-spectral temperature and area retrievals are not reliable, but is requires that the hotspot temperature exceeds ~600 K – which is the case for hotspots 2 and 3. FRE estimations are certain to the accuracy of a few tens of percent in all three cases.

A number of brighter areas were observed also in the MIR and TIR images of Etna obtained on 18 and 20 July 2003 – though Etna was partly clouded on 20 July 2003. The brightest of them are indicated with arrows. However, the Dozier analysis does not show any hot sources – the effective 'fire' temperature for the indicated bright spots lies in the range of 340-370 K.

3.5 HYPERION

During the ground based measurements campaign Hyperion data has been requested to be acquired over Mt. Etna in collaboration between INGV, USGS and NASA (Figure 3-4 and Figure 3.5). Hyperion is an imaging sensor payload of the Earth Observing (EO-1) platform. Launched on 21th November 2000 the EO-1 satellite is in a polar orbit at 705 Km of altitude and with a 16-day repeat cycle. The orbit is slightly to the east of Landsat-7 passing over the same ground-track one minute later. EO-1 joins a 'morning constellation' of earth observing satellites, including SAC-C and Terra, all examining electromagnetic radiation along the same ground track with different swath widths and with a range of spatial and spectral resolution.

The three primary instruments on board are Hyperion, ALI (Advanced Land Imager is a prototype for a Landsat-7 replacement instrument with ten spectral bands and a spatial resolution of 30m for the multispectral bands and 10m for the panchromatic band) and Leisa-AC (Linear Etalon Imaging Spectrometer Array – Atmospheric Corrector). (Table 3.8).

Parameters	ALI	Hyperion
Spectral Range	0.4-2.4 μm	0.4-2.4 μm
Spatial Resolution	30 m	30 m
Swath Width	36 Km	7.6 Km
Spectral Resolution	Variable	10 nm
Spectral Coverage	Discrete	Continuous
Pan Band Resolution	10 m	N/A
Total N° of Bands	10	220

Table 3.8 Hyperion main sensor parameters.
Tabella 3.8 Principali parametri del sensore Hyperion.

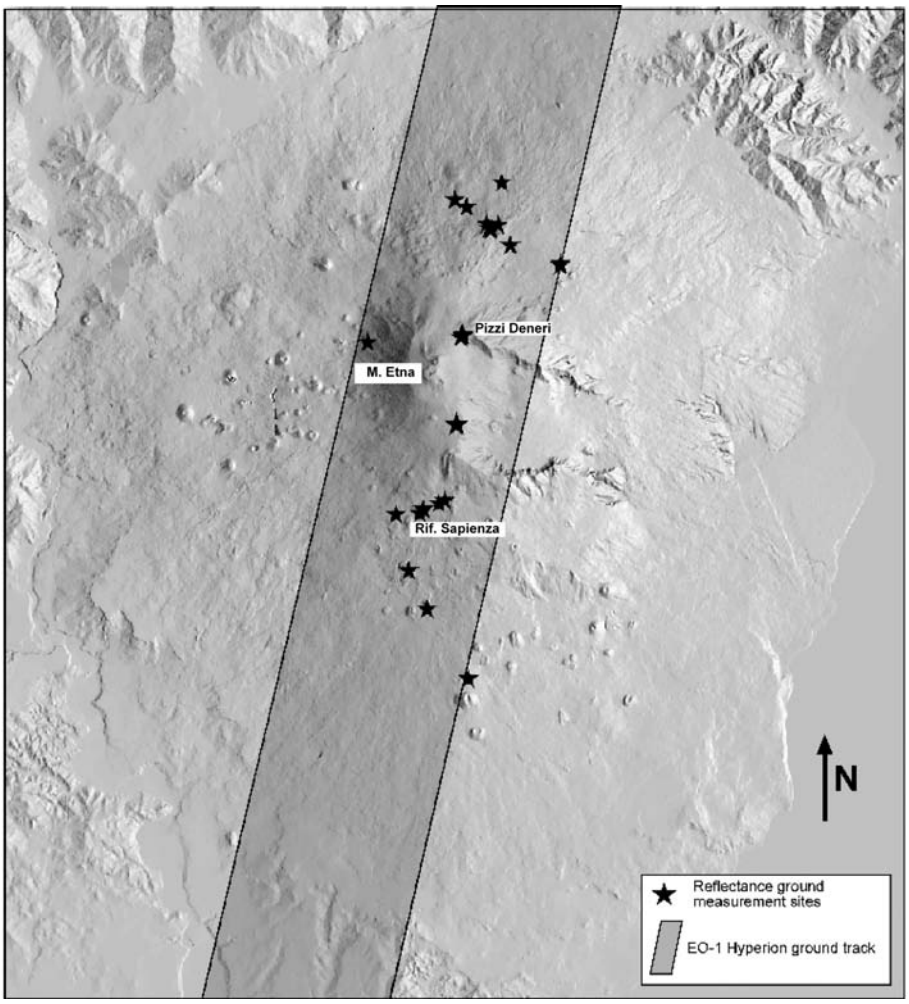

Figure 3.5 During the ground based measurements campaign Hyperion data has been requested to be acquired over Mt. Etna in collaboration between INGV, USGS and NASA: the figure shows the acquired footprint of the Hyperion sensor.
Figura 3.5 La figura mostra la strisciata acquisita con il sensore Hyperion.

The Hyperion Imaging Spectrometer is the first civilian high spatial resolution imaging spectrometer to orbit the earth. It collects 220 unique spectral channels ranging from 0.357 to 2.576 mm with a 10-nm bandwidth. The instrument operates in a pushbroom fashion, with a spatial resolution of 30 m for all bands. The standard scene width is 7.7 km. Standard scene length is 42 km, with an optional increased scene length of 185 km.

In the period 17-26 July Hyperion acquired data the 19th in the nadir view and the 26th with an inclination angle of about 8 degrees. In Table 38 sensors characteristics are reported.

3.6 AVHRR

Images from Advanced Very High resolution Radiometer (AVHRR/3) on board NOAA (U.S. National Oceanic and Atmospheric Administration) satellites have been directly received, calibrated and geo-referenced, at the IMAA HRPT receiving station during the whole period of the measurement campaign. AVHRR/3 is a scanning radiometer which thanks to two contemporary orbiting NOAA satellites, operating in parallel, guarantees at least four site revisitations per day (around synoptic hours). This high repetition rate, together with its 1.1km spatial resolution and spectral capabilities (six channels from the visible to the thermal infrared) make this sensor particularly useful (and widely used) for monitoring volcanic activity (Table 3.9).

The instrument has an instantaneous field-of-view of 1.3 milliradians providing a nominal spatial resolution of 1.1km (0.59 miles) at nadir. A continuously rotating elliptical scan mirror provides the cross-track scan, scanning

Oribital Characteristics	Satellite: NOAA-K, L, M Altitude: 833 km (450 nmi) Nodes: 3:30PM Ascending (NOAA), 8:30AM Descending (METOP)	
Optical Aperture	20.3 cm (8.0 inches)	
Method of Scan	Continuously rotating (360 rpm) scan mirror for cross-track line scanning	
Line Scan Accuracy	325 microradians line to line 98% of the time; 1300 microradians over 20 minute scan 98% of the time	
Spatial Resolution	1300 microradians (All channels)	
Channel Registration	Better than 100 microradians	
Sensitivity	CH1 and CH2: 9-1 S/N for 0.5% albedo CH3A: 20-1 S/N for 0.5% albedo CH3B, CH4 and CH5: <0.12K at 300K	
Design Life	3 to 5 years	
Size	11.5 x 14.4 x 31.3 inches	
Weight	72 pounds	
Power	28.5 Watts	
Spectral Band Specifications		
Channel Number	Wavelength	Detector Type
1	0.58 to 0.68	Silicon
2	0.725 to 1.00	Silicon
3A	1.58 to 1.64	In-Ga-As
3B	3.55 to 3.93	In-Sb
4	10.3 to 11.3	Hg-Cd-Te
5	11.5 to 12.5	Hg-Cd-Te

Table 3.9 AVHRR/3 design and spectral band specifications.
Tabella 3.9 Caratteristiche dei rivelatori alle diverse bande spettrali di AVHRR/ 3.

the Earth from +/- 55.4 degrees from nadir. The mirror scans at six revolutions per second to provide continuous coverage. A sixth channel has recently been added, designated 3A, at 1.6 microns for improved snow, ice and cloud discrimination. Channel 3A is time shared with the previous 3.7 micron channel, now designated 3B, to provide 5 channels of continuous data.

4. Ground campaign organization

In order to collect all the data necessary to validate and calibrate the remote sensed data a field survey, simultaneous with the DLR flyght plane (Table 2.5), was planned. Particular attention was devoted to the areas below the flyght lines overpassing the Etna volcano (Figure 41).

Originally, the field measurements campaign, made in July 2003, should have included Mount Etna, Vulcano Island and Campi Flegrei; even if all these three test sites were important a particular attention was given on Mt Etna, on which satellite acquisition was programmed. They summarize the various measurements acquired during the campaign that were performed on the Etna volcano. Figure 4.2 shows the synthetic representation of these measurements.

The following list summarize the scientific tools within the related applications:

- Atmospheric vertical profiles by means of meteorological radiosondes:
  Use: modeling of the atmospheric radiative contributes; modeling of the 3D distribution of the volcanic plume; SO_2 flux estimation;
- Surface spectral reflectance with a V-NIR and FTIR spectroradiometers:
  Use: characterization of the calibration sites for atmospheric modeling; ground truth for surface reflectance retrieval; spectral library for lithological interpretation;
- Ground surface temperature with an infrared

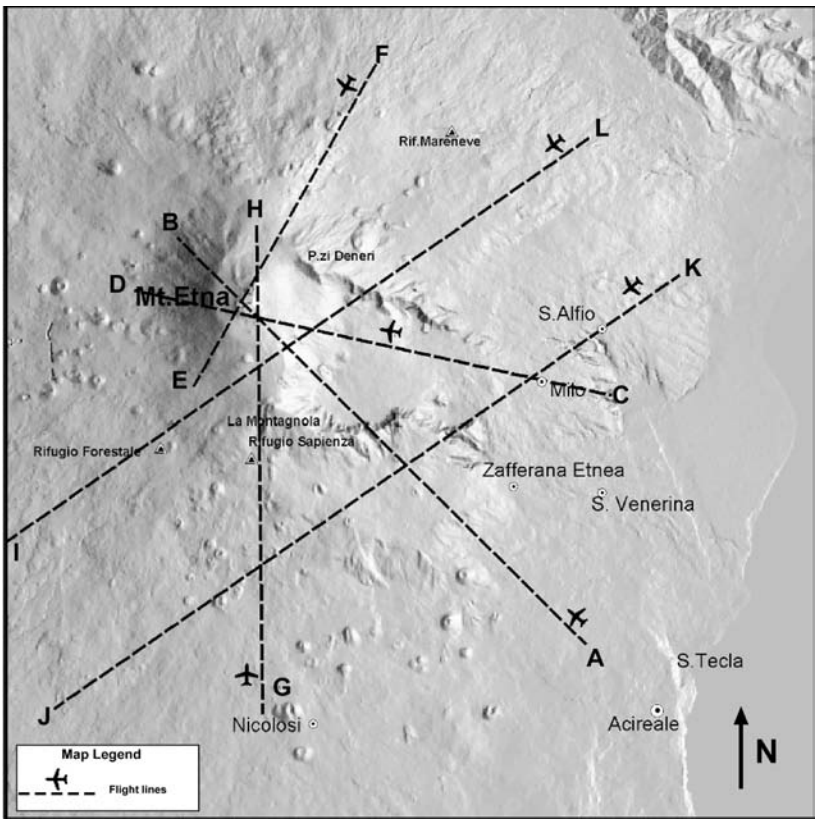

Figure 4.1 Flyght lines overpassing the Etna volcano.
Figura 4.1 Traiettorie di volo sul Monte Etna.

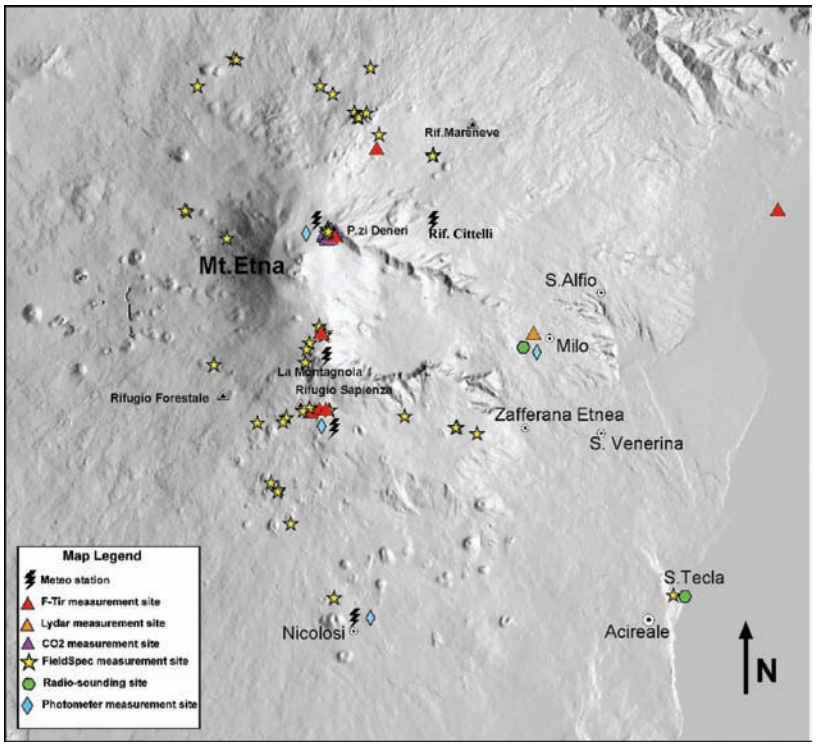

Figure 4.2 Mt. Etna: synthetic representation of all measurements performed on the Etna volcano.
Figura 4.2 Monte Etna: distribuzione dei siti di misura.

thermometer and thermocouples:
Use: characterization of the calibration sites for atmospheric modeling; ground truth for surface temperature retrieval;
- Measurements of the volcanic plume gases (relative) by ground based FTIR:
  Use: comparison with the estimates calculated with the MIVIS data;
- Meteorological measurements at the ground with a meteorological station:
  Use: modeling of the atmospheric parameters at the ground level; modeling of the distribution of the volcanic plume;
- Photometric measurements with a sun-photometer:
  Use: modeling of the atmospheric optical characteristics;
- Estimates of SO_2 concentration by a correlation spectrometer (COSPEC);
  Use: "ground truth" for the evaluation of the SO_2 content of the plume.
- Rock sampling for laboratory analyses:
  Use: ground truth for surface reflectance and emissivity retrieval; spectral libraries for lithological mapping.

4.1 Surface characteristics

4.1.1 Description of Mt Etna test site

4.1.1.1 Geology of the measurement sites

This section briefly describes the geological characteristics of the sites where the measurements were made. This is of particular relevance in the case of fieldspec radiance measurements, for which a number of sites with different characteristics were chosen, which are believed to represent the great variety of recent volcanic surfaces that is encountered at Mt. Etna.

Generally there are two types of volcanic surface: lava flows and pyroclastic deposits. The earlier differ greatly in their surface characteristics, including their surface morphology (‘a‘a and pāhoehoe) and vegetation cover, which in turn depends on (a) the age and (b) the location (elevation and exposure). Most lavas furthermore bear, to a certain degree, a pyroclastic cover that results from recent explosive volcanism at the summit craters (1990-2000) and from flank eruptive centers (2001 and 2002-2003). In order to obtain a record as representative as possible, sites were chosen on lavas on different flanks and of different age, and with pyroclastic covers that show different characteristics. The pyroclastic deposits were measured both at proximal and distal sites. They consist of lapilli-sized fragments in the earlier whereas ash is predominant at distal sites, as far as the eruptions of 2001 and 2002-2003 are concerned. Lapilli-sized scoriaceous fragments produced by short-lived paroxysmal episodes at the summit craters are abundant even at more than 10 km from their source and in many locations are mixed with the finer-grained pyroclastics of the 2001 and 2002-2003 flank eruptions. It is notable that re-working tends to affect much of these deposits within very short time after their emplacement and thus their characteristics at the time of the measurements differ strongly from those to be encountered immediately after deposition, especially in the more distal locations.

4.1.1.2 Lava flows

The by far most abundant type of lava surfaces at Etna is ‘a‘a, with pāhoehoe representing less than 10% of the exposed lava surfaces on the entire volcano. ‘A‘a lava is mostly of the blocky variety, with blocks ranging in size from a few centimeters to more than one meter. Flows (type A ‘a‘a) emplaced rapidly (a few hours to 1-2 days), at high effusion rates, are usually relatively thin (≤2 m) and have flat surfaces with poorly developed flow channels and levees, and show less variation in the block size spectrum than flows whose emplacement occurred over longer time spans (>2 days) (type B ‘a‘a). These latter are also characterized by well-developed levees and often have conspicuous flow channels whose floor may lie up to 10 m or more below the lateral levees. Among the measured flows, the 1981 lava on the NNW flank was emplaced in very short time, whereas the 2002 lava near Piano Provenzana (NE flank), emplaced over a period of about one week, belongs to the most chaotic lava fields to be seen at Etna. Bulbuous pāhoehoe, more rarely also ropy pāhoehoe, occurs within some predominantly ‘a‘a flow fields in coincidence with ephemeral (tube-fed) vents and is particularly frequent in the 1983 flow field on the southern flank, especially in its central portion. Some lava flows, such as that of 2002 near Piano Provenzana, contain considerable quantities of welded scoriae that were deposited near the source vents and entrained with the flowing lava.

There are several lava fields on Mount Etna that are largely pāhoehoe. In nearly all cases these are quite voluminous, including the 1614-1624 lava flow field, which was produced by the most voluminous historical flank eruption of the volcano (1-2 km^3). About 90% of the pāhoehoe shows ropy surfaces, with bulbuous and slabby surfaces being much less common.

The development of vegetation on Etnean lava fields does by no means proceed in a homogeneous manner from site to site, but depends strongly on the surface characteristics, exposure, altitude and location of the respective site. From one area to the other there are strong differences even with similar flow surfaces and at the same altitude, because of the extreme microclimatic variations even at short distances. Generally the progess of plant colonization on pāhoehoe is seen to take much longer than on ʻaʻa and is mostly due to the more compact nature of this lava type, which offers much less possibility for higher plants to take root. Lichens appear on both pāhoehoe and ʻaʻa within about a decade after emplacement. Grasses and shrubs are more abundant in depressed areas, where their growth is often facilitated by the presence of pyroclastics.

4.1.1.3 Pyroclastic deposits

Contrary to the widespread notion of Mount Etna as a non-explosive volcano, pyroclastic deposits abound in many areas of the volcano and are not only restricted to near-vent facies (pyroclastic cones), but also occur even on many recent to sub-recent lava flows. A high percentage of these deposits is of fairly recent origin, coinciding with the much intensified summit eruptions since the mid-1990s and the strongly explosive flank eruptions of 2001 and 2002-2003. Although similarly explosive eruptions have also occurred in the past, Etna's eruptions throughout the 20th century have been remarkably non-explosive except for a number of paroxysmal eruptive episodes at the summit that became more numerous towards the end of the century. Distal pyroclastic deposits are rapidly reworked and are prone to disappear quite fast from lava flow surfaces, so that the current situation may be unusual unless explosive volcanism continues at a similar rate as in recent years.

Currently, three types of pyroclastic deposits can be encountered at Etna. One, the most abundant and long-lived, occurs close to eruptive vents where pyroclastic cones or spatter ramparts are built. In the case of relatively mildly explosive activity, these deposists consist largely of bombs and spatter which show varying degrees of welding, and although the constructs are relatively small (from a few to a few tens of meters in height), they are most resistent to erosion and reworking. The second is produced by more explosive activity and constitutes larger cones (up to more than 100 m in height) but individual fragments are generally smaller (lapilli with varying quantities of loose bombs) due to a higher degree of fragmentation. Where such cones are particularly exposed (such as those of 2001 and 2002-2003 on the upper southern flank), the finer-grained fraction is rapidly eroded, particularly by the near-constant and often gale-force wind. Significant degradation was observed at the cones of the latest eruptions very shortly after their formation and continues at an impressive rate. Runoff during heavy rainfalls is accentuated in areas where fumarolic activity leads to a local cementation of the pyroclastics and is capable of undermining the flanks and crater rims on these cones.

The third type of pyroclastic deposit varies from a relatively proximal to a distal facies and consists of continuous to discontinuous sheets mantling the pre-existing topograpy away from the cones themselves. It can be distinguished in two sub-types, of which one consists of lapilli-sized, highly inflated scoriae that are the products of extremely violent, short-lived episodes of lava fountaining at the summit craters. Deposits of this type are discontinuous except close (about 1 km) to the source and contain centimeter-sized clasts even at up to 10 km distance when freshly fallen; these fragments commonly break into smaller pieces during the many heavy rainfalls that occur at Etna. Nearly all of the presently occurring deposits from lava fountains were produced in 2000, when the Southeast Crater produced 66 paroxysmal eruptive episodes.

In contrast, explosive volcanism during the flank eruptions of 2001 and 2002-2003 has produced deposits that maintain continuity far beyond the proximal areas. Closer to their source vents (but far beyond the pyroclastic cones themselves) they may be many tens of meters thick and reached thicknesses of dozens of centimeters even up to 5 km downwind from the vents. A characteristic decrease in the median diameter of the clasts is observed at increasing distance from the source, from lapilli-sized fragments within about 2 km from the vents to coarse ash farther away. On the downwind side such deposits were continuous at the time of deposition but much of the tephra was rapidly remobilized by rainfalls and removed from exposed sites whereas accumulation occurred in protected, depressed areas.

4.1.2 Sites measured during the June and July 2003 field campaigns

Measurements were concentrated mainly in two broad areas, on the southern and northern flanks of Mount Etna (Figure 4.3). Details of the geology and lithology of the sites are provided

in the following; the geographical coordinates of the sites are presented in Table 4.1.

n°	Lat N	Lon E	Description
1	37.76	14,96	(GPS coordinates are somewhat erroneous). W flank, about 1800 m elevation. 1843 lava flow immediately SE of M. Nunziata (cone formed during 1832 eruption), with blocky surface (type B 'a'a lava) and covered with abundant lapilli-sized scoriae produced by a lava fountain at the Southeast Crater on 5 January 1990. Minor amounts of 2002-2003 ash are also present. The 1843 lava flow was emitted from an impressive eruptive fracture ("bocche di fuoco del 1943"), higher upslope. The distal portion of the lava flow, ear the town of Bronte, was the site of the worst eruption-related disaster (in terms of human deaths) in the recorded history of Etna: the instantaneous evaporation of water in a cistern covered by the lava caused an explosion that killed about 60 people watching the advance of the lava flow.
2	37.78	14,94	(GPS coordinates are somewhat erroneous). NW flank, about 1680 m elevation. 1949 lava flow crossing the Forest Guard Road (strada forestale) about 2 km NW of M. Scavo. Type A 'a'a lava, covered with lichens; fresh cuts of the lava show dark grey to black color of the rock. Minor amounts of 2002-2003 ash in depressions. The 1949 eruption lasted only a few days but occurred simultaneously on the S and NW flanks, being the latest pre-2001 "bi-radial" eruption at Etna, and the first since 1879.
3	37.77	14,94	(GPS coordinates are somewhat erroneous). NW flank, about 1680 m elevation. 1949 lava flow crossing the Forest Guard Road (strada forestale) about 2 km NW of M. Scavo. See Point 23 for more detail.
4	37.80	15.01	NE flank, about 2350 m elevation. Uppermost portion of the eruptive fissure of 27 October 2002. Mostly lithic blocks scattered over older pyroclastic deposits and lavas, with very minor fresh scoriae which become more and more abundant downslope along the eruptive fissure.
5	37.80	15.06	NE flank, about 1600 m elevation. October-November 2002 lava flow at the junction of the "Mareneve" Provincial Road and the road to Piano Provenzana, substituted by a provisional jeep track. Extremely chaotic type B 'a'a lava, with blocks that reach even several meters in diameter. Colour of the lava varies from black to reddish and brown, due to the presence of oxidized welded scoriae that were entrained with the flow. Light cover of ash produced by the S flank vents of the same eruption after emplacement of the lava. The activity on the Northeast Rift during the 2002-2003 eruption lasted only 9 days, and most of the lava was emitted during the first three days of activity. The source vents lie at about 1850 m, only a few hundred meters away from the tourist facilities of Piano Provenzana, which was completely devastated by earthquakes and ground fracturing (caused by the slippage of the eastern flank of Mount Etna), which accompanied the eruption onset, before the place was inundated by lava.

6	37.82	15.01	(GPS coordinates are somewhat erroneous). N flank, about 1720 m elevation. Central portion of the 1614-1624 lava field in the Passo Dammusi-Grotta dei Lamponi area. Lava surface is nearly exclusively pāhoehoe with different morphologies, mostly ropy. The lava contains abundant plagioclase phenocrysts ("cicirara"), sometimes with diameters of up to 1 cm, which give a "grainy" aspect to the lava, which generally has a reddish-brown colour. This lava field shows a variety of peculiar features, such as terraces (confined rootless lava lakes), tumuli and lava flow channels often associated with drained lava tubes of highly variable dimensions. Lichens, herbaceous plants and a few bushes (ginestra aetnensis) are present locally. Black ash of the 2002-2003 eruption occurs in depressed areas. The 1614-1624 lava field is the product of the most voluminous historical flank eruption of Etna (1-2 km^3).
7	37.82	15.01	Lava of 1947.
8	37.81	15.02	NNE flank, about 1930 m elevation. Eruptive events and lavas of the 1643 eruption on E side of M. Timparossa and about 0.5 km W of M. Nero. Predominantly pāhoehoe surface, which also contains tree moulds ("pietracannoni"). Like all 17th century eruptive products, these lavas are "cicirara", with abundant plagioclase phenocrysts. Lichens and grasses are locally present. The 1643 eruption was the smallest of the 17th century and produced a series of very minor lava flows, but three years later another, much larger eruption in the same area produced the large pyroclastic cone of M. Nero and emitted a lava flow down to the Alcantara river. NNE flank, about 1950 m elevation. Uppermost portion of the main lava flow of the 1879 eruption, immediately below source vent(s). Type A 'a'a lava, with well-developed flow channel extending from source vent, and extensive presence of lichens. Light cover of 2002-2003 ash and scattered presence of scoriaceous lapilli produced during an early June 2000 lava fountain at the Southeast Crater. The 1879 eruption was characterized by a high degree of explosivity, which formed two huge craters on the flank of the prehistoric M. Pizzillo cone. The same eruption also produced a small lava flow on the SSW flank of Etna.
9	37.81	15.02	
10	37.81	15.03	NNE flank, about 1950 m elevation. 1923 lava flow at W base of M. Nero, with a conspicuous W-facing lateral levee consisting of sub-vertical slabs of relatively smooth lava (compared to the surrounding type A 'a'a surface). Source vent (a small, horseshoe-shaped pyroclastic cone about 10 tall) of this lava lies only about 200 m upslope. Light cover of 2002-2003 ash and scattered presence of scoriaceous lapilli produced during an early June 2000 lava fountain at the Southeast Crater. The 1923 eruption was similar to that of 1981 for its short duration and the rapid emission of a long (8 km) lava flow that reached the W margin of Linguaglossa.
11	37.81	15.03	NNE flank, about 1900 m elevation. Proximal portion of the 1646-1647 lava flow (M. Nero eruption) at the NW base of the source cone, composed of huge blocks of cicirara lava (type B 'a'a). Light cover of 2002-2003 ash and scattered presence of scoriaceous lapilli produced during an early June 2000 lava fountain at the Southeast Crater. The 1646-1647 lava issued to the N of M. Nero, breaching the cone and entraining portions of the crater rim to form two peculiar barriers on both sides of the lava flow. A minor lava flow issued in 1923 from the lower N slope of M. Nero.
12	37.83	15.03	NNE flank, about 1400 m elevation. 10 m-high W margin of a lava flow, possibly 1923 or 1879, type B 'a'a with numerous blocks and covered with lichens.
13	37.70	14,99	Lava 1983 and tephra.

n°	Lat N	Lon E	Description
14	37.70	14,99	S flank, about 1850 m elevation. March-August 1983 lava flow immediately SW of the Rifugio Sapienza tourist station. Type B 'a'a lava with occasional patches of bulbuous pāhoehoe at about 2 km distance from source vents (located at about 2500 m elevation), with ash of the 2002-2003 eruption. For background information on this eruption see Points 18 and 19.
15	37.70	14,97	SSW flank, about 1770 m elevation. 1780 lava flow at Piano Vetore (about 0.5 km NW of Monte Vetore). Type A 'a'a lava, relatively thin (not much more than 1 m), with individual blocks rarely exceeding 10 cm in diameter. Covered extensively with lichens, and partly reworked ash of the 2001 and 2002-2003 eruptions mixed with occasional scoriaceous lapilli of the 2000 lava fountains. Source vent lies less than 1 km to the north.
16	37.67	14,98	S flank, about 1350 m elevation. 1910 lava flow at N base of M. Sona, type A 'a'a with blocks no more than 0.5 m in diameter, and extensively covered with lichens, and ash of the 2002-2003 eruption. The 1910 eruption occurred from an impressive series of vents ("bottoniera") on the W flank of the Montagnola, in an area later used for the construction of ski lifts, ski tracks, and the Etna Cable-car. The area was repeatedly affected by lava flows (1971, 1983, 1985, 2001 and 2002-2003.
17	37.65	14,99	S flank, about 1100 m elevation. Distal portion of the main July-August 2001 lava flow (emitted from vents at 2100 m elevation), at the SE base of the lowermost cone of the Monti Ardicazzi., forming an impressive wall of lava up to 15 m high. This consists of a chaos of blocks (type B 'a'a) that range in size from a few centimeters to several meters. Actually the wall has several lobes with depressed zones between them, where there are a few remainders of burned trees. This entire lava flow (plus those emitted from eruptive vents at 2570 m) is characterized by the presence of abundant sedimentary inclusions (quartzarenites) of white to beige colour, and is rich in pyroxene (augite) phenocrysts up to 2 cm long, while there are also minor quantities of amphibole (kaersutite) that sometimes has lengths of more than 10 cm.
18	37.62	15.01	S flank, about 900 m elevation. 1886 lava flow about 1.5 km N of Monti Rossi (pyroclastic cone formed during the 1669 eruption). Type B 'a'a, vegetation more developed than on 1910 lava flow (point 57); ubiquitous presence of 2002-2003 ash. The 1886 lava flow was emitted much higher upslope, at M. Gemmellaro, and reached the NE base of the Monti Rossi, stopping extremely close to Nicolosi.

Table 4.1 Geographical coordinates of measuring Etna site discussed in the tex
Tabella 4.1 Coordinate geografiche dei siti di misura sul Monte Etna.

4.2 Surface reflectance spectroscopy

Purpose of the field activity was to collect data for the analysis of surface material composition. Reflectance measurements and sampling were performed on selected rock units, encompassing the compositional variability of the volcanic complex, and including lava flows of different geologic ages and from different effusive craters and fractures, and pyroclastic deposits on different Mount Etna sides.

4.2.1 FieldSpec reflectance spectroscopy for composition analysis and photometric evaluation

A FieldSpec Pro portable radiometer was used. Reflectance measurements were generally made from hights of 70 cm, and in some cases from 20-30 cm for individual detail detection. Two or more acquisitions were generally made at each target or station. Site location was determined by GPS. In several sites the measurements were made with different backward and forward observation angles in the sun-target-sensor plane (principal plane) (Figure 4.4), and

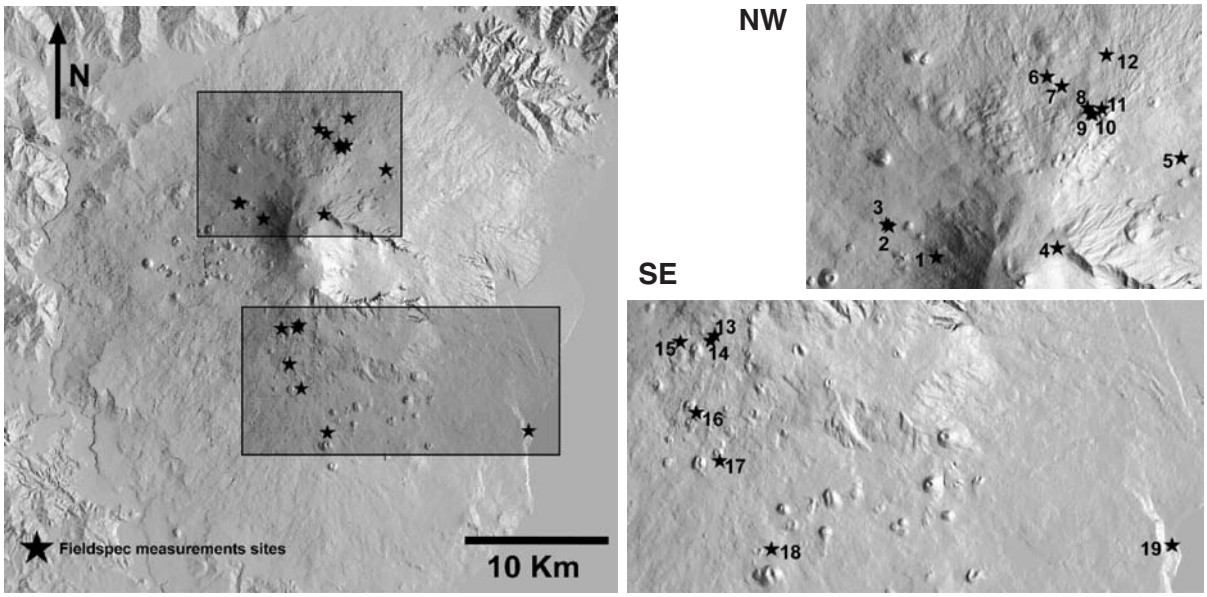

Figure 4.3 Mt. Etna: topographic position of the points described on Table 5.1.
Figura 4.3 Monte Etna: posizione topografica dei punti descritti a Tabella 5.1.

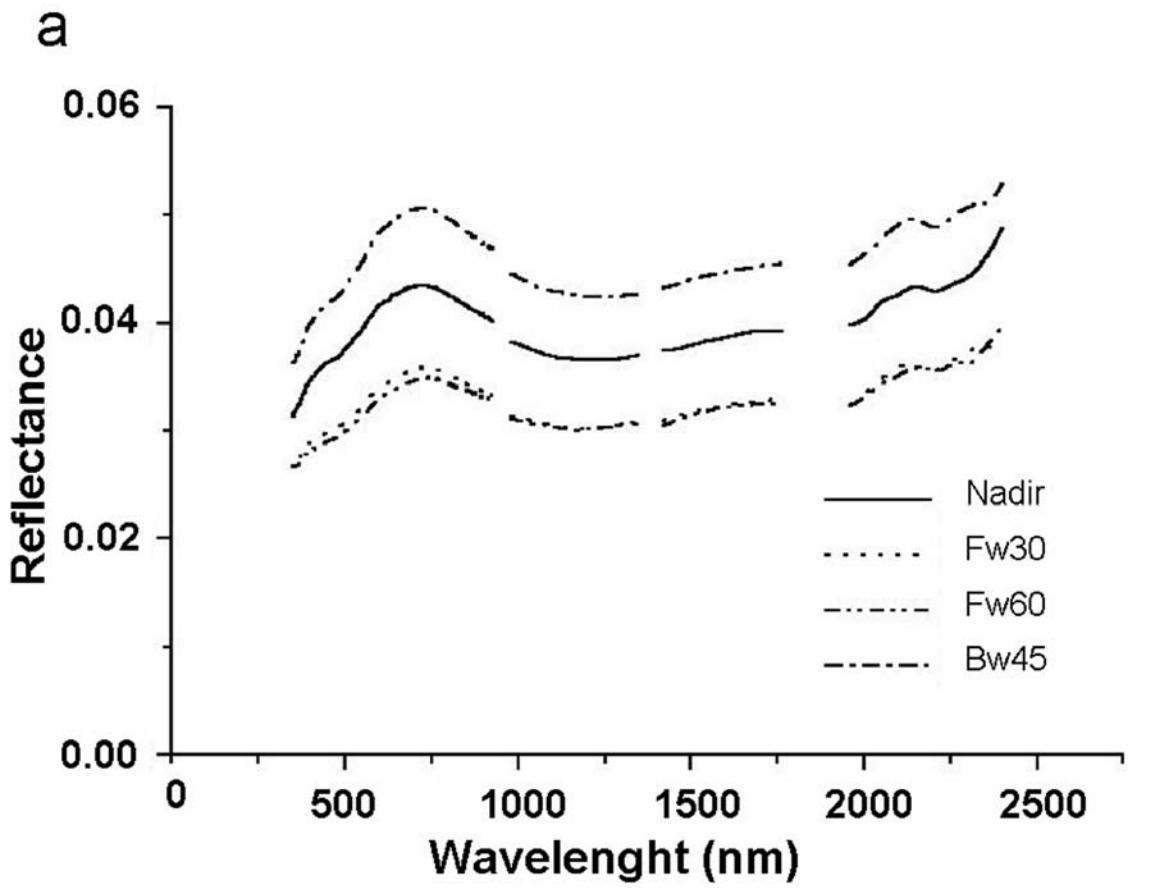

Figure 4.4 Reflectance of Pian delle Concazze surface, measured with different viewing angles in the principal plane.
Figura 4.4 Riflettanza della superficie di Pian delle Concazze, misurata a diversi angoli di vista nel piano principale.

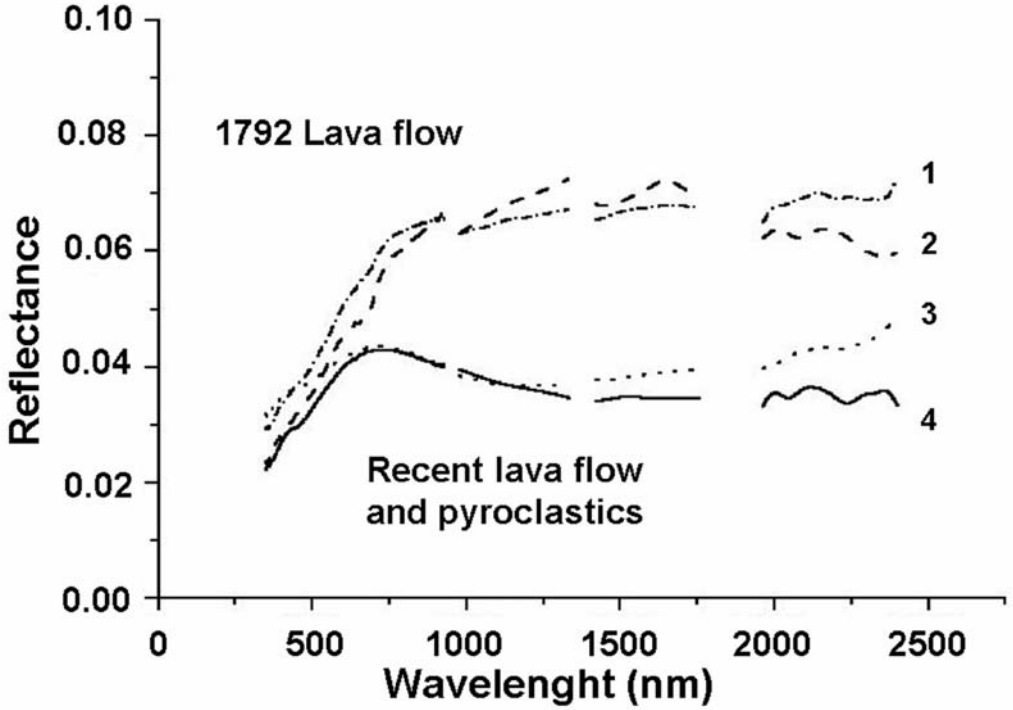

Figure 4.5 Spectra of pyroclastics and lava flows surfaces with different albedo and roughness. (1, 2): 1792 lava with centimetric (1) and decimetric (2) surface roughness; (3): Pian delle Concazze fine texture pyroclastics; (4): 2002 coarse texture lava flow surface.
Figura 4.5 Spettro delle superfici di piroclastiti e colate laviche avento diversi albedo e rugosità.

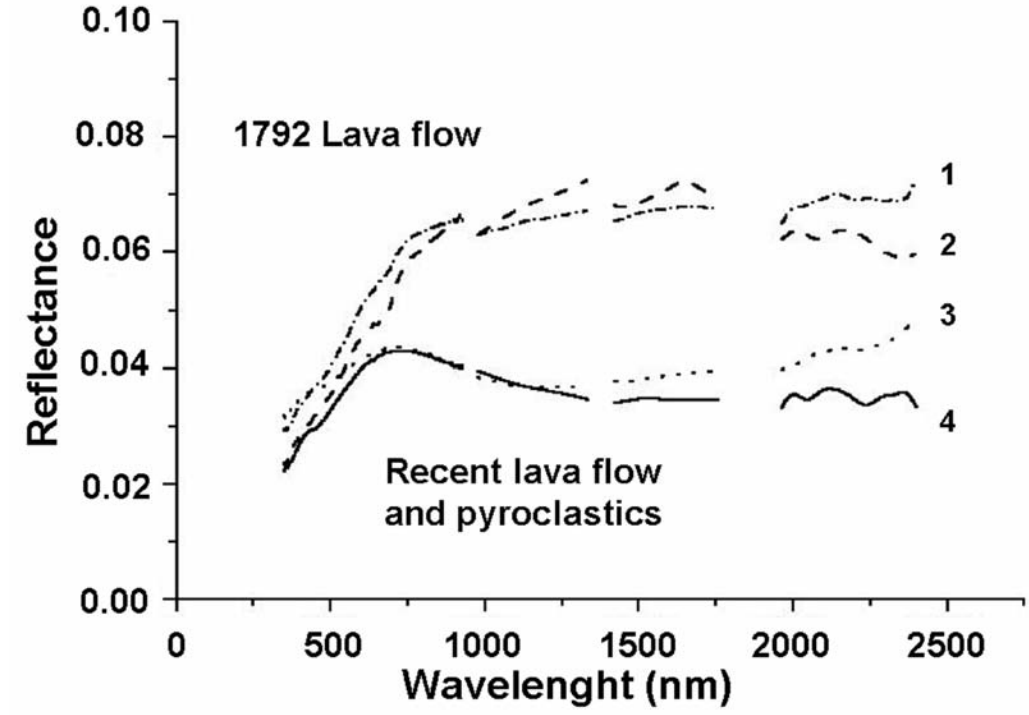

Figure 4.6 Spectra of two distinct areas of the 2002 lava flow, on the NE side of Mount Etna. The proximal area spectrum shows the effects of intense precocious oxidation.
Figura 4.6 Spettro di due distinte aree della lava del 2002, relativa al versante di nordovest del Monte Etna.

in the plane normal to the principal plane (normal plane), using a high precision sighting compass with clinometer for plane orientation and angle determination.

Sun elevation and azimuth were derived from local time.

The geologic units, object of FieldSpec measurements, include:

- historical lava flow (1792) along the S92 road
- recent (2001) lava flow on the southern side of Mount Etna, near Rifugio Sapienza
- recent (2002-2003) lava flow on the NE side of Mount Etna, at the interruption of the Milo-Linguaglossa road
- pyroclastic deposits, forming the Pian delle Concazze surface.

Lava unit surfaces mainly consist of ash and scoriae. Different lava units can be differentiated from one to another on the basis of relative abundance of the two endmembers, scoriae size, scoriae alteration and weathering level, liken coating and vegetal cover extension. These characteristics contribute to determine the surface texture on various scales, the radiometric effect of which is superimposed on the spectral charcteristics related to lava composition and alteration (Figure 45, Figure 46).

4.2.2 Description of units, sites and measurement setting

1792 lava flow

Site: km 32 of the S92 road, Mount Etna SE side, surface inclination below 10°

The surface consists of black ash and scattered centimetric size scoriae and decimetric scoriae intensively wathered. Liken coating are often present, and large areas are covered by bushes.

The targets selected for the measurements include: scoriae with liken coating, areas of mixed ash and centimetric scoriae, areas with decimetric scoriae concentration and scarse ash, and bushes, for a total of seven targets, with both nadir and inclined observation geometry.

2001 lava flow

Site: west of Monti Silvestri, Mount Etna South side, surface inclination lower than 10°.

The surface consists of black ash and variously altered scoriae, resulting, macroscopically, in colors varying from black to brown to reddish. The scoriae size also varies from a few centimeters to decimetric and metric.

Reflectance acquisitions were relative to surfaces with mixed ash and centimetric and, respectively, decimetric scoriae concentration. Close range measurements from 25 cm were made on very oxidized scoriae and on a xenolyth inclosed in a scoria. A total of five acquisition stations, with both nadir and inclined observation geometry was accomplished.

2002-2003 lava flow

Site: Rifugio Sapienza, Mount Etna South side, average surface inclination lower that 10°.

The surface is made up of prevalently decimetric up to metric scoriae, with limited ash spots. Lava and scoriae are only slightly altered. Measurements, both nadir and inclined, were made at only one station, relative to mixed scoriae and ash.

Site: Linguaglossa road interruption, on the NE side of Mount Etna, surface inclination below 10°.

Surface composition is similar to the previous one, with very coarse scoriae piled and randomly distributed. Five measurement stations were made on the coarse block surface, with different observation geometry, including panoramic views (zenith angle 80°)

Site: Piano Provenzana, Mount Etna NE side, surface with average inclination lower that 10°.

Surface consisting of piled bloks of scoriae, similar to the two previously described, but intensively oxidized. On this surface, four measurement stations were made, with different observation geometry, including two panoramic views.

4.2.3 Pyroclastic deposits

Site: Piano delle Concazze, Mount Etna NE side, horizontal surface.

Surface made up of black ash and small (centimetric) scoriae, equally sized, densely and uniformly distributed. Three measurement stations were made, with different viewing angles, including panoramic views. A fourth station consisted of a set of measurements along the diagonals of a square of about ten meters side, simulating the pixel of a satellite sensor. These measurements were made only from nadir.

Vertical section, exposing alternating snow and permafrost (sporadic mountain permafrost) strata, topped by the ash forming the Pian delle Concazze surface. Reflectance values of the top wet ash, an individual snow stratum, alternating snow and permafrost, and dry ash were measured. The reflectance of

mineral sublimate was also measured in the section proximity.

4.2.4 FieldSpec measurements for photometric evaluation

Surface roughness effects on relfectance of low albedo rocks and soils were evaluated considering surfaces with different roughness characteristics, and setting measurements with different viewing geometry. Of particular interest is the fact that very rough surfaces are made up of piled blocks, with very steep and often overhanging facets, creating cavities. The lava flows and pyroclastics selected for these experiments include units with different albedo, although still within the range of low albedo values.

Surfaces with centimetric and respectively decimetric scoriae of the relatively high albedo 1792 lava flow were selected, as well as the very rough surface of the 2001 and 2002 lava flows on the Southern and NE Etna sides and the relatively smooth surface of Piano delle Concazze, both characterized by very low albedo.

Observation geometry effects were evaluated on both "very rough" and "smooth" surfaces of the same geologic units indicated above, considering zenith angles of 30°, 45°, 60° in the principal plane, in the forward and backward directions with respect to the sun,. In the normal plane, observation angles of 30°, 45°, 60° were adopted in each quadrant at –90° and +90° in respect to the sun.

4.2.5 Lava and pyroclastics sampling and analysis

Forty six samples of lavas and pyroclastics were collected in the geologic units listed below. The attribution to the various units is based on the 1983 geologic map, and will be updated after discussion with Marco Neri and Boris Behncke.

The units include: 1792 lava flow, S92 road on the Mount Etna S side; 1766-1892 lava flow, S92 road on the S side; 2001 lava flow, Monti Silvestri, S side; 2002 lava flow, Rifugio Sapienza, S side; 1910 lava flow, near Rifugio Sapienza, S side; a group comprising the 1843, 1949, 1787, 1526-1614 lava flows along Strada Forestale on the W side; 2002 lava flow on the NE side, Elittico lava flow at Osservatorio geofisico, and ash and scoriae at Piano delle Concazze, NE side; sublimate sulfur from Cratere centrale; Trifoglietto lava flow at Pian del lago, S side.

4.2.6 Laboratory measurements: Preliminary laboratory spectroscopy and petrographic analyses

Laboratory reflectance spectroscopy is in progress, using a Perkin Elmer lambda 19 spectrometer, spectral range 350-2500 nm, a Zeiss MC 501, spectral range 220-1050 nm, and a Nicolet FTIR 740, spectral range 400-4000 cm^{-1}. The analyses are made on rock bulk samples in reflectance mode, and on particulate samples in transmittance mode in the Mid Infrared.

Raman spectroscopy has been made on a limited number of samples, to have a preliminary indication about the presence of minerals such as pyroxenes and olivine. Mossbauer spectroscopy will be made for Fe^{2+} and Fe^{3+} content evaluation.

Optical microscopy for petrographyc analysis, XRD and XRF analyses, and electron microprobe analyses are in progress for chemical and mineralogical composition determination.

4.3 Temperatures

4.3.1 Surface brightness temperature measurements: Description of the instruments characteristics and operational procedure

Measurements of temperature have been collected with an infrared thermometer by Everest Interscience(INGV and IMA team) and a ΩOMEGA-HH506R thermocouple (INGV team).

These kind of temperature are relevant for the validation and the calibration of remote sensed data acquired in the IR spectral range. The target have been selected according to homogeneity, sufficient extension and easy reaching criteria. Therefore they are easy recognisable from airborne and satellites. During this campaign has been possible to measure the temperature continuously pointing the same target observed by the F-TIR during the spectral emissivity measurement. These kind of measurement have been acquired by means a software application named *unilogger* able to measure in the same time also a GPS and a Meteo station signal. These kind of acquisition allows to know the details of the fluctuations.

4.3.2 Everest 130,2l

The EVEREST 130,2L is an infrared thermometer in the (8 -14)μm spectral range configured like a gun. An operator points the instrument at the target where he wishes to make a temperature reading. Instantly he can read that temperature measurement on the liquid crystal display, which gives a readout of the temperature of the outdoor target (*by*

Charles E. Everest).

The optical section, or front end of the infrared thermometer, collects a sample of the radiation given out by the turf. The instrument processes this sample through its circuitry and converts the information to a form that triggers the liquid crystal to display (Figure 47).

As no contact needs to be made between the thermometer and the territory to make a precise temperature measurement, the target is not altered. The Everest IR thermometer gives an instantaneous readout with 0.1°C resolution. Temperatures can be taken at a distance (maximum 300m) without any loss of accuracy.

The response time of a thermometer can be slowed down by switching to "Data Averaging" in order to read a temperature average over a period of time. This is especially helpful when wind gusts cause variations over the area being measured.

Operating Instructions

Operating the instrument is quite easy: pressing the middle "E" on the back readout panel turns the instrument on.

The abbreviations "IR" stand for current infrared surface temperature reading of the target that the instrument is focused on. While "A" stands for the Average Temperature Reading of the last five or ten readings taken, depending on the Average Mode being utilized.

The EVEREST 130,2L is equipped with a great number of functions. To access and change a variety of functions we use the keypads INDEX and ENTER (Figure 4.7)

The INDEX key is used to change display modes. The ENTER key is used to finalize functions or exit a mode. Repeatedly pressing the INDEX key will provide access to a variety of standard functions of the infrared thermometer Table 4.2.

The brightness temperatures of different surfaces: tephra, lava flow and asphalt were measured using the IR thermometer Everest 130.2L (serial N. 3558; see Figure 4.7). The technical characteristics are reported in Table 4.3.

This IR thermometer, working with emissivity compensation locked to 0.99, was put under test some days before the campaign. The test was done measuring the temperature of a small volume of water during a slow heating process (range about 30-40 °C). The measurements of the Everest IR thermometer were compared with the measurements done by a precise Negative Temperature Coefficient (NTC-4k). As expected the differences were about 0.2-0.3 °C.

This portable IR thermometer was used to measure the temperature of the surfaces, in the places and in the time intervals reported in Table

Function name	Function action
CHANGE F/C	Used to change from C to F
CHANGE AVE MODE:	Used to change from FAST to SLOW Averaging Mode. SLOW Mode takes the average of the last five seconds (or the last ten readings) while the FAST Mode takes the average of the last 2.5 seconds (or the last five readings)
CHANGE RS-232:	Used to change from ECHO to POLL Mode or vice versa. "ECHO" refers to when the computer is simply outputting all the information being processed by the instrument through the RS-232 port. "POLL" means that the instrument is switched to a duplex mode of operation whereby the computer requests the data it wants.
RESET PEAK	Used to reset the PEAK temperature value to current IR Temperature in Real Time Mode The PEAK Temperature is the highest temperature of a target that the instrument has had in its field of view since initial turn-on or after resetting the Peak Temperature value through the Reset Peak function.
RESET VALLEY:	Used to rest the VALLEY Temperature to the current IR Temperature in Real Time Mode. The VALLEY Temperature is the lowest temperature of a target that the infrared thermometer has had in its field of view since stabilizing after initial turn-on or after resetting the VALLEY Temperature value through the Reset Valley Function.

Table 4.2 EVEREST functions.
Tabella 4.2 Funzioni dell'EVEREST.

Figure 4.7 Everest reading taken on July 17, 2003 at Rifugio Sapienza; hot gases escaping from the 2003 lava flow.
Figura 4.7 Misura EVEREST al Rifugio Sapienza, Luglio 2003.

4.4. The measurements were usually taken normally to the surface and at a distance of about one meter or less then one meter; this means a spot on the surface of less than 7 cm of diameter.

On July 17 the measurements were taken on the 2001 lava flow, the part (first 100-200 m) leaving from the road at Rifugio Sapienza, just after Mt. Silvestri, and goes down toward Nicolosi. The measurements are related to tephra (ash or small fragments of volcanic rock), lava (big and small parts) and sometimes with the instrument looking to parts in the dark or, on the contrary, looking to surfaces practically normal to the incidence radiation. The result is an extremely variable time-increasing trend (see Figure 4.8, Figure 4.9).

Characteristic	value
Scale Range:	-30 °C to 100 °C
Resolution:	0.1 °C
Accuracy:	±0.5 °C
Noise Effective Temperature:	±0.2 °C
Spectral Pass Band:	8<λ<14 (μm)
Field of View:	4 degrees
Response Time:	0.1 s
Emissivity Compensation:	0.2 to 0.99
Operating Distance:	2 cm to 300 m

Table 4.3 130.2L Technical Characteristics.
Tabella 4.3 130.2L caratteristiche tecniche.

The bars correspond to one standard deviation. The mean standard deviation (SD) is reported in the last column (on the right) of Table 4.4.

The readings of July 20 where taken on the asphalt of a big parking area, after the Rifugio Sapienza pass, toward Nicolosi. On this uniform surface the thermal data show a time decreasing trend due to meteorological effects (see Figure 4.8). The bars correspond to one standard deviation. In Table 4.4 the mean value of the standard deviation is reported.

On July 19 the Everest measurements were taken at Pian delle Concazze. Pian delle Concazze is a very large (about 500 m x 500 m) flat area, mainly made of small piece of lava rock (tephra). The surface temperature measurements were performed on the perimeter of a square with a side of about 10 m. It was measured each 5 metres; that is in eight different points on the whole perimeter. In each point five different measurements were done (about toward north, east, south, west and north again). The four sides of the square were measured two consecutive times. The considered square was located in the central part of the plane of Pian delle Concazze. The time step between two consecutive points was about five minutes. The measurements toward north usually show larger values respect the other directions (the sun was mainly from south; i.e. the operator was with the

Place Date	Surface type	Long (deg min)	Lat (deg min)	Alt (m)	Start GMT hh:mm	End GMT hh:mm	Mean SD °C
Rif.Sapienza 17.07.2003	Lava flow	15° 0.219'	37° 41.946'	1895	07:30	09:30	3.9
Pian Concazze 19.07.2003	Tephra	15° 0.85'	37° 45.95'	2793	09:10	11:00	1.9
Rif.Sapienza 20.07.2003	Asphalt	14° 9.417'	37° 41.721'	1831	09:50	10:30	0.9
Pian Concazze 26.07.2003	Tephra	15° 0.81'	37° 45.95'	2793	09:40	10:20	1.6

Table 4.4 Places, surface type and measure time interval.
Tabella 4.4 Luoghi, tipo di superficie e tempi d'intervallo delle misure.

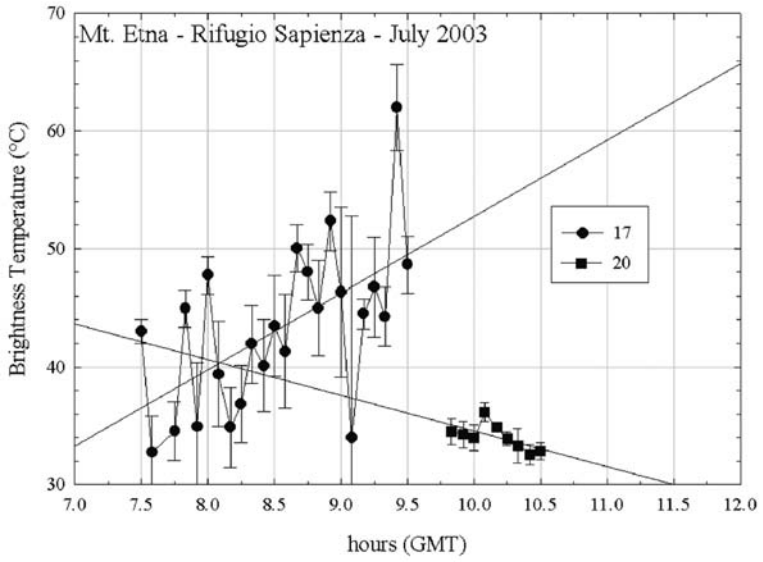

Figure 4.8 Surface brightness temperature.
Figura 4.8 Temperatura di brillanza superficiale.

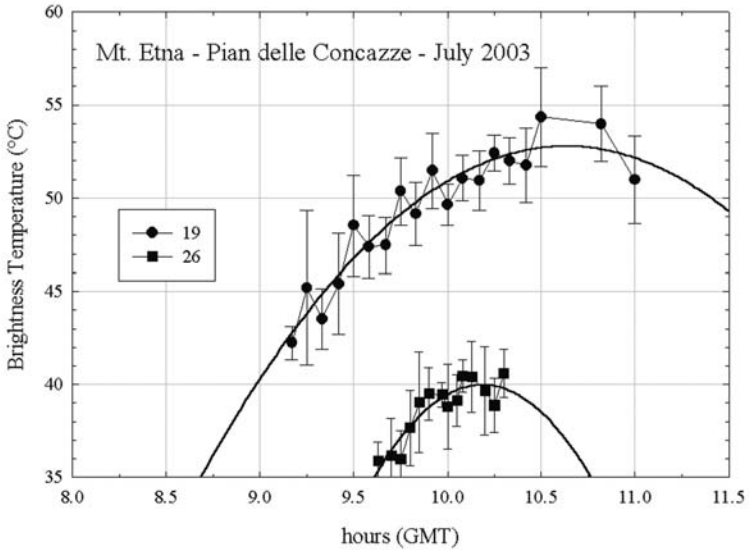

Figure 4.9 Surface brightness temperature.
Figura 4.9 Temperatura di brillanza superficiale.

sun on the back). During the last measurements (at 10:30) the wind was very weak. Some extra measurements (at about 10:50 and 11:00) were added due to the presence of the FASA system flying above the testing area. It was measured also the temperature of the snow; it changes from about –1.4 °C to 24-26 °C measuring clean snow or snow with many centimetres of ash over the snow respectively. Finally, before and after the measurements performed on the surface of Pian delle Concazze, it was measured in different points the temperature of the white domes of the roof of the INGV shelter at Pizzi De Neri (not reported here).

On July 26 (Pian delle Concazze) the Everest data were taken measuring along the diagonals of a square of about 20 m side; also this square is located in the central part of Pian delle Concazze area. In each diagonal were performed measurements in six different points at about 5 m step. The time step between the measurements in two consecutive points is usually less than five minutes. Finally, it was measured in different points the temperature of the white domes of the roof of the INGV shelter at Pizzi De Neri (not reported here).

Figure 4.9 shows the time increasing trend of the surface brightness temperature measured at Pian delle concazze on July 19 and 26. The bars correspond to one standard deviation; they are lower respect to the measurements performed on 17 July on the lava flow. A parabolic regression of the data is also reported. The mean values of the SD are reported in Table 4.4.

4.3.2.1 Description of surface brightness temperature measurements (DIMA-RU)

The temperature measurements have been realized using the IR thermometer Everest 130.2L joined to thermocouple and F-TIR acquisition. The sites of measurements were so coincident for the three instrument and the main information are summarized in one table. The data have been stored in one daily file.XLS containing a description of the measurements, a data sheet and a plot.

The EVEREST measurements were implemented in two different mode:

- O-MODE, by an Operator pointing the instrument at the target and
- C-MODE, by a Continuous acquisition using the RS-232 port of the instrument and saved as ASCII file and synchronize with a GPS. In this mode the instrument is fixed in a position during the whole time of measurement, pointing the same sample simultaneously measured by F-TIR.

C-MODE is particularly interesting because allows to give the exact temperature value in correspondence of measured sample.

The following table reports the details of the acquired data set.(Table 4.5).

Thermocouple ΩOMEGA-HH506R (INGV).

Figure 4.10 Infragold temperature measurements.
Figura 4.10 Misure di temperatura del riferimento *infragold.*

Measurements/day	Time in GMT	lat, long, z meters	Measurement Sites	XX_YYMMDD_YY_0000_ZZ xx: identify
17.07.2003 (Day)	From 9.16 To 11.57	N 37.7 E15.008 N 37.72844 E 15.00857 N 37.72855 E 15.00848	Etna: Pian del Lago. Volcanic scoria and ash	O-MODE pl_170703_et_om.xls
17.07.2003 (Night)	From 0:30 To 0:50	N 37.7 E15.011	Etna: crossway towards Nicolosi. Pavement	O-MODE 170703.xls
19.07.2003	From 11:58 To 13:05	N 37.72851 E 15.00850	Etna: Pian del Lago. Volcanic scoria and ash	C-MODE 19072003out.txt
20.07.2003 (Day)	From 11:25 To 12:50	N 37.7649 E 15.01494	Etna: Pizzo Deneri (Concazze). Volcanic scoria and ash	C-MODE 20072003.txt O-MODE Pd_030720_et_om.xls
22.07.2003 (Day)	From 11:30 To 13:50	N 38.406150 E 14.960891 N 38.40618 E 14.96116 N 384019 E 14.96142 N 38.40618 E 1496150 N 38.40614 E 14.96062 N 38.40614 E 14.96062	Vulcano: pumices and mixed gravels around Volcano edges. Older sulfur deposits Fresh sulfur deposits Weathered volcanic rock Pavement from chopper platform. Reddish Lava rock	O-MODE Vu_070723_et_om.xls C-MODE
23.07.2003 (Nigth)	From 23:55 To 01:15	N 37.69910 E 15.00377 N 37.69928 E 15.00372	Etna: Rifugio Sapienza. Volcanic scoria and ash	O-MODE Pl_030723_et_om.xls
26.07.2003 (Day)	From 10:10 To 12: 10	N 37.72852 E 15.00857	Etna: Pian del Lago. Volcanic scoria and ash	O-MODE pl_030726_et_om.xls
26.07.2003 (Nigth)	From 23:37 To 00:02	N 37.77688 E 15.22928 N 37.77727 E 15.22959	Fiume Freddo: Sand Fire	O-MODE ff_030726_et_om.xls
27.07.2003 (Day)	From 12:42 To 13:30	N 37.79785 E 15.03492	Etna: Piano Provenzana (lava flow)	O-MODE Pp_030727_et_om.xls

Table 4.5 EVEREST INGV team temperature description data set.
Tabella 4.5 Descrizione del *set* dei dati di temperatura dell'EVEREST.

This instrument is a 4½ digit, compact-sized portable digital thermometer designed to use external K -type thermocouples as temperature sensor.

The thermocouple has been used for the Gold reference and samples temperature measurements. (Table 4.6).

The thermocouple may operates in a Range 0°C to 50°C <80% with maximum display reading of 9999.9. Temperature indication follows Reference temperature/Voltage Tables (N.I.S.T. Monograph 175 Revised to ITS-90) for Ktype. Thermocouples.was used also to measure the infragold reference during F-Tir dwelling measurements (Figure 4.10).

Technical description	Values
Temperature Scale:	Celsius or Fahrenheit user-selectable
Thermocouple Range:	K-TYPE -200°C to 1372°C
Resolution:	K-TYPE 0.1°C
Accuracy:	Accuracy is specified for operating temperatures over the range of 18°C to 28°C for 1 year, not including thermocouple error. K -TYPE ±(0.05% rdg + 0.3°C) -50°C to 1370°C
Temperature Coefficient:	0.1 times the applicable accuracy specification per °C from 0°C to 18°C and 28°C to 50°C

Table 4.6 Thermocouple features.
Tabella 4.6 Caratteristiche della Termocoppia.

The Figure 4.11 shows the time increasing trend of temperatures measured at Pian del Lago on July 19 2003. EVEREST temperature of the surface data are plotted together the thermocouple acquisition.

4.4 FTIR spectrometer description

The validation of a spectral emissivity image retrieved from ASTER TIR data requires the independent measurement of the spectral emissivity. Reference ground truth measurements are provided by collecting surface emissivity spectra on the field. The last step of the validation process is represented by the comparison of these spectra with the corresponding points on the spectral emissivity image.

During the field campaign midwave and longwave infrared emissivity spectra of ground surface representative samples have been collected by means of a portable field spectroradiometer (Figure 4.12).

The instrument used was the Model 102F FTIR (Fourier transform infrared) spectrometer developed by Design and Prototypes for field measurements of Earth's surface and atmosphere spectral radiance. The spectrometer, called mFTIR, operates at wavelengths ranging from 2 to 16 mm with a spectral resolution of 2 cm^{-1}. It has two liquid nitrogen cooled detectors, HgCdTe (or MCT) and InSb, for measurements collection in the 8-14 mm and 3-5 mm atmospheric windows respectively. The main features of the mFTIR are resumed in Table 4.7.

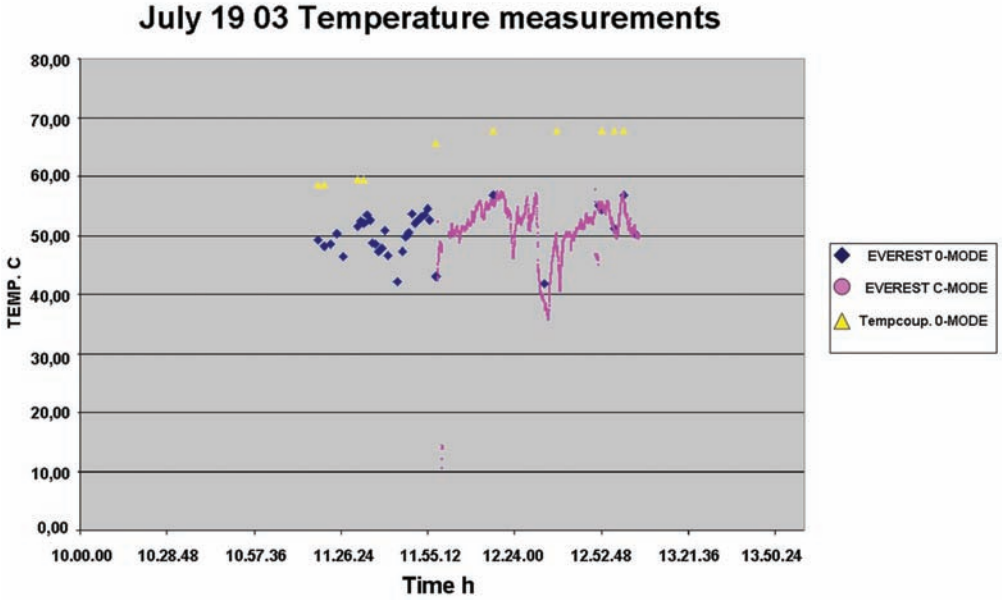

Figure 4.11 Time increasing trend of temperatures measured at Pian del Lago on July 19 2003.
Figura 4.11 Andamento delle temperature misurate a Pian del Lago il 19 Luglio 2003 in funzione del tempo.

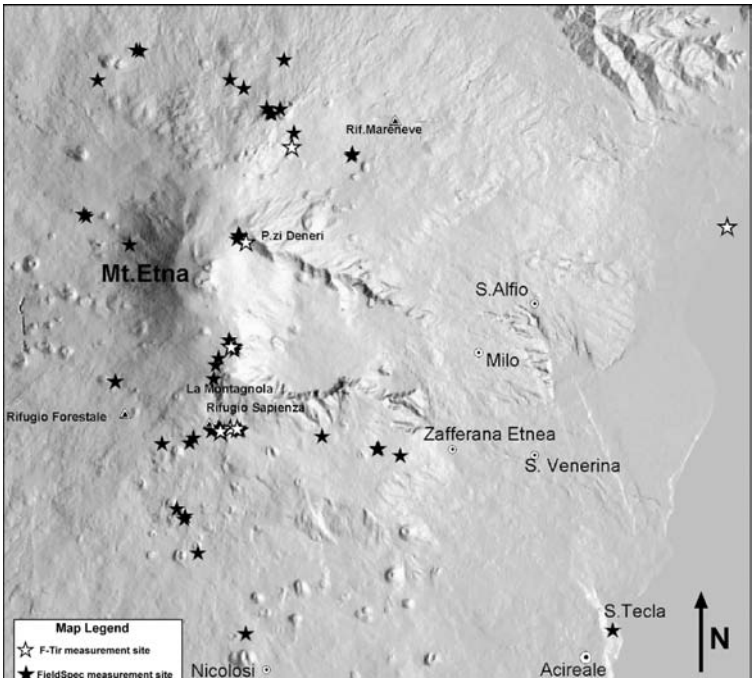

Figure 4.12 FTIR and FieldSpec measurements site.
Figura 4.12 Siti di misura per gli strumenti FTIR e FieldSpec.

4.4.1 Emissivity measurements

The core of the algorithm used in the mFTIR software to calculate the spectral emissivity is given by the equation

$$\varepsilon(\lambda) = \frac{L(\lambda) - L_{DWR}(\lambda)}{L_{BB}(T_S, \lambda) - L_{DWR}(\lambda)} \qquad \text{(Eq. 5.4.1)}$$

where

$L(\lambda)$ is the spectral radiance field measured by the spectrometer
$L_{DWR}(\lambda)$ is the downwelling radiance field composed of scattered, self-emitted and direct solar contributions integrated on the hemisphere centered on the target
$L_{BB}(T_S,\lambda)$ is the spectral radiance field of a black body at temperature T_S
$\varepsilon(\lambda)$ is the target spectral emissivity

Three radiance field measurements are for the instrument calibration and one for the target material. The three calibrations measurements are for the blackbody at two different temperatures and for the downwelling radiance field. Moreover the sample temperature T_S must be known by direct independent measurement or by inference with one of the temperature-emissivity separation (TES) algorithms given in the literature. This is needed to solve the under-constraint nature of the problem that rises when temperature and spectral emissivity of a sample are to be determined from the same multispectral data set.

Technical description	Values
Spectral range	2-16 μm
Spectral resolution	2,4,8,16 cm^{-1}
Operating temperature range	15-35 °C (instrument temperature)
FOV	4.8 ° (additional input optic 2.4 °)
Computer OS and type	DOS 6.22, 8GB HD, Pentium 166MHz/32MB
Input voltage range	12V DC (±10%)
Weight	7 Kg
Size	36cmx20cmx23cm

Table 4.7 Main features of the model 102F portable FTIR by Design & Prototypes,LTD.
Tabella 4.7 Caratteristiche principali del modello 102F FTIR.

A good choice of the two blackbody temperatures is just below the ambient temperature for the colder blackbody and just above the warmest temperature of the sample target for the warm blackbody. The radiance field of the sample will be then well within the two blackbody radiance curves and the calibration will be more precise. The instrument self-emission varies strongly with instrument temperature and thus the optical head of the instrument is temperature controlled to maintain his variations within 0.1°C for a better calibration accuracy. Nonetheless are good practices the repetition of the black bodies calibration measurements if the ambient temperature changes during long field measurements, the instrument thermalization for one hour, and the activation of the scan motor for 15 minutes before data collection.

The blackbodies radiance fields are measured by pressing the blackbody onto the instrument foreoptic. The blackbody provided is powered and temperature controlled by the instrument itself and the cold and warm calibration temperatures can be set from the acquisition software.

The downwelling radiance of the hemisphere above the target is measured with a reflector located on the target. A golden plate with emissivity $\varepsilon = 0.040$ on the MWIR TIR range is provided with the μFTIR. A good and cheap substitute is represented by randomly crinkled aluminium foil placed on a stiff surface. During the campaign only the golden plate has been used by our group and some difficulties have been experienced in the precise measurement of the plate temperature. The thermocouple measurements of the golden plate temperature have proved to be more stable and reliable than the measurements collected with the Everest TIR thermometer. These measurements display high fluctuations due to the variations of local meteorological parameters. The experience of the campaign led us to find and purchase a new thermometer for the reflector plate temperature measurement. This instrument is a radiometer with a special design that drives to unity the emissivity of the material of which the temperature is to be measured. A cone reflector is located at the apex of the thermometer probe. Applying the cone reflector on the target surface creates instantly a blackbody out of it.

The nature of Eq. 5.4.1 leads to a mathematical instability when the sample blackbody radiance $L_{BB}(T_S,\lambda)$ and the downwelling radiance $L_{DWR}(\lambda)$ approach each other. Furthermore the numerator of Eq. 5.4.1 will tend to zero or to negative values when the sample radiance will tend to $L_{DWR}(\lambda)$.This can happen in a number of actual cases, but a comprehensive discussion of their implications is beyond the scope of the present report. A general suggestion points out the early morning and the evening after the sunset as the more convenient time windows for emissivity data collection. The evening may be regarded as the more favorable moment because of the higher thermal contrast that may enhance the sample signal.

4.4.2 Description of the emissivity measurements

The sites (Table 4.8) where the ground measurements have been carried out have been chosen on the basis of the following criteria. They had to be as high as possible, wide, plane and open areas of homogenous surface material. The have to be easy to reach on the field and easy to recognize and locate on the image. On Mount Etna the highest places chosen were those of Pian del Lago and Piano delle Concazze. The first one is a slightly tilted surface of cineritic scoria of centimeter range diameter located between the Valle del Bove scarp, the two new 2003 eruption craters and the 2001 eruption new crater on the southeast flank of the volcano. An easy access is provided by the road that leads from Rifugio Sapienza to the point where was located the Torre del Filosofo mountain hut, now destroyed by the 2003 eruption. The choice of this site for collecting surface emissivity spectra has a possible serious drawback due to his location along one of the most probable directions of the plume: measurements of the downwelling radiance are very unstable if carried out under or inside the plume because of the continuously changing radiance of the plume itself. For instance, the wind direction has slightly changed from that of the early morning on July, 19 and unfortunately during the ground emissivity spectra acquisition the Etna plume was flowing over Pian del Lago. These measurements are thus to be considered unreliable for the reason explained above.

The second site is Piano delle Concazze, a plane area between the NE summit crater and Pizzi de'Neri observatory also covered with cineritic scoria of centimeter range diameter. The access is relatively easy during the day and is granted by a newly reopened road which crosses the 2003 eruption's lava flow that destroyed Piano Provenzana and the lower track of the old road to the mountain.

Both these places are at about 2700 m altitude where the atmosphere is relatively clean when there are good weather conditions. Just

Date	Site	GPS Coordinates
17.07.2003 (Day)	Etna: Pian del Lago	N 37.7 E 15.008 N 37.72844 E 15.00857 N 37.72855 E 15.00848
18.07.2003 (Night)	Etna: layby near the crossroad for Nicolosi	N 37.7 E 15.011
19.07.2003	Etna: Pian del Lago	N 37.72851 E 15.00850
20.07.2003 (Day)	Etna: Pizzo dei Neri (Concazze)	N 37.7649 E 15.01494
22.07.2003 (Day)	Vulcano: brecciolino su bordo cratere. Concrezione di zolfo bordo cratere Zolfo Roccia vulcanica solida lisciviata Piattaforma elicottero Lava litoide rossiccia	 N 38.406150 E 14.960891 N 38.40618 E 14.96116 N 384019 E 14.96142 N 38.40618 E 1496150 N 38.40614 E 14.96062 N 38.40614 E 14.96062
23.07.2003 (Nigth)	Etna: Rifugio Sapienza	N 37.69910 E 15.00377 N 37.69928 E 15.00372
26.07.2003 (Day) (Nigth)	Etna: Pian del Lago Fiume Freddo: Sand Fire	N 37.72852 E 15.00857 N 37.77688 E 15.22928 N 37.77727 E 15.22959
27.07.2003 (Day)	Etna: Piano Provenzana (lava flow)	 N 37.79785 E 15.03492

Table 4.8 List of the sites where emissivity measurements were carried out during the campaign.
Tabella 4.8 Lista dei siti dove sono state effettuate le misure di remissività durante la campagna di misura.

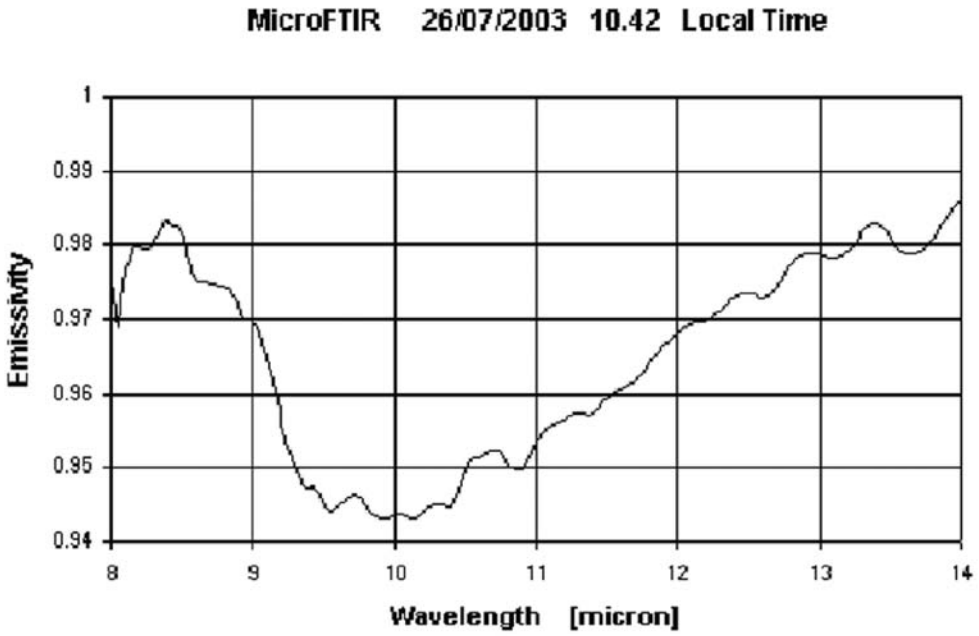

Figure 4.13 *Tephra* emissivity spectrum collected on Pian del Lago.
Figura 4.13 Spettro dell'emissività di *tephra* misurato a Pian del Lago.

because of the high elevation they are also exposed to sudden weather changes that can affect the downwelling radiance measurements.

A representative emissivity spectrum collected on July, 26 on the Pian del Lago site is shown in Figure 4.13.

4.5 Ground gas emission

4.5.1 CO_2 gas emission

Soil gas surveys were focused on the determination of diffuse CO_2 flux from the ground. Measurements were carried out on July 19, 2003 in an area close to Pizzi Deneri, on the upper northern flank of Mt. Etna at an altitude of about 2800 m asl, and on July 26, 2003 in an area of the lower north-east flank of the volcano, along the coast-line close to the village of Fondachello (B in Figure 4.14).

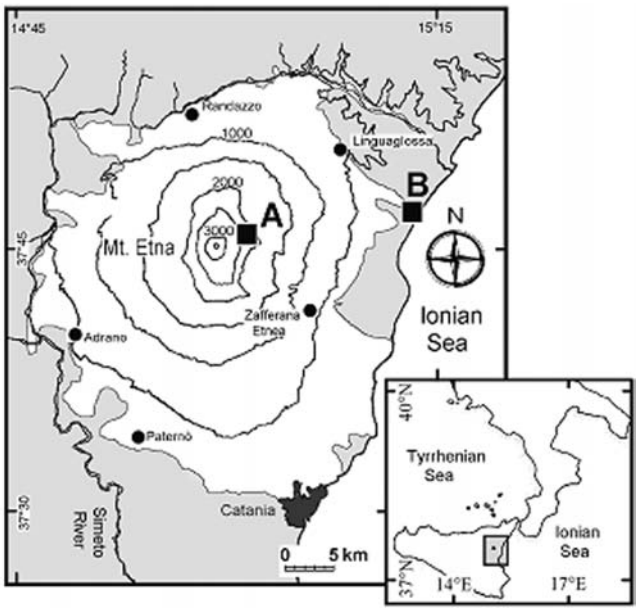

Figure 4.14 Location of the areas where the measurements of soil CO_2 flux have been carried out. A) Pizzi Deneri; B) Fondachello.
Figura 4.14 Aree di misura dell'emissione di CO_2 dal terreno A) Pizzi Deneri; B) Fondachello.

The method used for measuring the CO_2 flux from soil is that of the accumulation chamber [Chiodini et al., 1998]. The equipment used (Figure 4.15) consists of a cylindrical chamber open at the bottom, 10 cm high and with a surface of 308 cm^2, connected to an IR spectrophotometer calibrated for detecting CO_2 (Riken mod. 550A, CO_2 concentration range 0 – 5,000 μmol/mol, accuracy of ± 10 μmol/mol).

The accumulation chamber is placed firmly on the ground surface so as to avoid intrusion of air. The gas inside the chamber is constantly pumped from the chamber to the IR spectrophotometer and then sent again into the chamber. The chamber has an internal fan whose continuous motion allows an optimal mixing of the gas. Before being pumped to the spectrophotometer, the gas is filtered in order to trap any eventual water vapour, whose presence can create analytical interferences and can also damage the IR cell in case of vapour condensation.

The values of CO_2 concentration measured with time are visualised on a time graph in order to calculate the angular coefficient of the best-fit line obtained from the CO_2 data. The initial slope of this line (considering the first minutes of CO_2 concentration increase inside the chamber) is the key parameter to determine the soil CO_2 flux. In fact, it was experimentally observed by Chiodini et al. [1998] on the basis of previous experiences [Parkinson, 1981; Tonani & Miele, 1991] that the initial rate of CO_2 concentration increase inside the chamber is directly proportional to the soil CO_2 flux. Repeated measurements to calibrate the method were carried out by Chiodini et al. [1998] on synthetic soils imposing different known CO_2 fluxes, and the results showed deviations lower than 15 % from the imposed values and a reproducibility better than 10 %.

In the Pizzi Deneri area 24 soil CO_2 flux measurements were carried out over a surface of about 0.19 km^2 (Figure 4.16).

Values ranged from 0 g m^{-2} d^{-1} to 66.6 g m^{-2} d^{-1}, with an average value of 28.6 g m^{-2} d^{-1}. The daily output of CO_2 (Q_{CO2}) degassed from the soil of the surveyed area was estimated using arithmetic averaging and ordinary kriging. The Q_{CO2} obtained by integrating the arithmetic average of the 24 φ_{CO2} values over the 0.19 km^2 surface is 5.4 t d^{-1}. The Q_{CO2} estimated using the ordinary kriging is about 5.2 t d^{-1}. The two figures are very similar and therefore can be taken as a reliable estimate of the CO_2 output. In the Fondachello area 10 measurements of soil CO_2 flux were carried out over a surface of about 0.01 km^2. All values measured were zero.

4.5.2 Results of Measurements

The results of measurements carried out by the different Functional Units at Vulcano, in the framework of volcanic activity surveillance, showed a background level of activity for July 2003. This indication come from the compari-

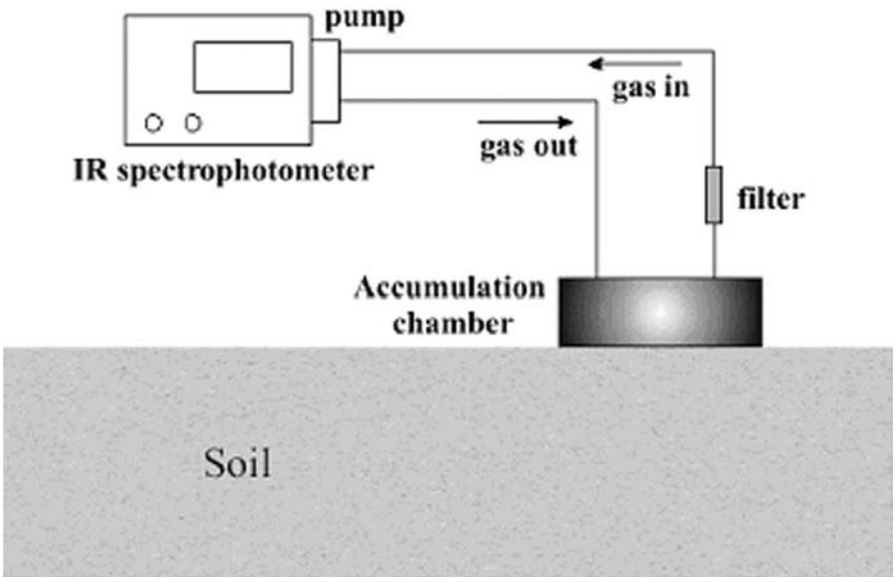

Figure 4.15 Sketch of the system used for measuring soil CO_2 fluxes.
Figura 4.15 Disegno del sistema usato per la misura del flusso di CO_2 dal terreno.

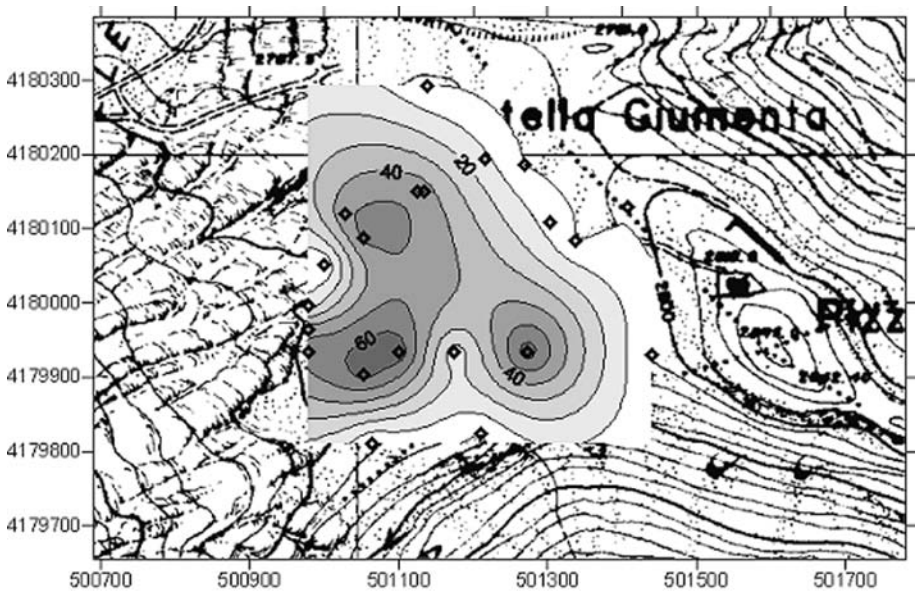

Figure 4.16 Contour map of soil CO_2 fluxes measured in the Pizzi Deneri area. Contours (expressed in g m^{-2} d^{-1}) were obtained by ordinary kriging. Coordinates are reported in the UTM-ED50 system (planar).
Figura 4.16 Mappa delle curve di livello delle misure di flusso di CO_2 effettuate a Pizzi Deneri.

son of the trends shown by various time series, relative to many geochemical parameters, from very different sources, sampled at Vulcano Island since 1990. In particular, they refer to:

- high temperature fumarole field of La Fossa Cone;
- thermal wells exploited inside Vulcano Porto area for domestic use;
- soil gas emissions measured around La Fossa Cone and at Vulcano Porto;
- soil (outside fumaroles) and air temperature
- rainfall amount.

4.5.3 Description of the instruments characteristics and operational procedure performed at La Fossa Cone

4.5.3.1 a) Temperatures

Spot data of fumarole temperatures have been measured by a Ni-NiCr thermocouple, inserted for a few cm in the same vent where fluids have been collected, in order to be representative of the temperature of sampled gases.

Continuous fumarole temperatures data have been acquired with hourly frequency in sites FA, F5, F5AT, and B1 (Figure 4.17) by a self-made station, using a Ni-NiCr thermocouple.

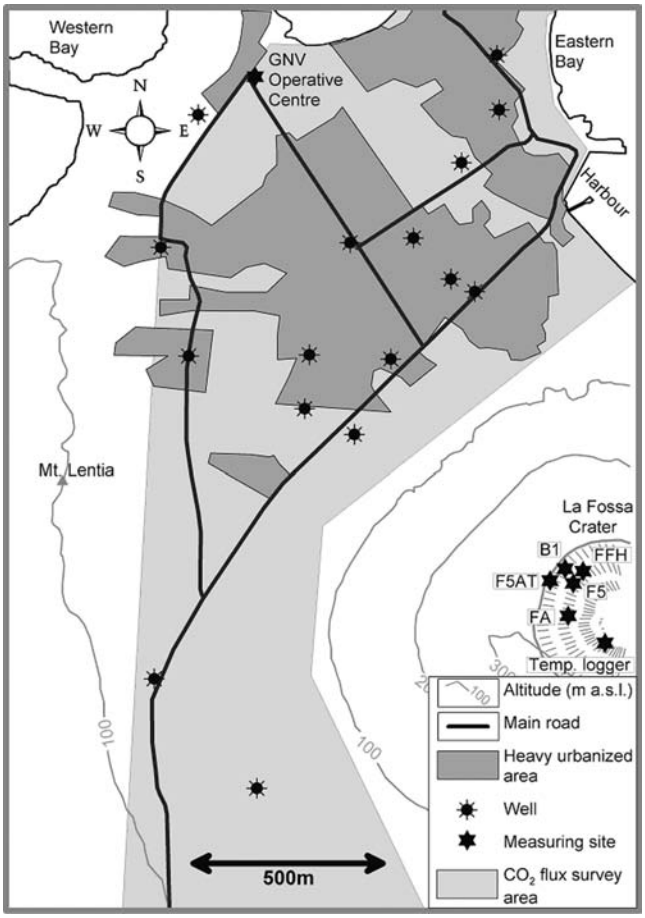

Figure 4.17 Location of the measuring sites at Vulcano Island (Italy).
Figura 4.17 Localizzazione dei siti di misura nell'isola di Vulcano (Italia).

The soil temperature outside fumarole field in La Fossa crater has been determined by a Gemini Tinytag plus Logger with external temperature sensor at 10 cm of depth, with sampling interval of 2 hours.

The air temperature has been measured by a Gemini Tinytag plus Logger with internal temperature sensor, installed inside a radiative wooden screen at 6 m from soil, with sampling interval of 2 hours.

4.5.3.2 b) Rainfall amount

Rainfall amount has been determined by a rain gauge, with diameter of 30 cm, coupled to a Gemini Tinytag plus event recorder, with a sampling interval of 2 hours.

4.5.3.3 c) Underground water level and temperature

The two parameters have been determined by the use of a PASI freatimeter with a PT100 temperature probe installed in the measuring head.

4.5.3.4 d) CO_2 flux from soil

The method used for systematic measurements of gas flux from soil is the dynamic concentration method [Gurrieri and Valenza 1988], calibrated in laboratory with an apparatus simulating a natural degassing system.

The instrumental devices used in the field consist of: a) probe with a 2.2 cm diameter inserted into the ground at 45 cm of dept for soil gas inlet; b) tube with 4mm diameter for air inlet; c) filter for dust and moisture; d) pump; e) infrared spectrophotometer with fixed wavelength to detect CO_2, the main constituent of soil gas emission.

With this method the CO_2 flux is obtained through the measurement of the dynamic concentration (Cd) in the soil, at a depth of 45 cm. Natural flux of CO_2 from the ground is indeed proportional to the CO_2 content (Cd) in a mixture of air and soil gases, reaching the infrared sensor when sucking gas at constant flow rate from the probe inserted in the soil. The value of dynamic concentration (Cd) is the constant value of CO_2 content, showed by the mixture a few minutes after the pump is turned on. Cd is multiplied to a constant value (K), that is empiric and depend on the physical characteristic of the ground, to obtain the unit CO_2 flux.

4.5.3.6 f) Description of the measurements

All data are presented will be briefly discussed in the next paragraphs.

4.5.3.7 g) Continuous monitoring of temperature at La Fossa Cone

Temperature values haven't shown significant variation during the last year of monitoring. Taking into account high temperature fumaroles, on July 22th 2003 the mean tempera-

ture values were 590 °K in site FA, 605°K in site F5AT and 460°K in site F5. These values indicate a low level of volcanic activity.

4.5.3.8 h) Meteorological, soil and underground waters measurements

Underground aquifer in the Vulcano Porto area is subjected to monthly measures of water table elevation and temperature in a network of 14 wells since 1995 (Figure 4.17) these measures are coupled to continuous temperature monitoring in 11 of the 14 wells. Water table elevation does not show significant variations during the hydrological year, being the feeding systems of the aquifer mainly related to the condensation, inside the volcanic edifice, of volcanic and geothermal fluids. Water temperatures do not show significant seasonal variations, but in some wells may be heavy influenced by seismic activity, with spikes up to 10°K in correspondence of seismic events. On July 22th the aquifer was in a quite phase, with values considered typical for the summer season.

4.5.3.9 i) CO_2 flux from soil

Diffuse emissions of CO_2 have been periodically evaluated since 1984. The investigated area, 2.2 Km^2 wide, is located inside the Caldera della Fossa and it includes the main village on the island of Vulcano. The sampling grid consists of 51 measurement points with a probe inserted in the soil. Investigation about the influence of different natural parameters on the mean CO_2 flux measured at Vulcano Porto, showed high correlations between mean CO_2 flux and other geochemical and geophysical parameters related to volcanic activity and coming from the other different sources, like plume, fumaroles, water wells, seismic stations and so on [Diliberto et al., 2002]. The mean CO_2 flux measured on July 22th was 6.31 x 10^{-5} cm^3 x cm^{-2} x s^{-1} . This value indicates a low level of exhaling activity for the investigated area. Moreover high CO_2 flux, from the fixed grid of measurement points, were observed only in the sites of Grotta dei Palizzi and Faraglione as it is usual in periods of not anomalous release.

5. Atmospheric characteristics measurements

In order to characterize the atmosphere at Mt. Etna, Solfatara, and Vulcano sites the Atmospheric groups participant the FASA-ASI and HYPSEO-ASI measurements campaign performed the following atmospheric measurements at the ground and from the ground:

- Vertical radiosoundings from two different sites at Mt. Etna and one at Solfatara;
- Meteorological parameters with three Meteorological stations at Mt. Etna and Vulcano;
- Aerosol observation with Lidar and with three different sun-photometers at Mt. Etna;
- Precipitable water measurements;
- Solar Irradiance measurements with two portables Spectrometers at Mt. Etna.

In the following paragraphs the measurements methods and instruments are described.

5.1 Vertical profile

Atmospheric correction is a fundamental step for the analysis of the radiance measured by remote sensed image. It can be performed using a radiative transfer code model like MODTRAN 4.0. [Acharya et al. 1998], adopted in order to evaluate the various radiative terms involved in the image acquired during the FASA campaign (Fire Airborne Simulator Arrangement).

Radiative transfer code needs a number of input data such as vertical distribution of pressure, temperature and humidity. These data were acquired, simultaneously with the FASA over flight, at the end of July.

The vertical profiles were made at two different locations considering the Etna structure, in particular one launch site was located at Milo (quota) and the second was located at Santa Tecla (quota).

5.1.1 Vertical atmospheric profiles at Milo (DIMA-RU)

The radiotheodolyte (AIR 3A RT) shown in Figure 5.1 is the instrument used by the DIMA-RU to carry out the vertical atmospheric profiles.

The meteorological radio-sonde (AIR IS 4A 1680) works at a frequency of 1680 (MHz) tunable (1660-1700 MHz). Table 5.1 reports the main characteristics.

This data are transmitted and received about each second. The ascension speed is about 5 (m s^{-1}) so this is the vertical resolution. Using pressure, temperature and relative humidity the hypsometric equation gives the geo-potential

	Pressure (hPa)	Temperature (°C)	Relative Humidity (%)
Range	1050 to 3	-50 to 90	1 to 100
Accuracy	± 1	± 0.5	± 2

Table 5.1 Air IS 4A 1680 specifications.
Tabella 5.1 Specifiche di Air IS 4A 1680.

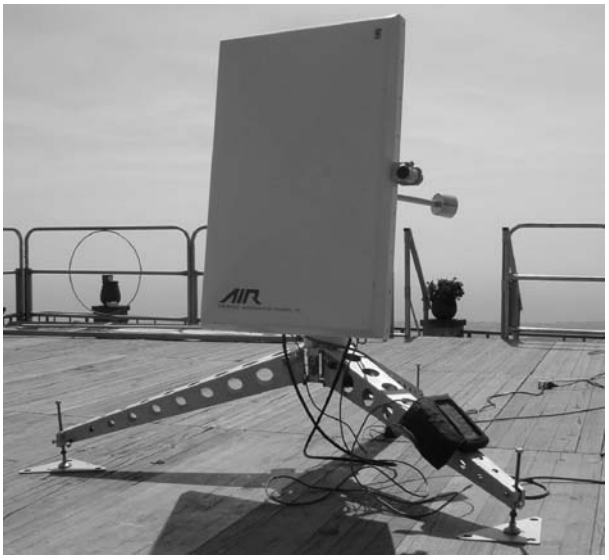

Figure 5.1 The radiotheodolyte. The rectangle is the flat antenna to track the sonde. The cylindrical column (behind the antenna) contains the receiver and the interface.
Figura 5.1 Il radioteodolite è composto da un'antenna rettangolare piatta per la rivelazione del segnale proveniente dalla sonda e da una colonna cilindrica contenente il ricevitore e l'interfaccia.

Figure 5.2 Flight train: balloon, parachute, sonde.
Figura 5.2 Treno di lancio: Pallone, paracadute, sonda.

altitude. The wind speed and direction are obtained tracking the sonde and deriving its velocity (i.e. the wind velocity). Tracking is done by means of the array antenna (made of eight small flat antennas inside the white rectangle searching the maximum signal of the carrier) (Figure 5.1). The accuracy of the wind speed is ±1 (m s^{-1}) if the wind speed is lower than 10 (m s^{-1}) or ±10% if the speed is greater than 10 (m s^{-1}). The accuracy of the wind direction is ±5 (degrees) if the wind speed is lower than 25 (m s^{-1}) or ±3 (deg) if the speed is greater than 25 (m s^{-1}). Figure 5.2 shows the so named fight train: balloon, parachute and sonde (Milo square).

During the Sicily 2003 campaign six vertical atmospheric profiles were carried out launching the meteorological sonde from the square of Milo village. Milo is located on the eastern flank of Mt. Etna at about 700m a.s.l.. The coordinates of the square of Milo are: Longitude 15° 7.033'; Latitude 37° 43.332'. Date, launch time, end time (balloon blast) and maximum altitude of the six radiosoundings are reported in Table 5.2.

The standard observations carried out at the Trapani WMO station 16429 (Longitude 12.50°; Latitude 37.91°; Altitude 14.0 m) have been collected too.

As an example Figure 5.3a reports the air temperature, the dew point temperature and the precipitable water while Figure 5.3b reports the wind speed and direction measured.

Date	Launch time (GMT)	End time (GMT)	Max altitude (m)
17.07.2003	08:16	09:56	17858
17.07.2003	21:06	22:41	18171
19.07.2003	09:25	10:42	18187
20.07.2003	09:38	10:57	23537
26.07.2003	09:10	10:53	18332
26.07.2003	20:32	22:21	17458

Table 5.2 Milo village radiosoundings; Longitude 15° 7.033', Latitude 37°43.332'.
Tabella 5.2 Radiosandaggi a Milo (CT); Longitudine 15° 7.033', Latitudine 37°43.332'.

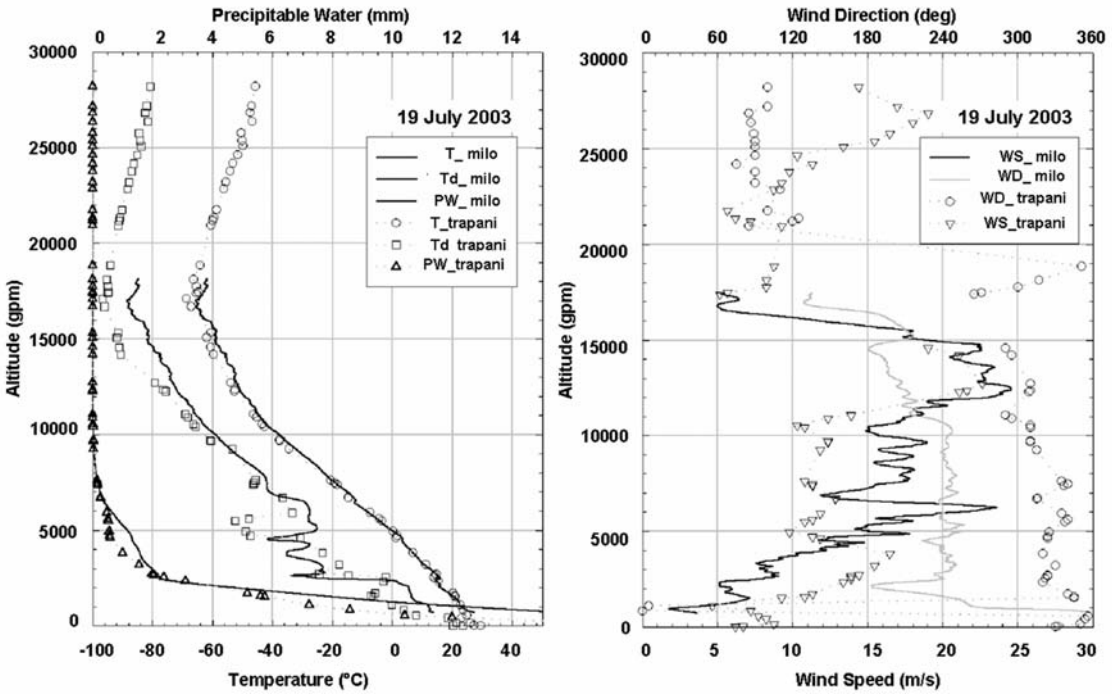

Figure 5.3 a,b Milo (CT) atmospheric profile. July 19, 2003; 09:25 GMT.
Figura 5.3 a,b Profilo atmosferico misurato a Milo (CT) il 19 Luglio 2003. Ora di lancio: 09:25 GMT.

The data were collected on July 19 2003 they are the atmospheric sounding performed at Milo village (solid lines; launch time 09:25 GMT) and the standard observations of Trapani 16429 WMO station (dotted line with symbols; launch time 11:00 GMT).

5.1.2 Vertical atmospheric profiles at Santa Tecla (IMAA-CNR)

The sounding system used during the July measurement campaign was a VAISALA PP15 processor and radiosondes used were the PTU RS80 ones, from VAISALA too. Radiosondes functioning was checked by a Ground Check Set, which checks for sensors accuracy (calibration with known and accurate references) and transmitter frequency.

Balloons were 1000g-type, 2.3m radius, inflated with helium gas. They have a mean ascent speed of 5m/s (300m/min). The whole system is equipped with a parachute for collecting measurements also during the descend-

Figure 5.4 Location of the radiosonde measurement site.
Figura 5.4 Localizzazione del sito di misura delle radiosonde.

Date [dd.mm.yyyy]	Time GMT [hh:mm]	Lat [deg,min]	Long [deg,min]	Elevation [m]	Measurement code
17.07.2003	07:53	37°36'N	15°10'E	5	ST_030717_VP_0001_NP
17.07.2003	08:17	37°36'N	15°10'E	5	ST_030717_VP_0002_NP
17.07.2003	21:23	37°36'N	15°10'E	5	ST_030717_VP_0003_NP
18.07.2003	12:53	37°36'N	15°10'E	5	ST_030718_VP_0001_NP
19.07.2003	09:19	37°36'N	15°10'E	5	ST_030719_VP_0001_NP
20.07.2003	09:52	37°36'N	15°10'E	5	ST_030720_VP_0001_NP
22.07.2003	09:51	37°36'N	15°10'E	5	ST_030722_VP_0001_NP
24.07.2003	09:01	37°36'N	15°10'E	5	ST_030724_VP_0001_NP
25.07.2003	09:59	37°36'N	15°10'E	5	ST_030725_VP_0001_NP
26.07.2003	09:35	37°36'N	15°10'E	5	ST_030726_VP_0001_NP
26.07.2003	20:48	37°36'N	15°10'E	5	ST_030726_VP_0002_NP

Table 5.3 Radiosonde launches performed during the campaign. ST=Santa Tecla; VP= Vertical Profiles; NP=Nicola Pergola.
Tabella 5.3 Lanci delle radiosonde da Santa Tecla (CT). ST=Santa Tecla; VP= Profili Verticali; NP=Nicola Pergola.

ing phase. The data transmission is performed on a radio frequency at 403Mhz, slightly tuneable (± 3Mhz).

The radiosonde measurements have been carried out from Hotel Santa Tecla, in Santa Tecla (CT) (Figure 5.4).

The site was located at the sea level, few kilometres north of Acireale, about 20 Km apart Catania, S-E of Mt. Etna volcano. Balloons were launched few meters apart the sea.

Site coordinates are: 37°36'N, 15°10'E.

In Table 5.3 the whole list of the launches carried out from 17/07/2003 to 26/07/2003 is reported.

Data collected during each launch were: Time (from the launch time, [min s]), Ascension Rate [m/s], Height a.s.l. [m], Pressure [hPa], Temperature [°C], Relative Humidity [%], Dew point Temperature [°C]. In Figure 5.5 an example of measurement is reported.

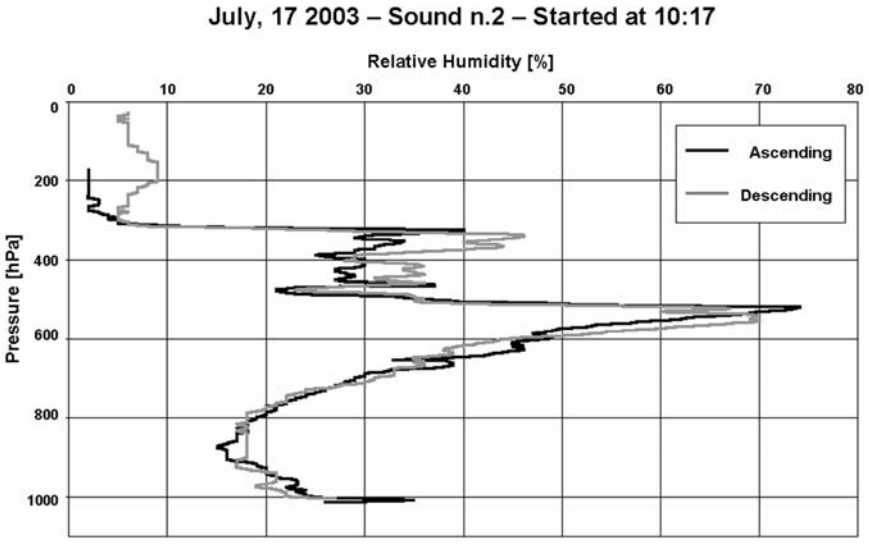

Figure 5.5 Results: an example of a vertical humidity profile, measured on July, 17th. Balloon was launched 10:17GMT.
Figura 5.5 Risultati: un esempio di profilo verticale dell'umidità misurato il 17 Luglio 2003. Il Pallone sonda è stato lanciato alle 10:17 GMT.

5.1.3 Vertical atmospheric profiles Solfatara di Pozzuoli (INGV-Telespazio)

The atmospheric vertical profile has been measured by MARWIN MW12 system [VAISALA inc.] launching RS80 radiosonde. This method provides vertical profile of pressure, temperature and humidity in real time. The measurements of these three quantities are carried out by means of Barocap® pressure sensor, Thermocap® temperature sensor and Humicap® humidity sensor. These sensor are produced by VAISALA and are stored inside the sonde which is string-connected to a meteorological balloon. The data from the sonde are transmitted to a receiver using frequency of about 400 MHz. A personal computer controls the receiver and provides also for data archiving and visualization in real-time. Technical characteristics of the RS80 sonde are listed in the following Table 5.4.

During the FASA campaign one launch has been performed from an area up the hill located at NE of the Solfatara of Pozzuoli (Naples), (Figure 5.6).

General specifications	
Battery	water -activated
Voltage	19 V
Transmitter frequencies	403 MHz, 1680 MHz
Meteorological sensors	
Pressure	BAROCAP® Capacitive aneroid
Measuring range	1060 hPa to 3hPa (mb)
Resolution	0.1 hPa
Accuracy	
Reproducibility (1)	0.5 hPa
Repeatability of calibration (2)	0.5 hPa
Temperature	THERMOCAP® Capacitive bead
Measuring range	+60 °C to - 90 °C
Resolution	0.1 °C
Accuracy	
Reproducibility (1)	0.2 °C up to 50 hPa, 0.3 °C for 50-15 hPa, 0.4°C above 15 hPa levels
Lag	< 2.5 s (6 m/s flow at 1000 hPa)
Repeatability of calibration (2)	0.2 °C
Humidity	HUMICAP® Thin film capacitor
Measuring range	0 to 100 % RH
Resolution	1 % RH
Accuracy	
Reproducibility (1)	<3 %RH
Repeatability of calibration (2)	2 %RHz
(1) Data based on WMO International Radiosonde Comparison, Phases I, II, and III (WMO/TD no 195 and 451) (2) Standard deviation between two successive calibrations	

Table 5.4 General specification of RS80 sonde.
Tabella 5.4 Specifiche generali della sonda RS80.

Time, location and other data concerning the launch are reported in.Table 5.5.

Launch Site	Latitude	Longitude	Altitude a.s.l.	Date	Time
Solfatara of Pozzuoli	40° 49‘ 54‘‘N	14° 08‘ 21‘‘E	184m	16.07.2003	13.45 GMT

Table 5.5 Site time and location of the launch.
Tabella 5.5 Ora e localizzazione del lancio.

Figure 5.6 Solfatara, Naples: Location map of the radiosonde measurement: the red point indicates the launch site.
Figura 5.6 Solfatara (NA): Localizzazione dei siti di lancio della radiosonda: il punto rosso indica il sito di lancio.

In this part the reports and the plots of the atmospherical profile are shown. The report contains the information in agreement with the WMO standard [W.M.O. 1984].

Each report contains:

- Date, time, location, latitude, longitude and elevation of the launch
- Surface data
- Standard levels
- Significant level
- Freezing interval

Surface data Table 5.6.

Alt	Pressure	Temp	RH	Dew dep.
Gpm	hPa	deg °C	%	deg °C
184	994.0	32.0	34	14.2

Table 5.6 Surface data.
Tabella 5.6 Misure superficiali.

Standard pressure levels (Table 5.7)

Time	Pressure	Height	Temperature	RH	Dew dep.	Asc. Rate
Min sec	hPa	gpm	deg °C	%	deg °C	m/s
NA	1000.0	132	NA	NA	NA	NA
2 35	925.0	820	25.2	27	4.9	NA
5 21	850.0	1558	21.9	38	7.0	4.5
11 38	700.0	3216	11.9	33	-3.8	4.4
21 9	500.0	5917	-8.7	15	-30.8	4.7
27 9	400.0	7607	-20.6	16	-40.0	4.7
NA	300.0	9664	NA	NA	NA	NA

Table 5.7 Standard pressure levels.
Tabella 5.7 Livelli standard della pressione.

Significant levels (Table 5.8).

Time	Pressure	Height	Temperature	RH	Dew dep.
Min sec	hPa	gpm	deg °C	%	deg °C
0 0	994.0	184	32.0	34	14.2
0 2	992.7	197	29.0	25	7.0
2 42	922.6	843	24.9	28	5.2
3 58	887.6	1181	24.6	19	-0.5
4 38	869.4	1362	23.5	12	-7.5
5 44	839.8	1663	21.1	41	7.4
7 50	787.0	2222	19.2	27	-0.2
16 0	602.8	4443	1.3	56	-6.5
18 34	549.3	5184	-4.7	49	-13.8
20 38	510.4	5758	-8.5	37	-20.6
21 36	492.1	6040	-9.4	9	-36.6
25 14	430.1	7066	-16.1	7	-44.2
29 38	363.7	8303	-26.1	20	-42.6
30 2	358.0	8416	-26.8	38	-36.9
30 40	349.6	8588	-28.1	17	-45.8
33 0	319.9	9217	-33.6	22	-48.2

Table 5.8 Significant levels.
Tabella 5.8 Livelli significativi.

Freezing Level (Table 5.9).

Time	Pressure	Height	Temperature	RH	Dewp
Min sec	hPa	gpm	deg °C	%	deg °C
16 32	591.4	4596	0	54	-8.2

Table 5.9 Freezing altitude.
Tabella 5.9 Altezza di congelamento.

The following graphs (Figure 5.7, Figure 5.8) show the value of the Temperature and RH listed above. The Y-axis of each graph represents the altitude from the ground up to 9217 m that was the bursting quote.

5.2 Ground meteo station

Ground atmospheric parameters were performed using meteorological stations situated around the Mt. Etna during the entire campaign period and in one day at Volcano.

5.2.1 Ground meteorological stations (DIMARU)

Two different kinds of standard meteorological stations were used: DAVIS and MICROS stations. DAVIS is an independent, automatic, complete and quite economic data logger. The data automatically collected by DAVIS may be downloaded calling its internal mobile cellular phone. Two of these ground meteorological stations were installed in two fixed places located at different altitudes: Nicolosi village, CT (about 750 m asl; Long. 15° 1.160'; Lat. 37° 36.800') at the INGV building (Ex Poseidon building; see Figure 5.9) and Rifugio Citelli (about 1750 m a.s.l.; Long. 15° 3.583'; Lat. 37° 45.913'; see Figure 5.10).

These two fixed meteorological stations were installed to estimate the temperature gradient and to compute the two parameters of a vertical exponential function representing the vertical profile of the precipitable water. The meteorological fields measured by DAVIS stations, each 15 minutes, are: pressure, temperature, relative humidity, wind speed and direction, precipi-

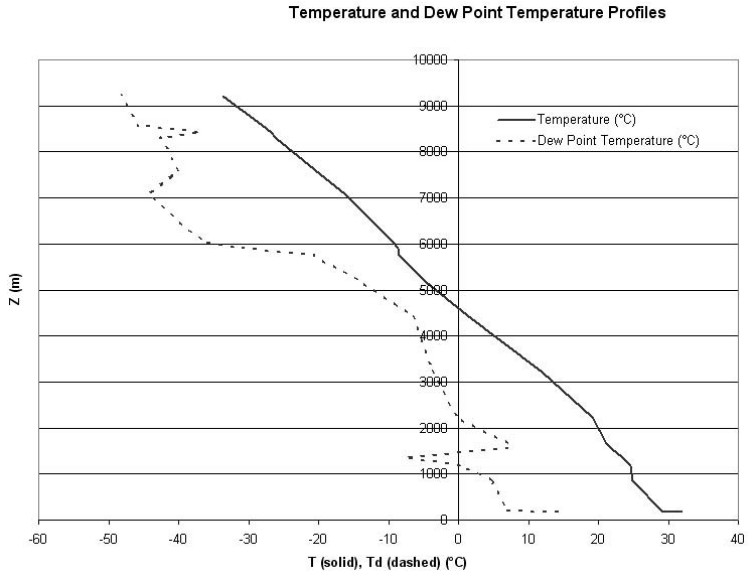

Figure 5.7 Temperature and Dew Point Temperature profiles: freezing occurs at about 4600m a.s.l..
Figura 5.7 Profili della Temperatura e Temperatura di *Dew Point*: 0 °C corrispondono ad una altezza di 4600 m s.l.m..

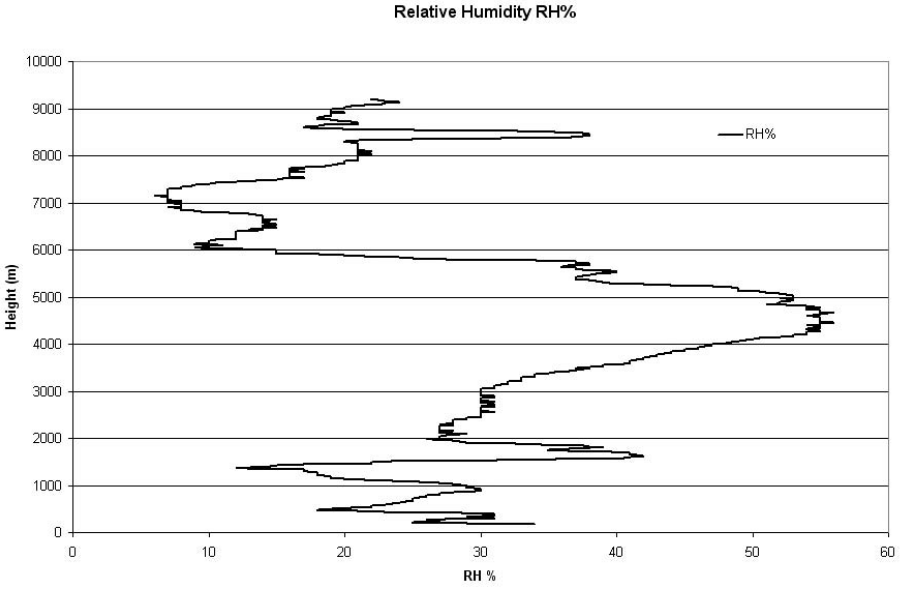

Figure 5.8 Relative Humidity Profile.
Figura 5.8 Profilo di umidità relativa.

tation and global irradiance.

The MICROS data-logger (named Pico) is a micro data logger having few input ports but it is very light and friendly to use as mobile station. A PC, via RS232 interface, is required to download the data and to configure the data logger. This logger was used to collect meteorological data at Rifugio Sapienza and at Pizzi De Neri peak. See the INGV shelter on Figure 5.11 at Pizzi De Neri; it is close to Pian delle Concazze where many other measurements were carried out.

The meteorological fields measured by the Pico logger each minute, are: pressure, temperature, relative humidity, wind speed and direction. Table 5.10 indicates the name of the places, their Longitude and Latitude, the date and the measuring time interval (GMT) of the mobile Pico data logger.

Figure 5.9 Nicolosi INGV building (750 m asl). DAVIS station down on the small meadow. Longitude: 15° 1.160'; Latitude: 37° 36.800'.
Figura 5.9 Edificio INGV a Nicolosi (CT).

Figure 5.10 Rifugio Citelli (1750 m asl). DAVIS station fixed at the rail terrace. Longitude: 15° 3.583'; Latitude: 37° 45.913'.
Figura 5.10 Stazione meteorologica DAVIS al rifugio Citelli (Monte Etna). Longitudine: 15° 3.583'; Latitudine: 37° 45.913'.

Figure 5.11 Shelter Pizzi Deneri peak (2850 m asl). Meteorological sensors were on the top-peak. Longitude: 15° 1.033'; Latitude: 37° 45.899'.
Figura 5.11 Rifugio di Pizzi Deneri (2850 m asl). I sensori metereolgici sono posti sul tetto. Longitudine: 15° 1.033'; Latitudine: 37° 45.899'.

Place name	Place Longitude deg. minutes	Place Latitude deg. minutes	Date	(GMT) Start time hh:mm	(GMT) End time hh:mm
Rifugio Sapienza	15° 0.219'	37° 41.946'	17.07.2003	07:32	10:36
Pizzi De Neri	15° 1.033'	37° 45.899'	19.07.2003	08:38	11:46
Rifugio Sapienza	14° 59.417'	37° 41.721'	20.07.2003	09:21	10:35
Pizzi De Neri	15° 1.033'	37° 45.899'	26.07.2003	08:56	10:32

Table 5.10 Ground meteorological stations measurements (DIMA-RU).
Tabella 5.10 Misure delle stazioni metereologiche di terra (DIMA-RU).

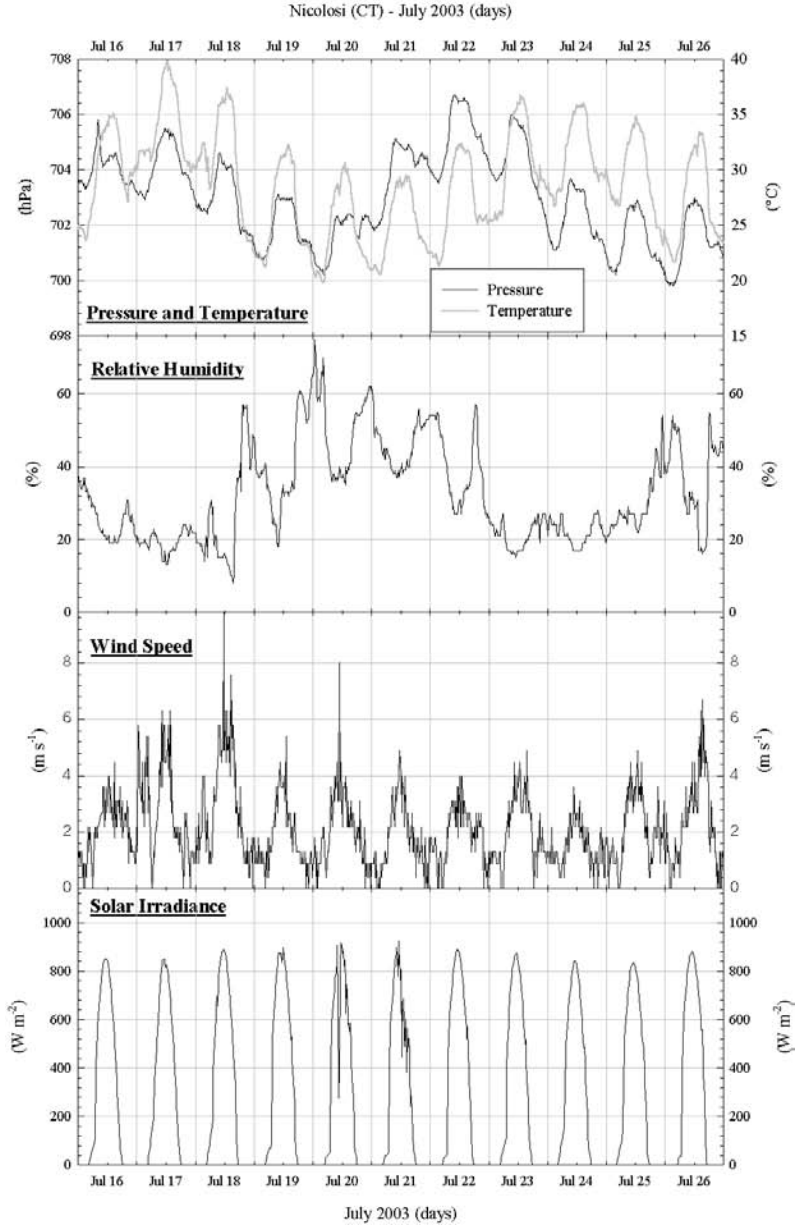

Figure 5.12 The figure shows the trend of the atmospheric fields measured at Nicolosi. The time interval is July 16 - July 26, 2003.
Figura 5.12 La figura mostra l'andamento dei campi atmosferici misurati a Nicolosi dal 16 al 26 Luglio 2003.

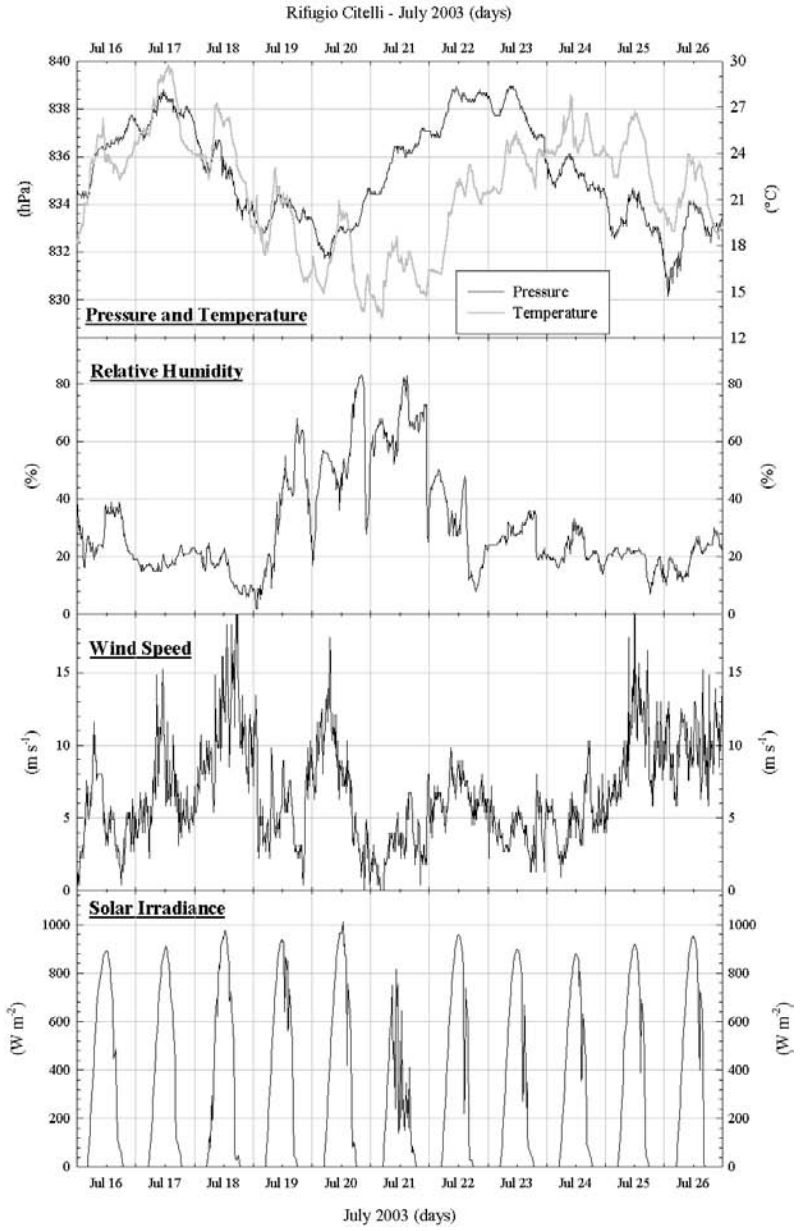

Figure 5.13 The figure shows the trend of the atmospheric fields measured at Rifugio Citelli. The time interval is July 16 - July 26, 2003.
Figura 5.13 La figura mostra l'andamento dei campi atmosferici misurati al Rifugio Citelli dal 16 al 26 Luglio 2003.

Figure 5.12 and Figure 5.13 show the trend of the atmospheric fields measured at Nicolosi and Rifugio Citelli respectively. The time interval is July 16 - July 26, 2003.

Rifugio Citelli is located on the northern flank of Mt. Etna while Nicolosi village is on the southern flank. This means a different microclimate of the two sites. A high pressure filed characterized the weather during the considered period (July 16-26); this reduces the microclimatic effect.

The main difference between the trends measured at Nicolosi and at Rifugio Citelli stations is related to the fact that Nicolosi presents a well-defined daily cycle while this is not so clear in the Rifugio Citelli data.

Another thing can clearly be seen: the barometer of the DAVIS logger is not temperature compensated. The atmospheric pressure directly follows the air temperature. A first analysis of the Nicolosi data indicates a pressure change of about 0.36 (hPa $°C^{-1}$). This will represent a problem computing, GPS zenith hydrostatic delay with a good approximation (see

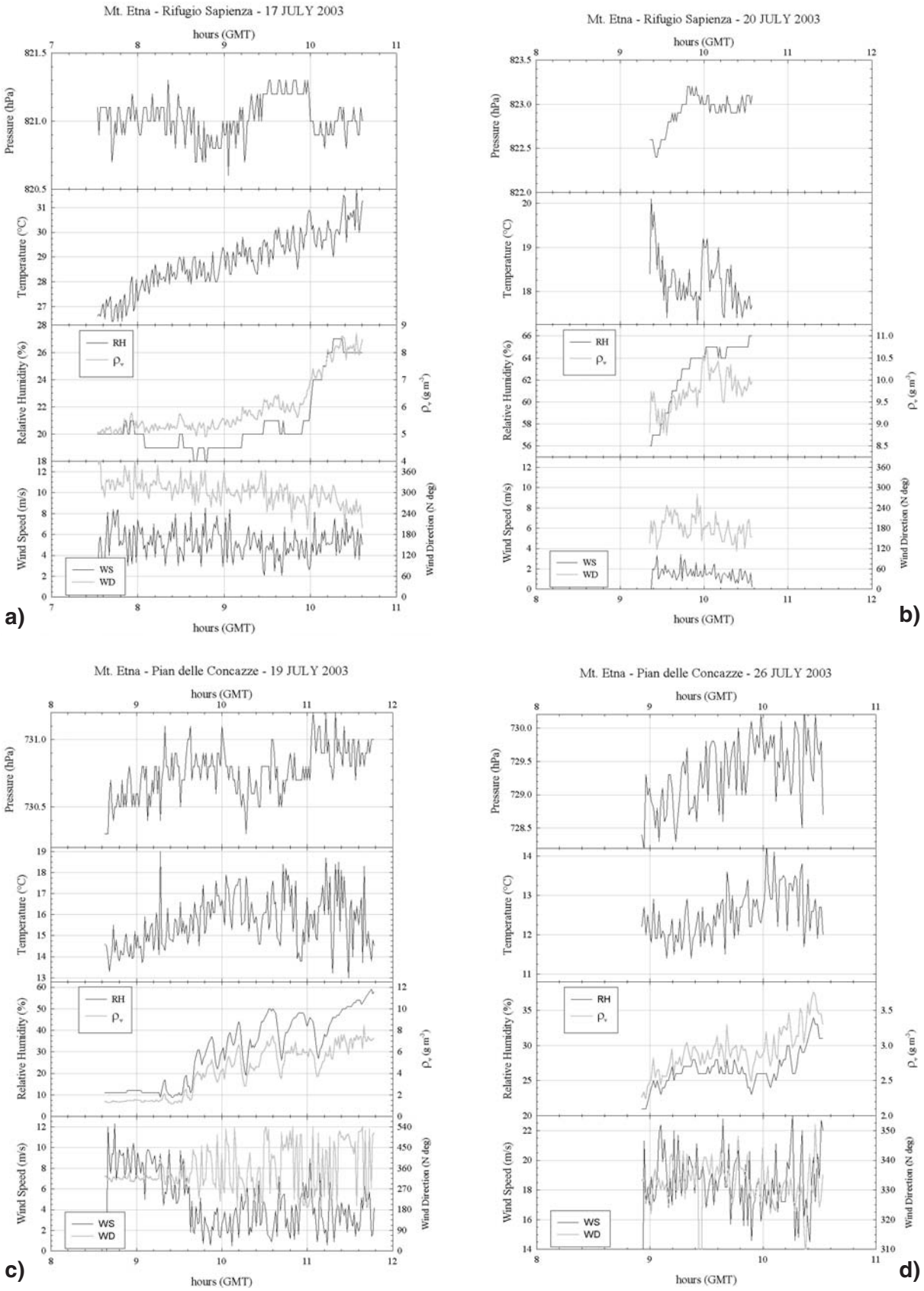

Figure 5.14 a,b,c,d. Meteorological data trend at Rifugio Sapienza using a Pico data logger.
Figura 5.14 a,b,c,d. Andamento dei parametri metereologici al Rifugio Sapienza usando il Pico "data logger".

later; precipitable water using the GPS data).

Figure 5.14a, and Figure 5.14b report the behaviour of pressure, temperature, relative humidity (also water vapour density), wind speed and direction measured using Pico data logger (one minute time step) at Rifugio Sapienza on July 17 and 20, 2003 respectively.

On July 17 atmospheric pressure is practically constant around its mean value of 821.0 (hPa); air temperature clearly shows the daily increase; similarly but, probably related to a dynamic effect (valley breeze), a relative humidity and water vapour density increase can be seen; wind speed is quite constant (about 5 m s^{-1}) while wind direction slowly rotate from the initial north direction to the final east direction.

On July 20 the upper and northern part of Mt. Etna was cloudy. As can be seen the air temperature decreases while the relative humidity again show the typical increase between 9:00 and 10:00 GMT; wind speed and wind direction (about from south) are quite constant.

It must be remarked that DAVIS data indicate as cloudy day July 21. The reason of this is not clear at the moment.

Figure 5.14c, and Figure 5.14d report the behaviour of pressure, temperature, relative humidity (also water vapour density), wind speed and direction measured using Pico data logger (one minute time step) at Pizzi De Neri (close to Pian delle Concazze) on July 19 and 26, 2003 respectively.

On July 19 the weather was sunny and dry (perfect). The atmospheric pressure is practically constant between 730.5 and 731.0 (hPa; mean value 730.76 hPa); air temperature shows the expected increase but also some fluctuations; relative humidity and water vapour density show the expected daily dynamic increase but they also show some fluctuations, similarly to the ones of the temperature; wind speed shows a clear reduction (from about 9 m s^{-1} to about 3 m s^{-1}) while the water vapour increases; wind direction results very stable during the strong wind and fluctuates during weak wind; during the whole period (on 19 July) the mean value of the wind direction is quite stable from north.

On July 26 the weather was sunny, chilly and windy. As can be seen the air temperature is mainly between 12 and 13 °C. Relative humidity again show the typical increase after 10:00 GMT. The wind speed (quite strong) and wind direction (about from north) are quite constant.

5.2.2 Ground meteorological stations (INGV)

The Ingv meteorological station is a portable Davis Vantage pro wireless model [Davis inc., 2003] (Figure 5.15).

The acquired data are transmitted to a console and the controlling software collects the data. In Table 5.11, the precision of the single sensors is reported.

The meteorological data acquired at 1.50m altitude from the ground has been archived by the Log software Ingv made. This software described in cap. 4 permits to acquired the data of GPS, Ground Temperature, Brightness temperature and meteo parameters every 10 seconds. However, meteo parameters are transmitted at the controlling software with a delay, so has been taken every 1 minutes. With this acquisition system is possible to characterise locally in the view angle of the FTIR the temperature of the ground and the temperature of the air, and the correlation between the wind speed and the cooling surface temperature. The station has been situated on the same site of the FTIR. In the Table 5.12 the measurements sites are reported.

It is interesting to note that the 19th July the measurements site were under the volcanic plume. So the measured atmospheric parameters are representing of the plume thermalised.

In the following figures comparison of measurements taken at Mt. Etna and Volcano for air temperature (Figure 5.16), relative humidity (Figure 5.17) and wind speed (Figure 5.18) are reported.

Figure 5.15 Davis Vantage Pro meteorological station.
Figura 5.15 Stazione metereologica Davis Vantage Pro.

Date	Site
17.07.2003	Etna: Pian del Lago. Volcanic scoria and ash
18.07.2003 (night)	Etna: crossway towards Nicolosi.
19.07.2003	Etna: Pian del Lago. Volcanic scoria and ash
20.07.2003	Etna: Pizzo Deneri (Concazze). Volcanic scoria and ash
22.07.2003	Vulcano: pumices and mixed gravels around Volcano edges.
23.07.2003 (Nigth)	Etna: Rifugio Sapienza. Volcanic scoria and ash.
26.07.2003	Etna: Pian del Lago. Volcanic scoria and ash.

Table 5.11 Characteristics of Davis Vantage Pro station sensors.
Tabella 5.11 Caratteristiche dei sensori della stazione Davis Vantage Pro.

Date	Site
17.07.2003	Etna: Pian del Lago. Volcanic scoria and ash
18.07.2003 (night)	Etna: crossway towards Nicolosi.
19.07.2003	Etna: Pian del Lago. Volcanic scoria and ash
20.07.2003	Etna: Pizzo Deneri (Concazze). Volcanic scoria and ash
22.07.2003	Vulcano: pumices and mixed gravels around Volcano edges.
23.07.2003 (Nigth)	Etna: Rifugio Sapienza. Volcanic scoria and ash.
26.07.2003	Etna: Pian del Lago. Volcanic scoria and ash.

Table 5.12 INGV Meteorological station measurements sites.
Tabella 5.12 Siti di misura delle stazioni metereologiche INGV.

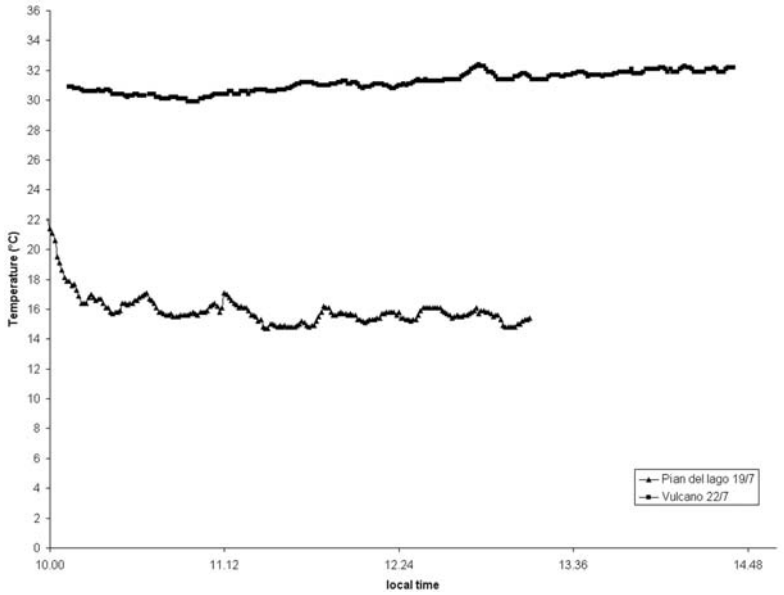

Figure 5.16 Example of Air temperature measurements.
Figura 5.16 Esempio di misure di temperatura dell'aria.

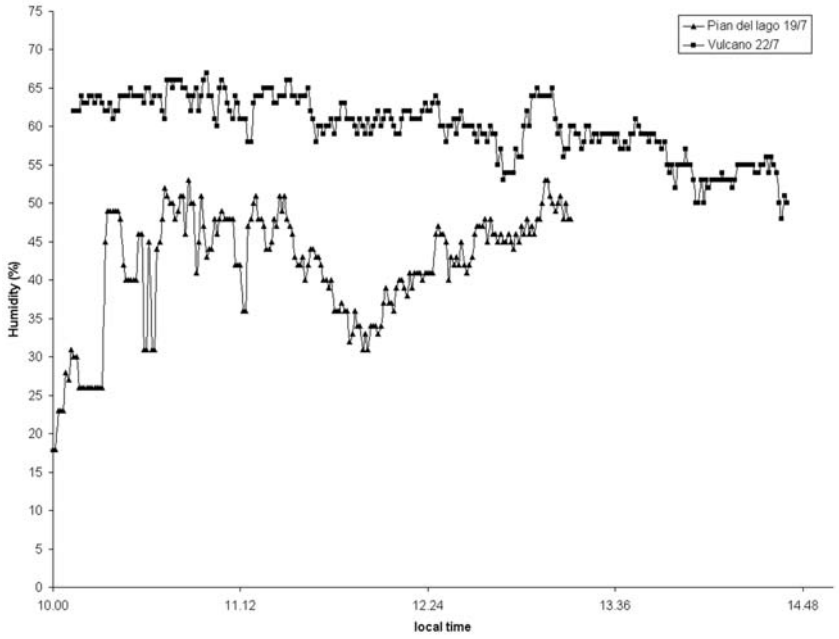

Figure 5.17 Example of relative humidity measurements.
Figura 5.17 Esempio di misure di umidità relativa.

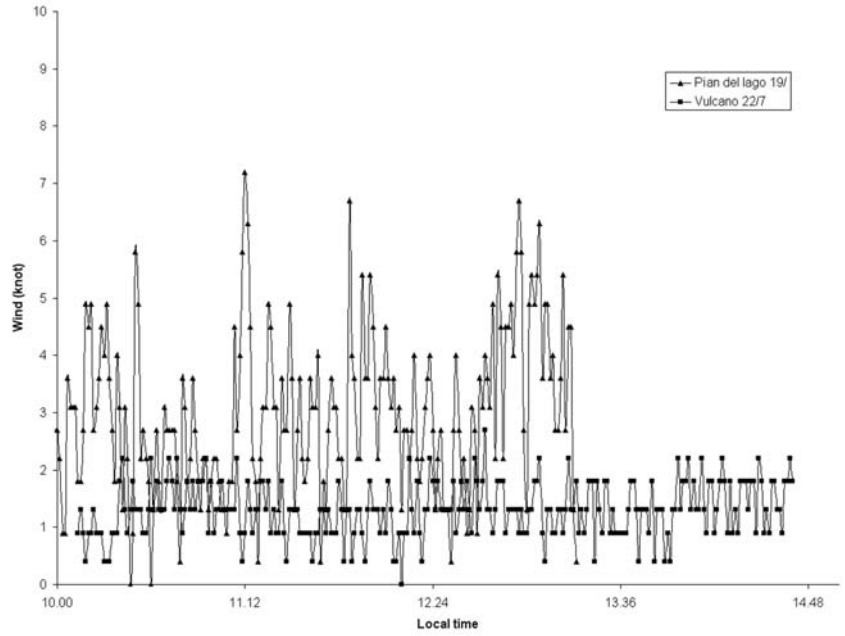

Figure 5.18 Example of wind speed measurements.
Figura 5.18 Esempio di misura di velocità del vento.

5.3 Aerosol and precipatable water measurements

5.3.1 Lidar and Sunphotometer observations (ISAC-CNR)

ISAC-CNR participated in the FASA-Satellite campaign by deploying the VEhicle-mounted LIdar System, VELIS [e.g., Gobbi et al. 2000] and a MICROTOPS sunphotometer. During the campaign VELIS was located at Milo (37° 43.876' N - 15° 6.767' E, 815 m asl), approximately 11 km east of the Mt. Etna sum-

mit. Both VELIS and the MICROTOPS operated from July 16 until July 27. The periods and number of relevant observations are reported in Table 5.13:

DAY	START (UT)	STOP (UT)	VELIS Profiles	Microtops Records	PLUME	WIND (kts) @3000m	NOTES
16.07.2003	09.01	18.10	9	23	$C_{am} - L_{am}$	SW, 30	Dust (am+pm)
17.07.2003	07.28	22.00	18	42	$C_{am} - L_{am}$(?)	NW, 25	Dust (am+pm)
18.07.2003	09.08	18.46	10	18	$C_{am} - L_{am}$(?)	NW, 40	Dust (am)
19.07.2003	07.40	17.43	19	51	L_{am}	NE, 20	
20.07.2003	07.50	15.00	14	48		N-NW, 15	
21.07.2003	08.57	19.48	11	21	L_{am}	N, 10	
22.07.2003	09.18	19.48	15	39		N/A	Dust (pm)
23.07.2003	09.10	19.38	10	36	L_{am}(?)	NW, 15	Dust (am+pm)
24.07.2003	08.42	19.32	10	30	$C_{am} - L_{am}$(?)	NW, 15	Dust (am+pm)
25.07.2003	08.20	19.00	21	54	$C_{am} - L_{am+pm}$	W-NW, 35	Dust (am+pm?)
26.07.2003	07.10	19.52	20	54	L_{am+pm}(?)	NW, 45	Plume transect
27.07.2003	11.00	14.01	6	21	L_{am}	N-NW, 25	

Table 5.13 Operation times of the VELIS lidar and Microtops sunphotometer at Milo. Plume presence over Milo is reported when detected by the INGV-Catania Cospec (C) or by the lidar (L). Question marks (?) indicate uncertain assessment.
Tabella 5.13 Tempi operative del lidar VELIS e del fotometro Microtops a Milo (CT).

Lidars operate by sending laser pulses into the atmosphere and collecting the backscatter light by means of telescopes provided with highly sensitive photodetectors. Similarly to radars, the return time of the laser pulse indicates the distance of the scattering object. Analysis of the signal intensity allows for retrieval of physical and chemical properties of the atmospheric constituents.

VELIS is a compact polarization system operating at 532 nm and developed for day and night field observations of aerosol and thin clouds between 150 m and 20 km altitude above the lidar site. Time and altitude resolution of the profiles are 5 min and 37.5 m, respectively. VELIS-retrieved variables are: aerosol extinction (σ) and backscatter (β) coefficients, backscatter and depolarization ratios (R and D), plus aerosol volume and surface area [e.g., Gobbi, 1998; Barnaba and Gobbi, 2001]. The backscatter ratio R represents the aerosol versus molecular contribution to backscatter, while D indicates the ratio between radiation backscattered on the perpendicular and parallel planes, with respect to the laser beam one:

$$R = 1 + (\beta_{aerosol} / \beta_{molecular}) \quad (1)$$

$$D = \beta_{Perpendicular} / \beta_{Parallel} \quad (2)$$

Since spherical particles (as liquid aerosol) do not depolarize while non-spherical ones do, the aerosol thermodynamic phase (liquid, solid or mixed) can be inferred from the depolarization measurement [e.g., Gobbi et al., 2000].

The MICROTOPS sunphotometer measures aerosol optical thickness (AOT, i.e., the integral of aerosol extinction over the whole atmosphere) at four wavelengths (λ = 440, 500, 675 and 1020 nm) plus total precipitable water (PW), i.e., the total column (cm) of water vapor

if condensed at STP. The spectral behavior of the aerosol optical thickness is related to the dimension of the particles suspended in the atmosphere. In fact, sub-micron particles shows a marked spectral dependence (AOT (λ) $\propto \lambda^{-a}$, with $1 < \alpha < 4$), whereas the presence of supermicron particles strongly reduces such dependence ($\alpha < 1$). For the campaign period, the parameter α (generally referred to as Angstrom coefficient) has been computed from the MICROTOP AOT record as:

$$\alpha = - [\ln (AOT_{500} / AOT_{1020}) / \ln (500/1020)] \quad (3)$$

where AOT_{500} and AOT_{1020} refer to AOT (λ= 500 nm) and AOT (λ = 1020 nm), respectively.

5.3.1.1 Lidar Observations

Lidar profiles representative of the various conditions encountered during the campaign are presented in Figure 5.19. In particular, Figure 5.19 reports a profile collected during the Dornier 228 flight of July 17, showing the aerosol and dust layer extending from the ground up to 6 km.

The Mt. Etna plume was also embedded in this layer (e.g.,Table 5.13), possibly in the region at ≈ 3.5 km. Figure 5.19 (July 19, second flight of the Dornier 228) reports a case of Mt. Etna plume detection, as revealed by a layer at 2.8 km and of a second, broader one at 2 km. It is interesting to note that the plume shows depolarization levels D ≈ 10%, indicating the presence of solid particles within a plume mainly composed of liquid ones. AOT_{500} in this case is ≈ 0.25 and $\alpha \approx 1.3$, i.e., plume particles are submicrometric. Figure 5.19 describes the conditions of July 25, when again Saharan dust and the Mt. Etna plume were located over Milo. In this case, the dust reached up to ≈ 5.5 km while the plume was mainly located at 3 km. $AOT_{500} \approx$ 0.5 and $\alpha \approx 0.4$ indicate the optical depth to be mainly determined by Saharan dust supermicron particles. In both Saharan dust events the plume seemed to ascend above the craters level, while it usually descended below in normal conditions. Figure 5.19 shows observations collected on July 26, at about 17 UT. Only boundary layer aerosol as present at that time. Milo was right at the northern edge of the Mt. Etna plume (see also next section), which is just visible by the increase in backscatter and depolarization between 2 and 3.5 km in the lidar trace.

A complete picture of the lidar record during the campaign is given in Figure 5.20, showing a contour plot of the VELIS-measured aerosol extinction from 1 km (i.e., ≈ 150 above the observational site) up to 10 km. The variability of the aerosol load observed during the campaign is clearly visible in this plot. Typical local aerosol conditions (particles below 3 km,

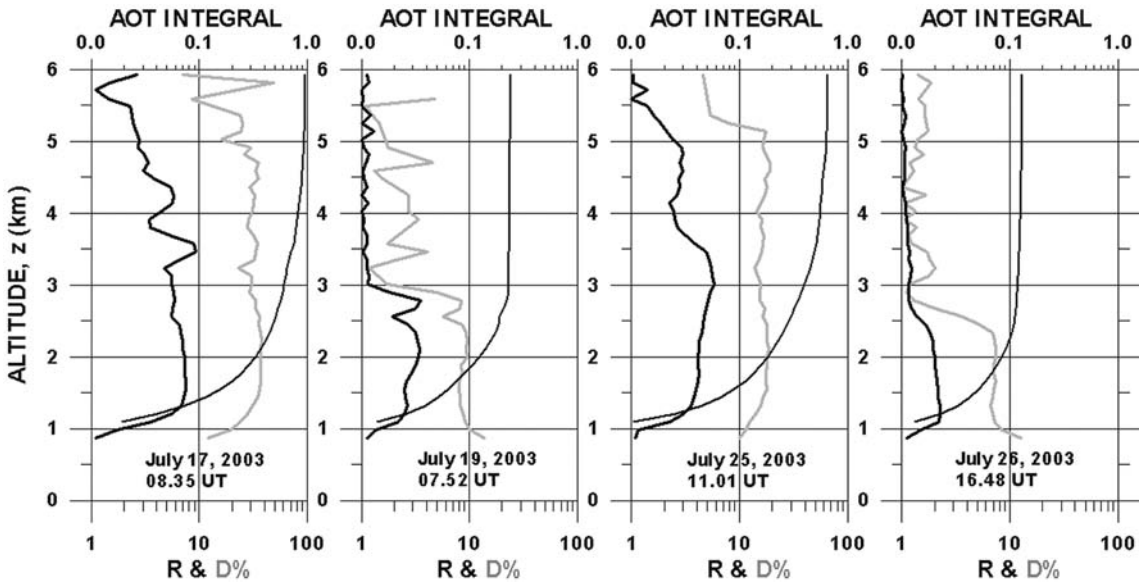

Figure 5.19 VELIS profiles of backscatter ratio R (thick black line), depolarization ratio D% (thick gray line) and integral AOT (from ground up to z, dotted black line), as measured at Milo during the FASA campaign.

Figura 5.19 Profili VELIS del rapporto di retrodiffusione (linea nera spessa), del rapporto di depolarizzazione (linea grigia spessa), ed AOT integrale (da terra fino a z, linea nera tratteggiata), misurati a Milo durante la campagna FASA.

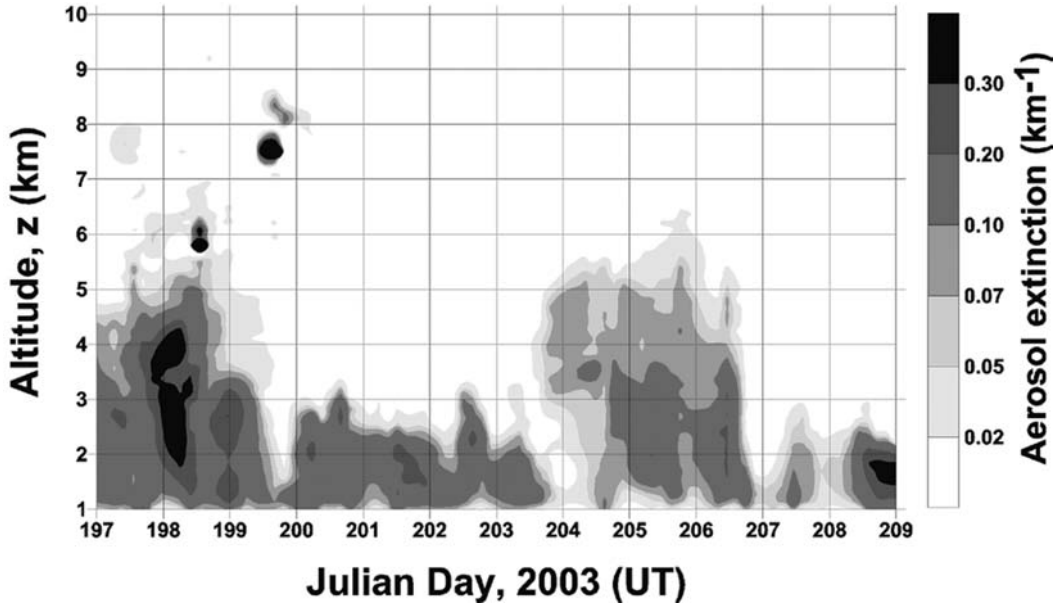

Figure 5.20 Contour plot of aerosol extinction at 532 nm as observed by the VELIS lidar during the FASA campaign (Julian days 197-208 correspond to the period July 16-27).
Figura 5.20 Contour plot del coefficiente di estinzione a 532 nm osservato con il lidar VELIS durante la campagna FASA dal 16 al 27 Luglio 2003.

mainly liquid, i.e. hygroscopic) are only observed in the periods July 18(pm)-22(am) and July 26-27. In the remaining periods (July 16-18(am) and 22(pm)-25) two major dust events affected the atmospheric visibility up to 6 km, showing rather high extinction coefficient (σ > 0.05 km^{-1}) up to 5 km.

5.3.1.2 SunPhotometer Observations

The total record of aerosol optical thickness at 500 nm, AOT_{500}, and of the Angstrom coefficient, α, is presented in Figure 5.21.

Similarly to the lidar retrievals, the sunphotometer record shows that two Saharan dust events were registered over the site during the

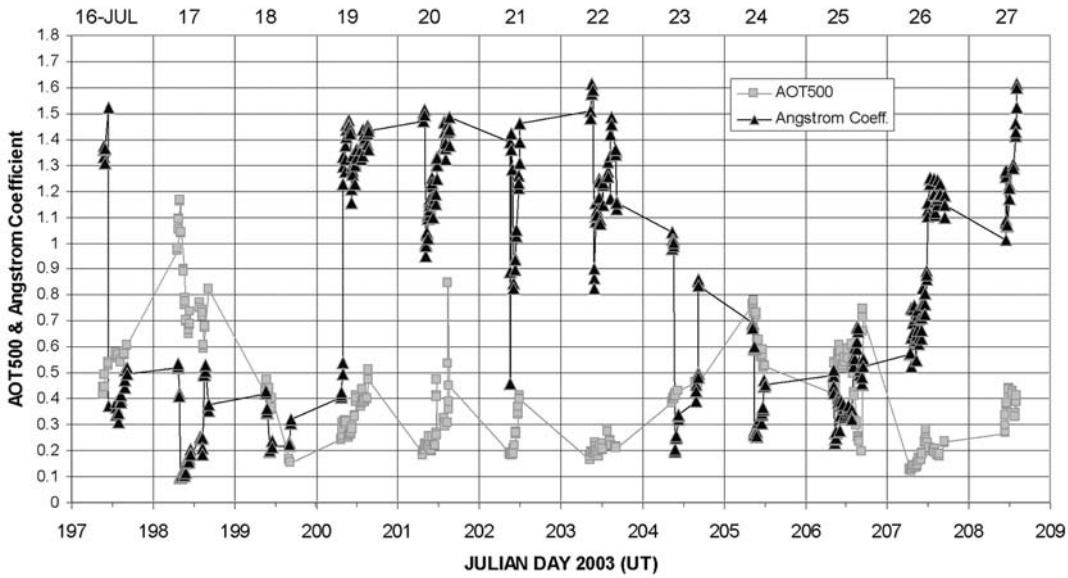

Figure 5.21 The sunphotometer 500 nm AOT and Angstrom Coefficient (a) measured during the FASA campaign at Milo.
Figura 5.21 AOT a 500 nm AOT e coefficiente di Angstrom (a) misurato dal fotometro durante la campagna di misura FASA a Milo.

FASA campaign (16-18 July and 23-25 July, see alsoTable 5.13). These events are characterized by a sharp increase in AOT (in the range 0.8-1 at 500 nm) and a corresponding decrease in α (0.1-0.5). In fact, as already mentioned, values of $\alpha > 1$ are typical of small, sub-micron aerosol sizes, while super-micron aerosols generate Angstrom coefficients $\alpha < 1$. In particular, Saharan dust was present during the DLR-Dornier 228 flight of July 17, with $AOT_{500} \approx 1$ and $\alpha \approx 0.3$.

Figure 5.22 reports sunphotometer observations made on July 26 during a 6-km, N-S-N transect from Milo to Zafferana and back to

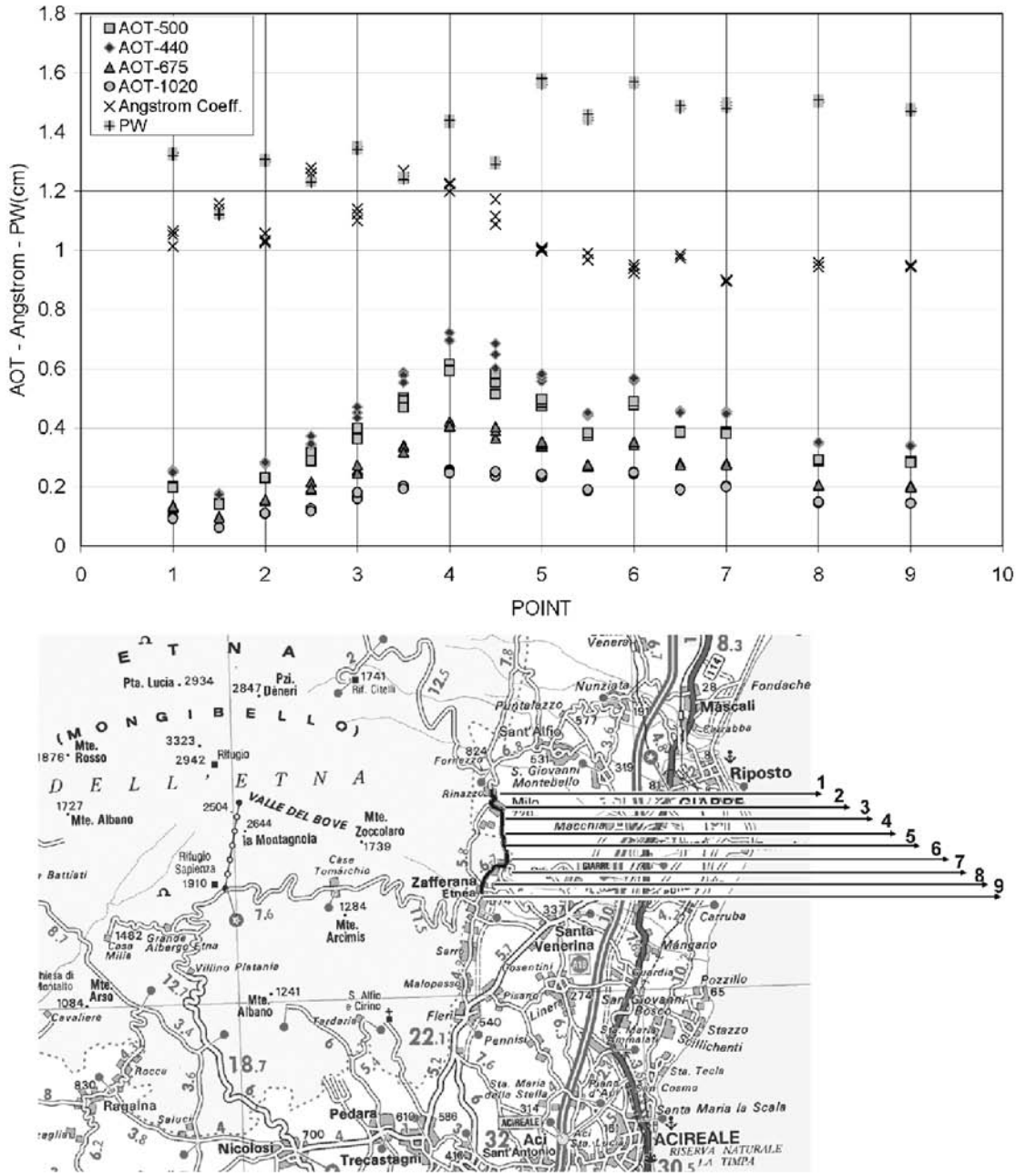

Figure 5.22 (a) Sunphotometer transect across the Mt. Etna plume on 26-07-03 at 15.40 - 16.40 UT. Aerosol optical thickness at 440 nm (diamonds), 500 nm (square), 675 nm (triangle) and 1020 nm (circle) is reported together with precipitable water (PW, cm) and Angstrom coefficients (crosses). Measurement points (1-9, along a 6 km road) are reported in the map (b) by increasing-length arrows. Fractional points (.5) represent the return transect

Figura 5.22 (a) Misure fotometriche eseguite attraverso un transetto comprendente del plume dell'Etna il 26-07-03 alle 15.40 - 16.40 UT. (b) I punti di misura sono riportati sulla mappa ed indicati dalle frecce.

Milo (fractional points, e.g. 1.5, represent the return trip measurement at point 1).

The transect was performed between 15.40 and 16.40 UT, i.e. just before the lidar observation of Figure 5.19d. Figure 5.22 shows the maximum of the plume ($AOT_{500} \approx 0.6$ and $\alpha \approx 1.2$) to be located at point 4, i.e., 2 km south of Milo. With respect to the background values, the plume is characterized by an increase of ≈ 0.4 in AOT_{500} and ≈ 0.2 cm in PW. The anticorrelated behavior of α and PW clearly reveals the hygroscopic growth of the plume particles. These observations confirm that at that time the plume was mainly composed by submicron particles in the liquid phase. However, as in the case of July 19, the lidar depolarization of Figure 5.19d reveals that some solid matter (≈ 20%) contributed to the total volume of the plume particles.

5.3.2 Photometric measurements (DIMA-RU)

Two different sun photometers were available during the field campaign: Cimel CE 318, installed at Nicolosi (CT), on the roof of the INGV building (736 m asl; Longitude: 15° 1.166' E; Latitude: 37° 36.810' N; see (Figure 5.9) and a mobile Cimel CE 317.

The CE 318 is part of the NASA AErosol RObotic NETwork (AERONET; it is #254) http://aeronet.gsfc.nasa.gov/. The #254, Mt. Etna data, are available and downloadable at this site: http://aeronet.gsfc.nasa.gov/cgi-bin/type_one_station_new3?site=ETNA&nachal=1&level=1.

The central wavelength of each band of the CE 318 (AERONET #254) was measured at NASA during calibration (end of year 2002). Photometer #254 was installed at Nicolosi in February 2003. Initially the instrument doesn't work properly, it shown a tracking problem. We waited a new ring to reduce (possible saturation of the a sensor) the light entering the optical window, which drive the fine track operation. In July, just before Sicily 03 campaign, the real reason of the problem was known and repaired: it was a pin of the optical head connector.

The two photometers (CE 317 and CE 318) have different spectral characteristics but four bands (considered standard) have the same nominal central wavelength. The central wavelength and the calibration constant of each band are reported in Table 5.14. The bandwidth of all the bands (except band 5 of CE 317, which is 40 nm) is about 10 (nm).

Bands (or channels) 5 and 6 of CE 317 are related to precipitable water and are not calibrated because the method to compute precipitable water with CE 318 is different from that foreseen for CE 317. In fact, CE 317 uses two channels with the same central wavelength and different bandwidth while CE 318 uses only one channel in the tau absorption band of the water vapour. The water vapour transmittance in the tau absorption band (about 940 nm) is assumed to be $T_w = \exp(a * w^b)$. Where w is the total precipitable water along the slant column (i.e. $w=m \cdot PW$); m is the relative air mass and PW is the precipitable water (in the vertical direction). The two constants (a and b) have the following values: $a = 0.6548$; $b = 0.574$. The field of view (FOV) of CE 317 is one degree; the FOV of CE 318 is 1.2 degrees.

The portable sun photometer CE 317 was used in the places and in the time intervals reported in Table 5.15.

It shows the total ozone abundance measured by TOMS over the Mt. Etna.

Photometer	band 1	band 2	band 3	band 4	band 5	band 6	band 7	band 8
CE 318 λ (nm)	1019.7	870.2	674.5	439.4	501.5	940.2	380.0	340.3
CE 318 calibration	17803.9	15728.5	19067.4	13344.0	15241.4	18900.5	48285.4	42058.6
CE 317 λ (nm)	1020	870	670	440	936	936	----	----
CE 317 calib.const.	17742	28104	24199	9296	----	----	----	----
CE 317 St.Dev.	198	205	134	53	----	----	----	----

Table 5.14 CE 318 and CE 317 wavelengths and calibration constants.
Tabella 5.14 Costanti di calibrazione per CE 318 e CE 317 alle diverse lunghezze d'onda.

Place	Date	Long (deg)	Lat (deg)	Alt (m)	Start GMT	End GMT	O_3 (DU)
Rif. Sapienza	17.07.2003	15.00	37.70	1895	07:40	10:00	279
Pian Concazze	19.07.2003	15.01	37.77	2793	09:10	11:10	304
Pian Concazze	26.07.2003	15.01	37.77	2793	09:40	10:20	305

Table 5.15 Sun photometric measurement: place, date, time interval and O_3.
Tabella 5.15 Misure fotometriche: luogo, data, tintervallo temporale e O_3.

These ozone data were used to compute AOT from the raw CE 317 data. CE 317 AOTs are shown in Figure 5.23, Figure 5.24 and Figure 5.25.

The large AOT values on July 17 (Figure 526) are due to a dust event (from Sahara desert). AOT at Nicolosi (736 m asl) and at Rifugio Sapienza (1800 m asl) are practically the same; aerosols were above.

The trend on July 19 (a lot of fluctuations between 9:30 and 10:00) should be due to liquid aerosols coming directly from the volcanic plume. The Northeast crater is close to Pian delle Concazze where these measurements were done. The wind direction was from 240-270 north degrees (i.e. mainly from east and a little bit from south). See also meteorological data (relative humidity at Pizzi De Neri). On July 19 a small cloud formed and disappeared just above the Pizzi De neri Peak.

Vice versa, on July 26 the atmosphere was very clear due to a strong wind coming mainly from the north. AOT at 1020 (nm) is larger than the other wavelengths.

The value of the Angstrom turbidity parameter alpha (the exponent of the wavelength) is related to the particle size distribution. The typical alpha value is 1.3-1.4. Small value of alpha (lower than 1) means mainly large particle dimension, vice versa, big alpha value (greater than 2) means mainly particles of small dimension. From CE 318 data (Nicolosi) an

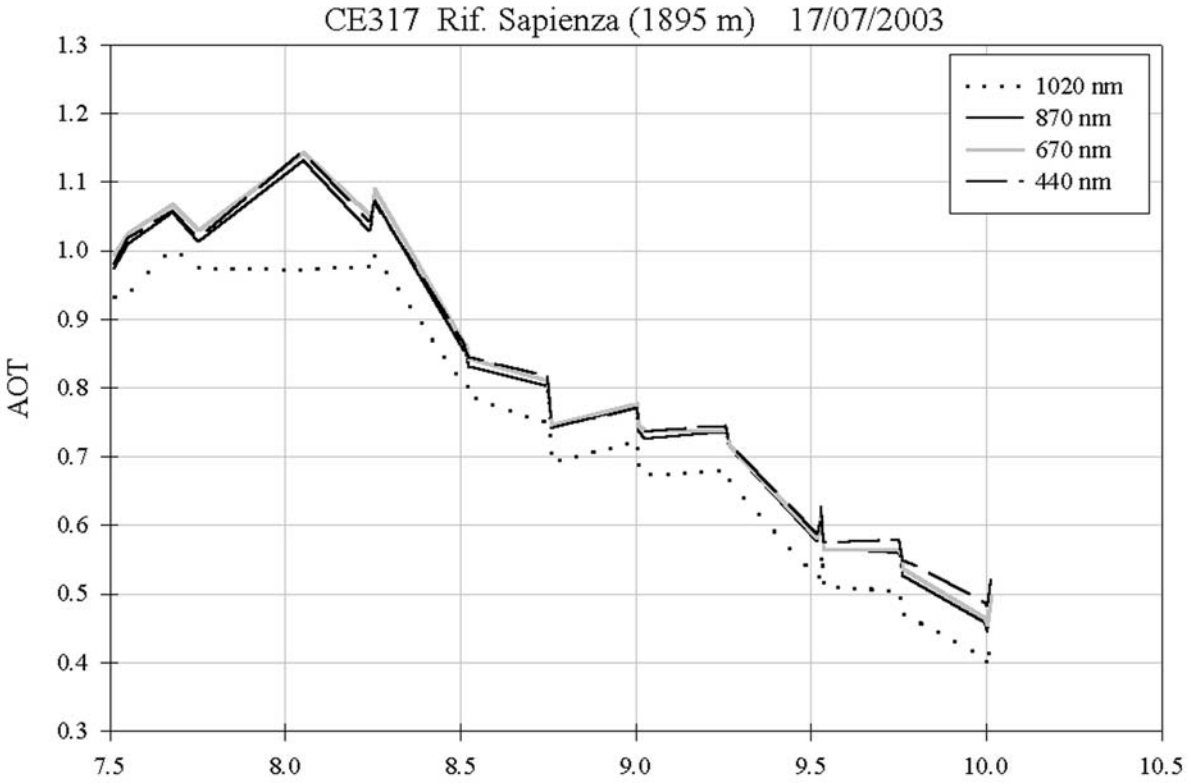

Figure 5.23 Rifugio Sapienza – July 17 2003. The ozone data (see Table 5.15) were used to compute AOT from the raw CE 317 data.
Figura 5.23 Rifugio Sapienza – 17 Luglio 2003. I dati dell'ozono sono stati utilizzatii per calcolare l'AOT dal dato grezzo CE 317.

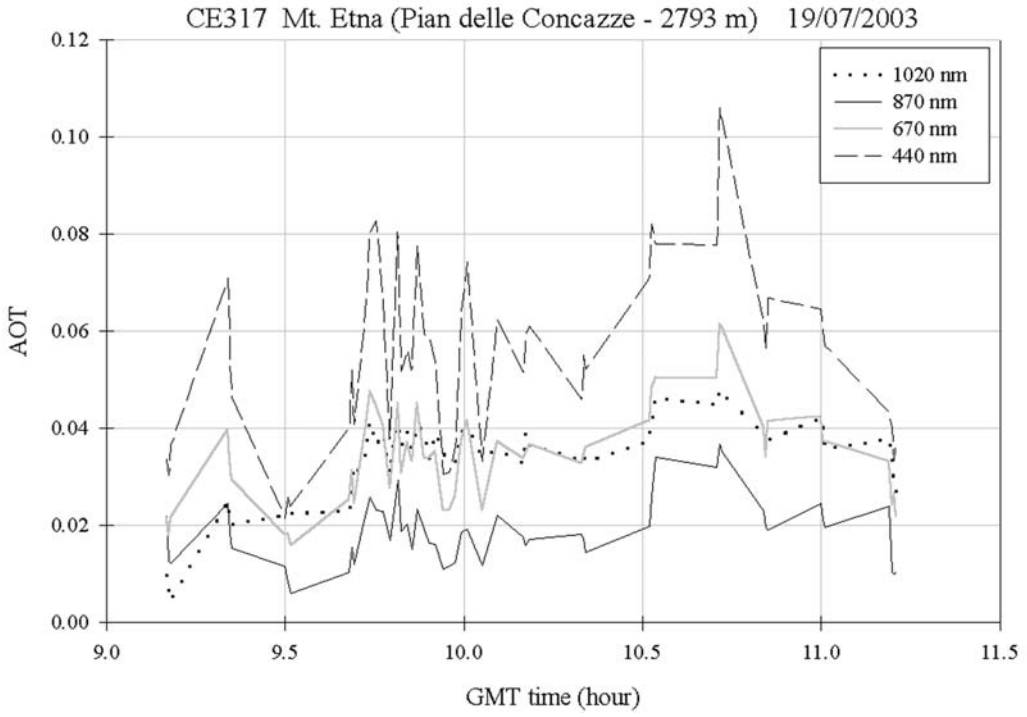

Figure 5.24 Pian delle Concazze – July 19 2003. The ozone data (see Table 5.1 5) were used to compute AOT from the raw CE 317 data.
Figura 5.24 Pian delle Concazze – 19 Luglio 2003. I dati dell'ozono sono stati utilizzatii per calcolare l'AOT dal dato grezzo CE 317.

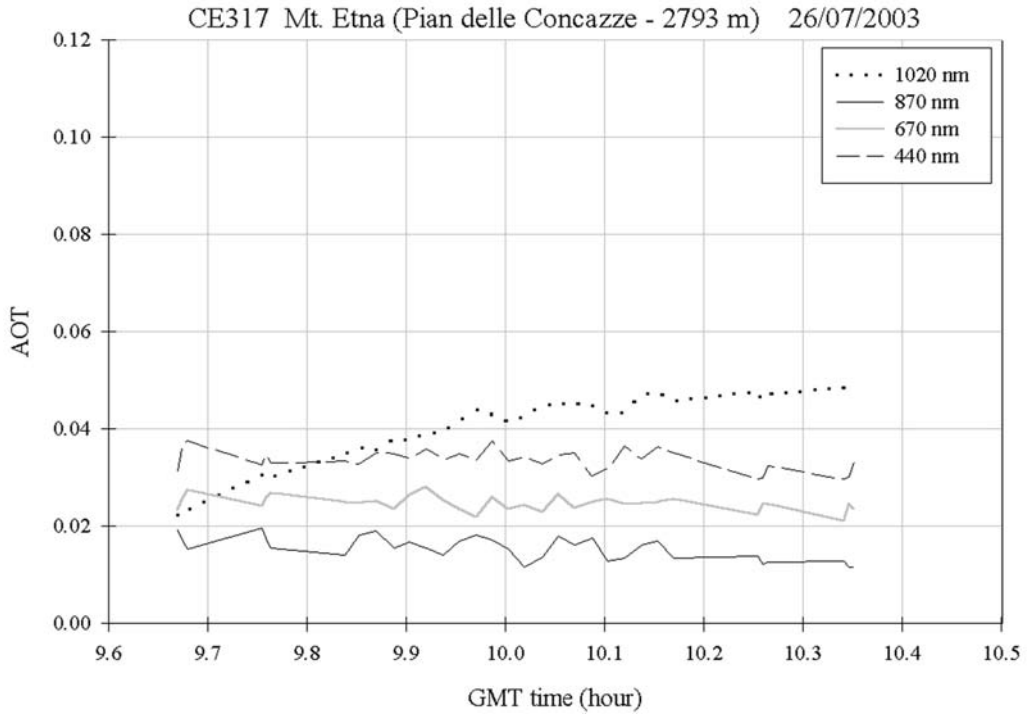

Figure 5.24 Pian delle Concazze – July 19 2003. The ozone data (see Table 5.1 5) were used to compute AOT from the raw CE 317 data.
Figura 5.24 Pian delle Concazze – 19 Luglio 2003. I dati dell'ozono sono stati utilizzatii per calcolare l'AOT dal dato grezzo CE 317.

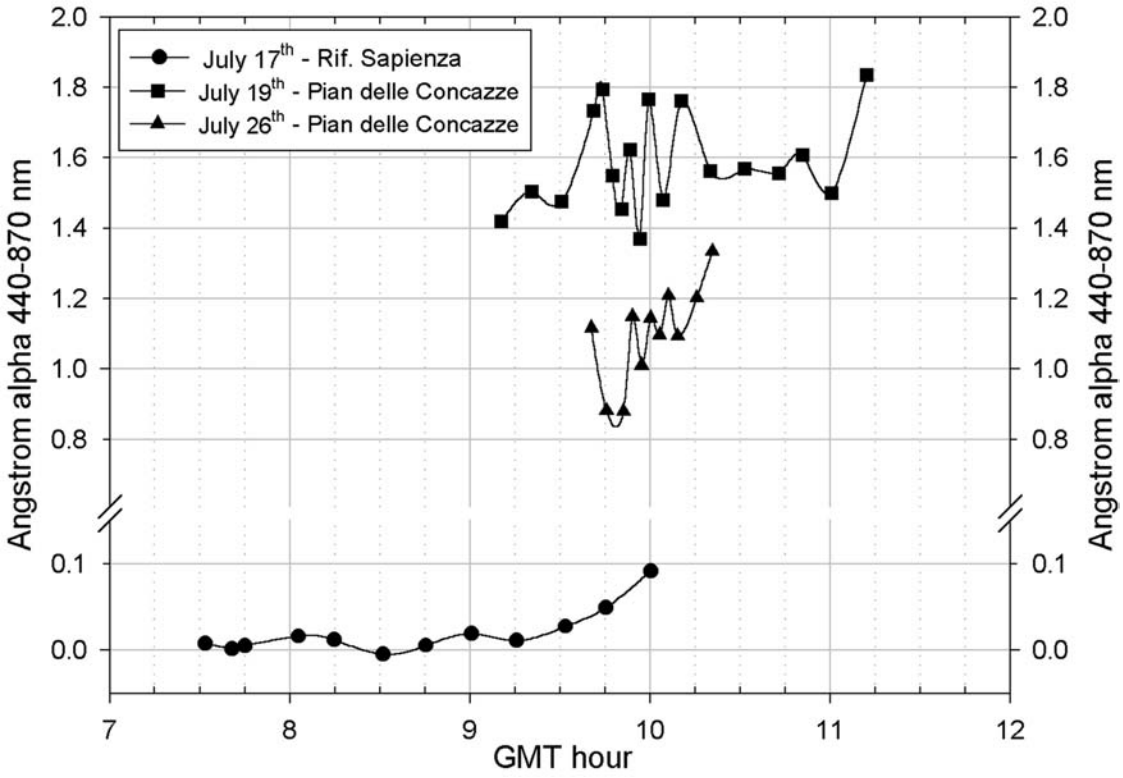

Figure 5.26 July 17, 19, 26 – Alpha trends parameter as measured at Rifugio Sapienza and Pian delle Cocazze.
Figura 5.26 17, 19, 26 Luglio 2003 – Andamento del parametro Alpha misurato al Rifugio Sapienza e Pian delle Cocazze.

alpha (440-870) value of about 1.6±0.2 can be usually seen. Small values (in the range 0.0-0.4) were found during the dust events (July 16, 17, 18 and 24, 25).

Finally, Figure 5.26 shows the trend of alpha parameter as measured at Rifugio Sapienza (July 17, dust event) and at Pian delle Cocazze on July 19 (no dust but water droplets fluctuations) and 26 (after a second dust event).

5.3.3 Precipitable water measurements (DIMA-RU)

The total Precipitable Water (PW) in the vertical direction can be directly computed using the vertical atmospheric profiles of pressure, temperature and relative humidity. The atmospheric water vapour is, in fact, present only in the first 10-12 kilometres (i.e. altitude usually reached by the meteorological sonde).

Again, precipitable water can be estimated considering the absorption bands of the water vapour in the Near Infrared (NIR) range. Sun photometric readings estimate PW measuring the attenuation of the solar irradiance at 940 (nm). AOT at 940 (nm) is obtained interpolating the AOT values at 870 and 1020 (nm). Of course, these measurements may be done only when the sun is present.

Finally, a new methodology to investigate the precipitable water is related to the analysis of the tropospheric delay of an electromagnetic signal (e.g. GPS signal). The tropospheric delay depends on dry air and water vapour densities along the atmospheric path (a specific mapping function is used to have the vertical part). The so named Zenith Total Delay (ZTD=ZHD+ZWD*) is the sum of two terms: Zenith Hydrostatic Delay (ZHD) and a part of the Zenith Wet Delay (i.e. ZWD*). The atmospheric pressure measured at the GPS antenna permits to estimate ZHD=0.002277 Ps. From the wet part: PW=ZWD* 0.15 (Bevis et al. 1992). That is: PW = 0.15 (ZTD – 0.002277 Ps). The delays are in (m) and the pressure in (hPa).

Comparison among GPS results and other different type of instruments (e.g. microwave radiometer and sun photometer) and also with meteorological models have been done (Pugnaghi et al. 2002).

From June 2003 (see

Code	Site description	Receiver
EIIV	Catania P. Roma INGV build	Trimble 4000
NICO	Nicolosi INGV building	Trimble 4700
ESLN	Serra la Nave – Oss. Astrofisico	Trimble 4000
EMEG	Monte Egitto	Trimble 4700
EMAL	C.da Monte Maletto	Trimble 4700
EMFN	Monte Fontane	Trimble 4700
EFAR	C.da Farelle	Trimble 4700
EMGL	Etna Monte Gallo	Trimble 4700

Table 5.16 List of the eight standard INGV GPS stations.
Tabella 5.16 Lista delle otto stazioni GPS standard dell'INGV.

http://www.ct.ingv.it/UfDGG/DispositiviMisura.htm) the standard Mt. Etna GPS INGV network has eleven stations. We had (Giuseppe Puglisi) the GPS data (July 14-26) of eight of the eleven standard stations; they are reported in Table 5.16

The analysis of the GPS data is under work but some first results are already available. They are reported in Figure 5.22. The Bernese 4.2 software was used to analyse GPS data. The procedure used to compute the PW data shown in Figure 5.22 uses three International Geodynamic Stations (IGS): Noto (SR), Matera and Medicina (BO). The analysis of the data of the three aforementioned IGS stations together with the station of Nicolosi gives the results of Figure 5.22. Two hours GPS integration results were reported in Figure 5.22; the mean difference between GPS data and sun photometer data is 2.0±2.8 mm.

It must be remarked that some GPS data present high ambiguity reducing the possibility of a good estimation of the PW. In particular on July 15 (DOY 196) and on July 22 (DOY 203) only Matera and Medicina of the three IGS stations were used due to the large number of ambiguities in the Noto measurements.

5.4 Solar irradiance

ASD FieldSpec Pro FR portable, battery powered, spectroradiometer permits to detect individual absorption features due to specific chemical bonds in a solid, liquid or gas. Detection is dependent on the spectral range, spectral resolution, and signal-to-noise of the spectrometer (parameters that describe the instruments capability), the abundance of the material and the strength of absorption features for that material in the wavelength region measured (see Par. 5.1).

The spectrometer (Table 5.17) permits to operate in three detector ranges, 350-1050 nm, 1000-1800 nm, 1800-2500 nm, with just one instrument.

Then the radiation is led by an optic fibre into the detector system with 10 nm spectral resolution where wavelength components are separated and reflected for independent collection by the detectors. The original field of view is 25°. With a foreoptic it can be reduced up to 1°.

The optimisation of the spectroradiometer is performed immediately prior to the start of data collection. This process may need to be repeated periodically.

Each spectrometer detector converts the incident photons in electrons and accumulates a signal over a period defined by the integration time (typically set at 17 milliseconds). The integrated signal is converted to a voltage and then digitised by a 16-bit analogue to digital (A/D) converter.

The instrument is controlled and data displayed and stored using a notebook computer providing foreoptic information, recording dark current and registered spectra. Since the dark current varies with time and temperature it is gathered for each integration time. Spectral data from ASD FieldSpec Pro FR spectroradiometer has been obtained for several test-sites locations spread across the study area.

The ASD FieldSpec Pro FR spectroradiometer has also been also used to make solar irradiance measurements with a field of view of 180° on a horizontal receiver surface. Solar irradiance at the ground depends to a great extent on solar elevation angles. Their diurnal variations are maximum in June. The daily maximum of solar elevation occurs at 12 TST (True Solar Time). The spectrometer unit and computer are carried on a special tripod, while power is supplied from a battery pack carried around the waist. The Remote Cosine Receptor (RCR) is used for the purpose of global irradiance meas-

Name	FieldSpec® Pro FR
Spectral Range	350-2500 nm
Spectral Resolution	3 nm @ 700 nm 10 nm @ 1400 & 2100nm
Sampling Interval	1.4 nm @ 350-1050 nm 2 nm @ 1000-2500 nm
Scanning time	100 milliseconds
Detectors	One 512 element Si photodiode array 350-1000 nm Two separate, TE cooled, graded index InGaAs photodiodes 1000-2500 nm
Input	1.4 m fiber optic (25° field of view) Optional foreoptics
Calibration	Wavelength, reflectance, radiance*, irradiance*. All calibrations are NIST traceable (*radiometric calibrations provided)
Noise Equivalent Radiance (NeDL)	UV/VNIR 1.4 x 10^{-9} W/cm^2/nm/sr @ 700nm NIR 2.4 x 10^{-9} W/cm^2/nm/sr @ 1400nm NIR 8.8 x 10^{-9} W/cm^2/nm/sr @ 2100nm
Notebook Computer	Pentium processor, 800 MB hard disk, 16 MB Ram, 3.5" floppy disk drive, battery, AC power supply
Weight	7.2 kg or 15.8 lbs

Table 5.17 FieldSpec® Pro FR instrument characteristics.
Tabella 5.17 Caratteristiche dello strumento FieldSpec® Pro FR.

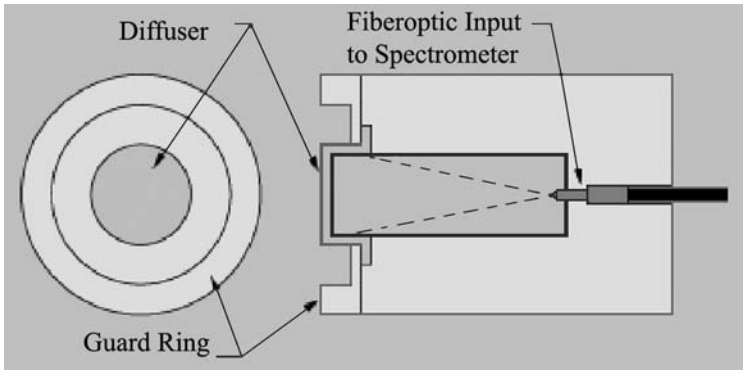

Figure 5.27 Instrumental receptor (RCR) scheme.
Figura 5.27 Schema del rivelatore strumentale.

urements. The RCR is attached to the fiber-optic probe and this enable it to collect the radiant flux incident on a receiving surface from all direction per unit of area in unit of W m-2 nm-1. The RCR is a tube with one end covered by a diffusion-disc (Figure 5.27). The bubble level atop the tripod level is used so that the optics are pointing straight up. Solar irradiance measurements are collected by notebook about every 15 minutes from 350 nm to up 2500 nm.

5.4.1 Global and direct spectral Irradiance measurements IMAA - CNR

In Table 5.18 type and sites of measurements are reported. The first measurement site was at the Hotel S. Tecla (37°.36'N, 15°10'E), few meters a.s.l.. One of the global Irradiance measurements performed at S. Tecla site (17/7/2003) is showed in Figure 528.

AOT values from 1.6 up to 2.0 were measured at this site during all the days of campaign from 17 to 25 July. Only on 26 July lower AOT values (from 1.1 to 1.4) were observed. The second measurement site was Piano delle Concazze (37°46'N, 15°00', 2800m a.s.l.), where we have performed quantitative measurements of global and direct spectral irradiance for AOT (Aerosol Optical Thickness) estimation. On July, 19th

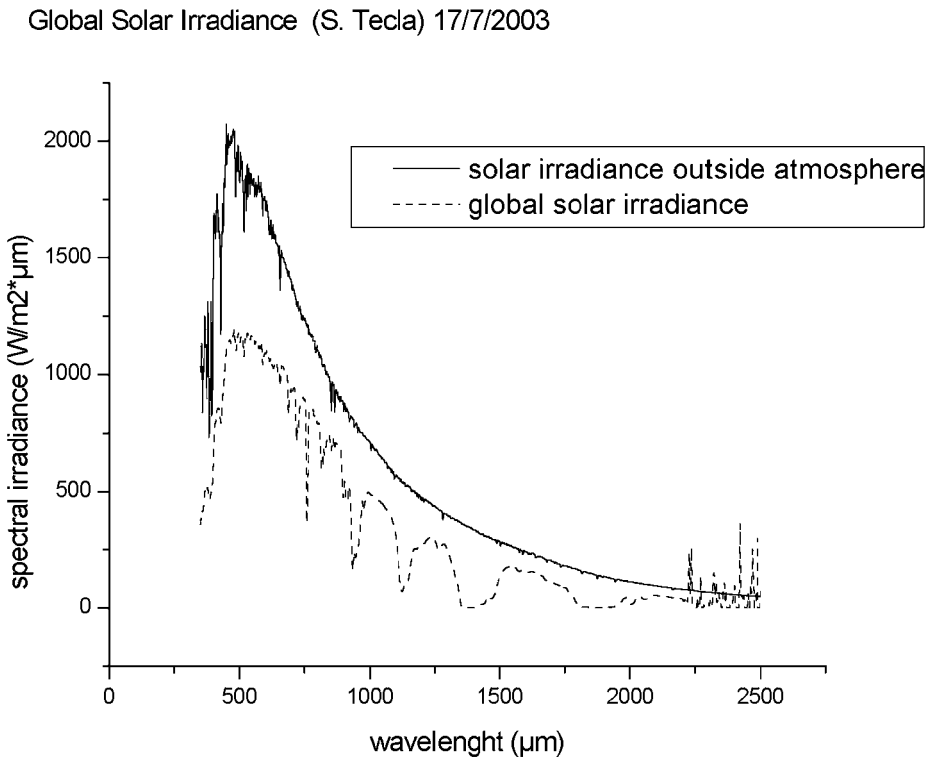

Figure 5.28 An example of Global Irradiance Measurements performed at S. Tecla site (17/7/2003).
Figura 5.28 Esempio delle misure di Irradianza Globale eseguite a Santa Tecla (17/7/2003).

Date	Time GMT [hh:mm]	Lat [deg,min]	Long [deg,min]	Elevation [m]	Measurement code
18.07.2003	09-15	37°36'N	15°10'E	5	ST_030718_OT_0001_VL
19.07.2003	08:15-11:03	37°46'N	15°00'E	2784	PC_030719_OT_0001_VL
19.07.2003	08:15-11:03	37°46'N	15°00'E	2784	PC_030719_GI_0001_VL
24.07.2003	09-11:33	37°36'N	15°10'E	5	ST_030724_OT_0001_VL
24.07.2003	09-11:33	37°36'N	15°10'E	5	ST_030724_GI_0001_VL
25.07.2003	09:32-12:28	37°36'N	15°10'E	5	ST_030725_OT_0001_VL
25.07.2003	09:32-12:28	37°36'N	15°10'E	5	ST_030725_GI_0001_VL
26.07.2003	08:43-12:45	37°36'N	15°10'E	5	ST_030726_OT_0001_VL
26.07.2003	08:43-12:45	37°36'N	15°10'E	5	ST_030726_GI_0001_VL

Table 5.18 Global Solar Radiation and AOT measurements performed by the IMAA CNR group. ST=Santa Tecla ; PC=Piano delle Concazze; OT=Aerosol Optical Thickness; GI=Global Spectral Irradiance; VL=Vito Lanorte.
Tabella 5.18 Radiazione Solare Globale e misure di AOT eseguite dal gruppo IMAA CNR.

2003, from Piano delle Concazze the atmosphere appears to be limpid and clean. The boundary layer upper limit was clearly visible around to 2500m above sea level. Global Irradiance Measurements performed at Piano delle Concazze site (19/7/2003) is show in Figure 5.29.

Additional measurements include direct irradiance. The ASD Direct Irradiance Attachment couples with the Remote Cosine Receptor (RCR) for the purpose of collecting the direct component of downwelling Solar Irradiance. A suntracker carrying the direct irradiance sensor can be used in order to perform long-term automatic tracking. Aerosol Optical Thickness (AOT) at 550nm has been derived from the direct irradiance measurements using the Bouguer-Langley method

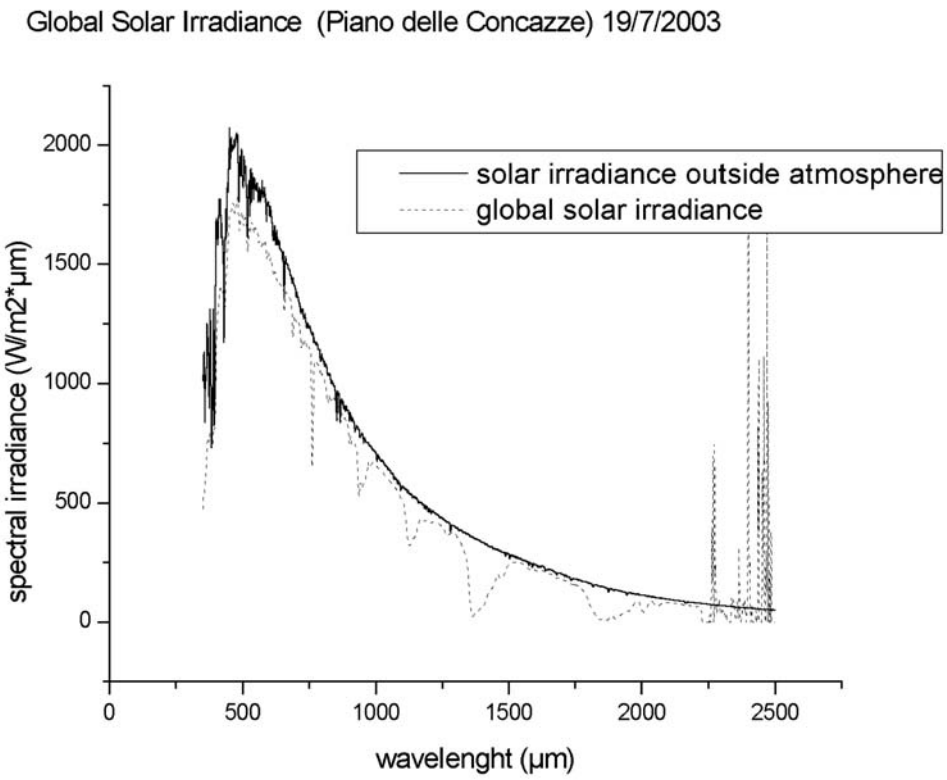

Figure 5.29 An example of Global Irradiance Measurements performed at Pian delle Concazze (19/7/2003).
Figura 5.29 Esempio delle misure di Irradianza Globale eseguite a Pian delle Concazze (19/7/2003).

described in Lenoble [1993].

The measured optical thickness values were indeed very small (from 0.2 to 0.4 during the observation time) and as expected very lower than in the S. Tecla case.

5.4.2 Global spectral Irradiance measurements INGV

The remote sensing receptor was mounted at the cable fore optic over a tripod at 145 cm ground altitude (Figure 5.30). Both the tube and the disc are designed with geometry and material that optimises the cosine response. The radiometer sensors acquired radiant energy that is transmitted through the diffusion-disc, and is directly visualized by the controlling software.

During the campaign period 5 times was decided use the FieldSpec to measure the solar irradiance. These measurements were contemporaneous with other type of measurements. In the following Table 5.19 the measurements days

Figure 5.30 Measurements configuration .The remote sensing receptor was mounted at the cable fore optic over a tripod at 145 cm ground altitude.
Figura 5.30 Configurazione delle misure eseguite con il rivelatore strumentale (FieldSpec).

Date	Starting GMT time	End of GMT time measuring	During time	Number of Spectrum	Site	Elevation a.s.l.	Contemporaneous
20.07.2003	9:22:00	11:08:00	106 min	96	Santa Tecla	0 m	with CNR FieldSpec Irradiance with FASA system flight with Modis on Terra, Bird and Avhrr
23.07.2003	11:18:00	11:20:00	2 min	11	Passo Dammuso	1710 m	test with ISPESL radiometer
24.07.2003	12:34:00	12:35:00	1 min	7	Santa Tecla	0 m	test with ISPESL radiometer with Avhrr
26.07.2003	9:30:00	10:35:00	65 min	52	Pian del Lago	2665 m	with Ali, Avhrr, Eros, Hyperion and Modis on Terra

Table 5.19 Mt Etna Solar Irradiance measurements performed by the INGV and ISPELS group.
Tabella 5.19 Misure dell'Irradianza solare sul Monte Etna eseguite dal gruppo INGV e ISPESL.

are reported.

In the following figures the spectral irradiance measured at the sea level (Figure 5.31) and at the summit crater zone inside the plume degassing (Figure 5.32), respectively are reported.

In Figure 5.32 it is possible to see the evidence of the effect of the volcanic plume presence on the spectral irradiance especially in the visible and near infrared wavelength range. Besides the irradiance from to is filtered by the RCR and any measurement on this range is possible.

5.5 Gas emission measurements

Active volcanoes are important sources for many trace gas species in the atmosphere; approximately 10% of the global flux of S has been attributed to volcanic activity [Bluth et al. 1993]. Volcanic degassing is driven by magma dynamics that also control volcanic activity, hence much work has been done to estimate the flux and composition of gas emitted from volcanoes. Validation of volcanic gas data obtained by remote sensing tools is logistically difficult and opportunities are rare. However data validation occupies the main role in testing remote observation on atmospheric gas composition, principally for the study of volcanic clouds. Remote sensing is an essential tool to comprehend volcanic processes from a safe distance avoiding tragic consequences; this is especially true for volcanologists concerned with active volcanoes. Observation of volcanic gas emission is the key to analysing volcanic dynamic evolution and may aid to predict eruptive activity. Long-term monitoring of gas emitted is useful to establish baseline emission rates and correlate changes with volcanic activity. Besides the estimation of total volcanic gas discharged in the atmosphere, it provides significant information to study the modifications of climate conditions and health effects of volcanic smog (called VOG) on people [Sutton et al. 1997]. Technological improvements in satellite or aircraft data, need ground-based constraints for testing, processing and interpretation of results. COSPEC and FTIR spectrometers are the most widely used ground-based instruments to perform remote acquisition of volcanic gas data. They offer complementary capabilities and are widely used side-by-side. FTIR is used primarily to determinate relative abundances of various gases [Francis et al. 1998, Burton et al. 2000]. In contrast, the COSPEC instrument is used to quantify the flux of a single gas species, sulfur dioxide (SO_2). It operates in the UV region measuring absolute path densities. Sicilian active volcanoes present different behavior in volcanic activity, controlled by structural features within the geo-dynamic region where they are located [Romano, 1982, Cristofolini et al. 1979].

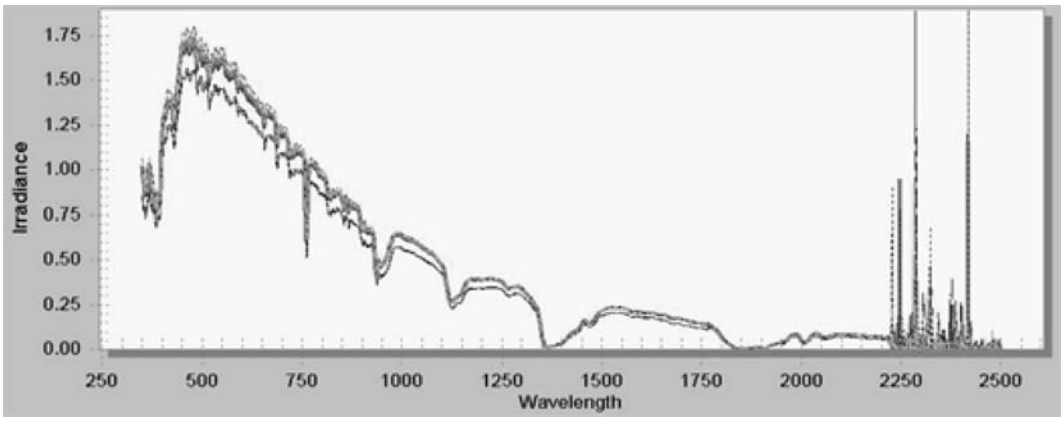

Figure 5.31 AIrradiance measured at the sea level at Santa Tecla (20/7/2003).
Figura 5.31 Irradianza misurata al livello del mare a Santa Tecla (20/7/2003).

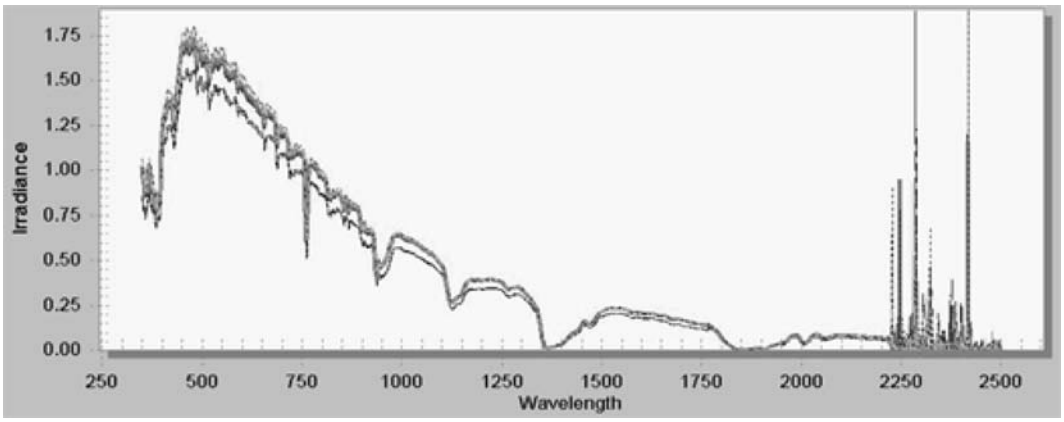

Figure 5.32 Irradiance measured at Pian del Lago (26/7/2003).
Figura 5.32 Irradianza misurata al Pian del Lago (26/7/2003).

5.6 Cospec and ftir sampling

Volcanic gas emission monitoring using remote sensing techniques is becoming a standard tool in the armory of the volcanologist to survey and study volcanic activity. COrrelation SPECtroscopy (COSPEC) and Fourier Transformed Infra-Red (FTIR) spectrometry are two approaches used by our group to measure gas flux and content in volcanic plumes emitted from Etna, Stromboli and Vulcano. These techniques were used during the FASA Campaign to provide a ground truth comparison with simultaneously measured air- and space-borne instruments.

5.6.1 Methodology: COSPEC (correlation spectrometer)

COSPEC is a passive remote sensing spectrometer which utilizes sky ultraviolet scattering at those wavelengths where the absorption bands of SO_2 have particular absorptions, to measure SO_2 content in the atmosphere.[Millan, 1984, 1978; Millan and Hoff, 1977, Newcomb and Millan, 1970; Moffat and Millan, 1971]. The use of COrrelation SPECtroscopy [Stoiber et al. 1983] to estimate SO_2 emission rates is perhaps the most common application of remote sensing measurements in Volcanology [Krueger et al. 2000]. Sulphur dioxide emission rates have yielded a wealth of information regarding magma supply rates [e.g. Chartier et al. 1988; Sutton et al. 2001; Caltabiano et al. 1994; Allard et al. 1994; Allard, 1997], contributions to the global SO_2 budget in the atmosphere and to comprehend another gas constituent of volcanic plumes. Rayleigh scattering of solar radiation takes place throughout the atmosphere, and therefore during daylight hours the sky is a source of ultraviolet radiation. Active volcanoes emit SO_2, which has a strong UV absorption band between 290 and 330 nm. Down-welling scattered solar UV radiation is therefore absorbed by volcanic SO_2 and may be measured by zenith-sky viewing UV spectrometers. The

COSPEC receives the sky radiation in an opening angle of 10 x 30 mrad and directs it to a diffraction grating to disperse scattered sunlight onto a rotating disk (correlation mask). Slits in this disk have been selected to allow radiation at wavelengths where SO_2 absorbs strongly to be measured by a photomultiplier tube. Other slits are selected to allow non-SO_2 absorbing wavelengths to be transmitted. By comparing the voltage from these two wavelength ranges, a signal that is proportional to the amount of SO_2 present above the instrument can be calculated, and this forms the uncalibrated output signal from the spectrometer with a resolution of 1 parts per million per meter (ppm◊m). The output voltage can be calibrated by placing cells with known amounts of SO_2 into the field of view of the instrument. We normally use two calibration cells with a concentration path-length of 133 and 344 ppm◊m. The calibrated COSPEC may then be transported underneath a volcanic plume while viewing vertically and thereby derive a two dimensional cross-section of the volcanic plume SO_2 content. If the position of measurements is achieved using a GPS receiver during the traverse underneath the plume, the raw SO_2 cross-section may be geometrically corrected to produce a cross-section quite perfectly straight and orthogonal to the wind direction. COSPEC measurements at Mt. Etna were made along traverses under the volcanic plume with the instruments mounted on a ground-base vehicle at distance of 7–15 km from the summit craters. We also performed SO_2 flux measurements using aircraft, helicopter, or boat (especially for Stromboli and Vulcano Islands) and from fixed positions (Vulcano Island, Mt. Etna) analysing the emissions from different sources during eruptive phenomena. A flux of SO_2, express in metric tonnes per day (t/d) may then be calculated integrating the corrected cross/section and multiplying by the wind speed. The uncertainty in wind speed value produces proportional uncertainty in the amount of SO_2 flux value [Casadevall et al. 1987]. The inaccuracy in the measures of wind speed at high altitudes was estimated between 15-20% [Malinconico, 1987] and 10-20% [Elias et al. 1998]. If the total uncertainty is taken into account this results in an overall uncertainty ranging from 20 to 30% on reported SO_2 flux values, very near to that reported from Stoiber et al. [1983]. Total uncertainty includes also the incorrect estimation of the plume height and the different wind speed inside the plume, even if the latter can affect significantly the flux estimate only under cases of severe wind shear [Hoff and Millan, 1981]. Italian Air Force Meteorogical Service provides us the data for wind speed. High altitude wind speed was sometimes simultaneously measured during some COSPEC surveys with an anemometer at the altitude of Mt. Etna's summit craters [Caltabiano et al. 1994], giving results comparable to those of Air Force data (deviation of about 15%). On Mt. Etna COSPEC methodology has been applied intermittently between 1975 and 1986 [e. g. Haulet et al., 1977; Malinconico 1979; Jaeschke et al. 1982; Carbonnelle and Zettwoog, 1982] and routinely since 1987 [Caltabiano et al. 1994; Bruno et al. 1999, Badalamenti et al. 2004]. The measurements were carried out on a weekly basis since 1987 and two to three times per week since October 1996. COSPEC measurements have been scheduled for daily measurements in presence of an eruptive event, both on Mt. Etna and on Aeolian Volcanoes.

5.6.2 FTIR (fourier transform infra-red)

Most gases emitted by volcanoes absorb infrared radiation, and therefore can be detected and measured using an infrared spectrometer with an appropriate source of infrared radiation. Fourier transform infrared spectroscopy (FTIR) offers the possibility to monitor multiple gases. A generally applicable technique is a passive method using solar occultation [Francis et al. 1995, Francis et al. 1998], measuring the absorption of solar radiation passing through the volcanic plume, or collecting infrared spectra emitted by hot rock or lava.

Solar spectra are analyzed by simulating the complete atmospheric transmittance, based on a 50 layer FASCODE standard atmosphere, together with an idealized volcanic plume layer with homogeneous pressure and temperature. Passive spectra were simulated by assuming a single-layer atmosphere containing both atmospheric and volcanic constituent. FTIR uses a Michelson interferometer [Michelson, 1892] to produce an interference pattern which is the Fourier transform of the spectrum of incoming light. Data were collected with a Bruker OPAG-22 FTIR spectrometer at 0.5 cm-1 resolution using medium Norton-Beer apodization. The detector was a LN_2-cooled InSb photovoltaic semiconductor with sensitivity between 1,500 and 6,000 cm^{-1}. Recorded infrared spectra were analyzed using a non-linear least squares fitting program based on the Rodgers optimal estimation algorithm and the Oxford RFM radiative transfer model, using spectral line data from the HITRAN 96 database [Rothman et al. 1998]. Each spectrum was analyzed to produce a path

amount of SO_2, HCl and HF, three gases which have negligible concentrations in the unpolluted free troposphere but which are abundant within volcanic emissions. The nature of the FTIR is such that all detectable wavelengths are measured simultaneously. This means that, despite the swiftly changing concentrations of gas in the line of measurement between the spectrometer and the sun, each measured spectrum records the instantaneous composition of all the measurable volcanic gases. Unlike COSPEC, FTIR measurements do not allow measurements of a gas flux; they are performed from a fixed point and with a fixed viewing, so that they provide only the concentrations and the molar ratios of different gas species. Molar ratios are determined by measuring 50 or more spectra of a particular gas plume, and then plotting retrieved amounts of SO_2 against HCl and HF. Since the year 2000 regular measurements of the chemical composition of Mt. Etna's plume gas emissions have been performed using a rugged, portable Fourier transform infrared spectrometer (FTIR) and the sun as a radiation source [Burton et al. 2003]. With this configuration we measure SO_2, HCl and HF within the volcanic plume; volcanic gases such as H_2O and CO_2 are unfortunately obscured by the much more abundant atmospheric burdens of these gases. Radiation at these wavelengths cannot penetrate dense clouds, and atmospheric water vapour absorption reduces the sensitivity with increasing distance. By combining the molar ratios of SO_2/HCl and SO_2/HF with the SO_2 flux determined by COSPEC we may derive the flux of SO_2, HCl and HF. The analytic errors on concentrations range from 4% to 10%.

5.6.3 Description of Measurements for Etna, Vulcano and Stromboli

This section describes COSPEC and FTIR campaign in the FASA project. Groundbase remote sensing measurements were performed during the whole period of the test campaign, except for adverse weather conditions and the contemporaneous activity in Aeolian Archipelago. COSPEC measurements were carried out from the ground campaign on Mt. Etna, Vulcano and Stromboli islands. In the step of FASA's acquisition data, COSPEC is a constrain of SO_2 flux data, so for the gas emissions data that obtain FASA system. In the stage of ground activity particular consideration is assigned on Mt. Etna than Vulcano and Stromboli, so in our collection data we have several data on Mt. Etna than another location, in exception of Stromboli island because we perform a daily COSPEC measurements as a consequences of the Stromboli eruption 2002-2003. In Vulcano we made only one campaign of measures in coincidence to air fly. COSPEC activity was executed using different methods depending on the location of sampling and the measured volcano. On Mt. Etna we performed SO_2 flux measurements using a car mounted COSPEC, on Stromboli we used the COSPEC mounted on a boat, while on Vulcano island we make measurements from a fixed point (tripod-based). The first method was

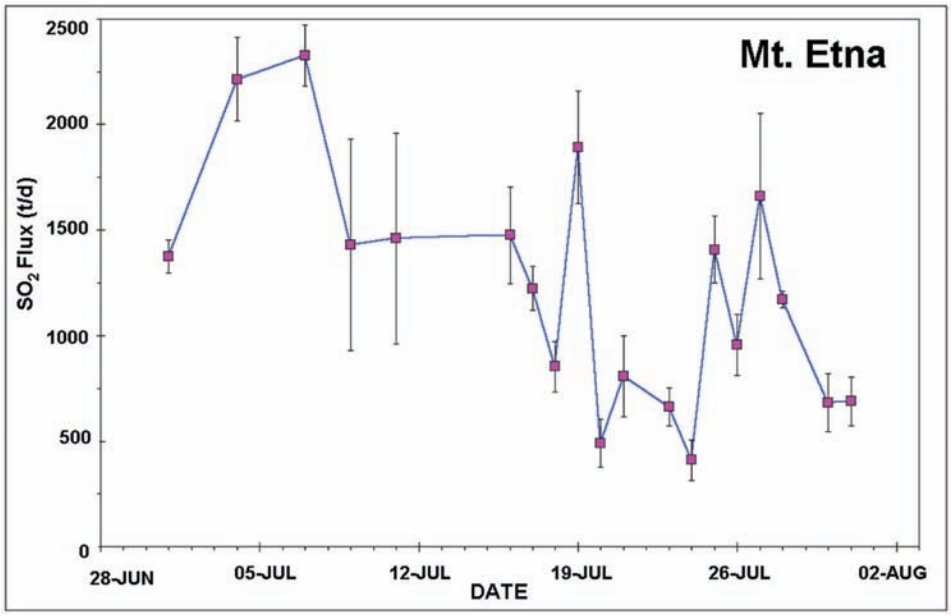

Figure 5.33 COSPEC SO_2 flux from Mt. Etna.
Figura 5.33 Monte Etna: flusso di SO_2 rilevato con COSPEC.

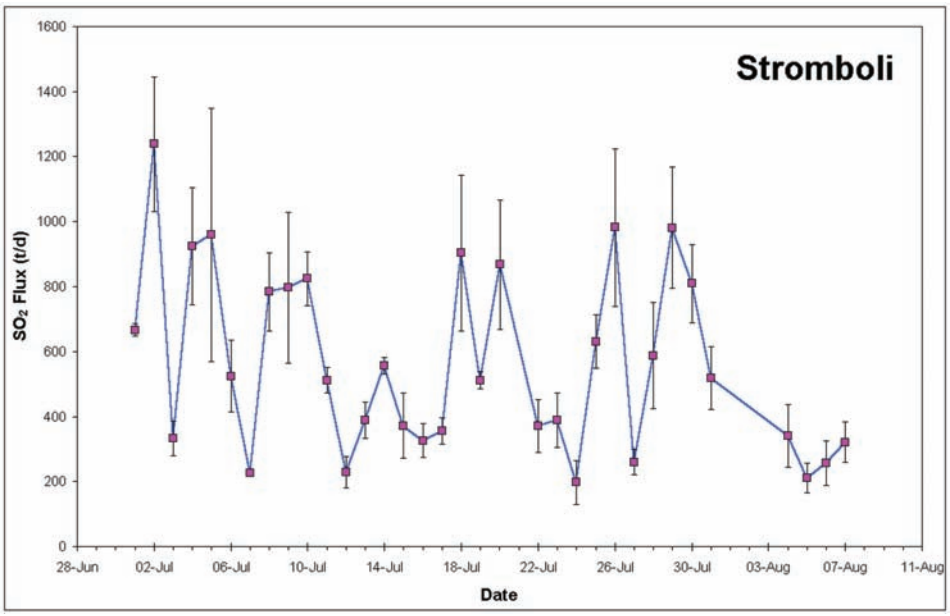

Figure 5.34 SO_2 flux from Stromboli. Standard deviations of each day of measurements are shown as vertical bars.
Figura 5.34 Stromboli: flusso di SO_2. le barre verticali rappresentano le deviazioni standard per ogni giorno di misura.

Date	Etna - COSPEC					
	Traverse	h start (GMT)	h stop (GMT)	Wind 3000 mt.	Wind 5000 mt.	Site
17.07.2003	6	06:59	11:27	NW 25	NNW 25	Fornazzo-Pedara
18.07.2003	5	07:23	11:52	NW 40	NW 35	Fornazzo-Pedara
19.07.2003	6	07:25	11:54	NE 20	NE 30	Ragalna-Zafferana
20.07.2003	8	07:44	12:13	NNW 15	NW 25	Trecastagni-Ragalna
21.07.2003	4	07:56	11:23	N 10	NW 15	Nicolosi-Adrano
23.07.2003	4	07:42	10:24	NW 15	NW 30	Monterosso- Ragalna
24.07.2003	5	07:08	11:36	NW 15	NW 15	Trecastagni- Fornazzo
25.07.2003	4	07:28	09:20	WNW 35	WNW 32	Monterosso-Fornazzo
26.07.2003	9	08:10	12:39	NW 45	W 30	Fleri-Nicolosi
27.07.2003	4	08:05	12:33	NNW 25	NW 10	Fleri - Ragalna

Table 5.20 COSPEC measurements at Mt Etna.
Tabella 5.20 Monte Etna: misure COSPEC.

performed mounting the COSPEC on a vehicle with the telescope pointing vertically using a 45 degree mirror outside a lateral window. The acquisition system consists in laptop, a data-logger and a GPS. Traverses were made under the volcanic plume on roads that depending on the plume direction in order to execute traverses as straight and perpendicular as possible. The length of the traverses depends mainly on the wind speed and on the activity of the volcano. The fix-point measurement was performed mounting the spectrometer on a tripod under or off to the side of the plume. With a correct aligned and levelling of COSPEC with the plume axis, the rotation of the 45 degree mirror of the telescope has permitted the scanning of the volcanic plume. This method produced a different yielded of the effective measurements of SO_2 flux than vehicle-based method, [Sutton et al. 2001, Andres et al. 1987, 1989].

Results from Mt. Etna and Stromboli are graphically shown in Figure 5.33 and Figure

Date	Vulcano - COSPEC				Stromboli - COSPEC		
	Traverse	h start	5.6.3.1 h stop	Site	Traverse	h start	h stop
17.07.2003					4	05:30	07:45
18.07.2003					6	07:30	08:59
19.07.2003					4	08:51	10:00
20.07.2003					4	07:17	08:10
21.07.2003							
22.07.2003	26	11:57	13:22	P.so del Piano	8	9:20	12:00
23.07.2003					6	07:00	09:00
24.07.2003					4	16:00	17:00
25.07.2003					4	07:20	08:45
26.07.2003					4	07:15	08:45
27.07.2003					6	09:47	10:29

Table 5.21 COSPEC measurements at Vulcano and Stromboli.
Tabella 5.21 Misure COSPEC a Vulcano e Stromboli.

5.34 respectively. Standard deviations of each day of measurements are shown as vertical bars

In Table 5.20 and Table 5.21 the results of COSPEC measurements reported.

On Mt. Etna the interval time of acquisition data is length 4 hours, usually in this time we obtained in mean 6 cross-sections of measures. In the whole campaign we collected 13 days of SO_2 flux measurements, executing 67 traverses. During the campaign the plume was located in south-western and south-eastern flanks of Mt. Etna. In Figure 5.35 an example of a single traverse path with SO_2 cross-section of the volcanic plume is reported.

Average SO_2 flux was about 1080 t/d, the highest value was about 1890 t/d (19 July 2003) while the lowest value was about 410 t/d (24 July). As far as the single traverse was concerned the maximum peak value of concentration was about 294 ppm◊m and recorded in the first traverse of the 27 July near the site of Nicolosi, correspondent to longitudes degrees 15.0186, and latitude degrees 37.6148. Minimum peak value of concentration was about 78 ppm◊m recorded in the eighth traverse of the 20 July near the site of Nicolosi, correspondent to longitudes degrees 15.0258 and latitude degrees 37.6180.

FTIR measurements of the volcanic gas emissions from Mt. Etna (Figure 5.36) were carried out every day between 18 and 24 July, apart from the 20th (see Table 5.20).

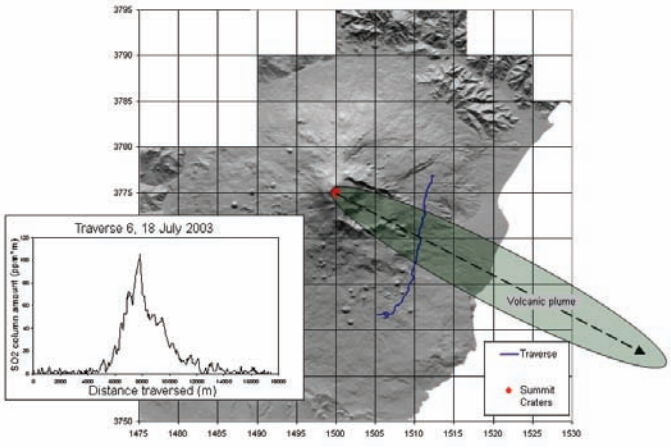

Figure 5.35 An example of a single traverse path (blue vertical line) on Mt. Etna with SO_2 columnar amount.
Figura 5.35 Esempio di singolo transetto (blu) e nel riquadro: andamento del contenuto colonnare SO_2.

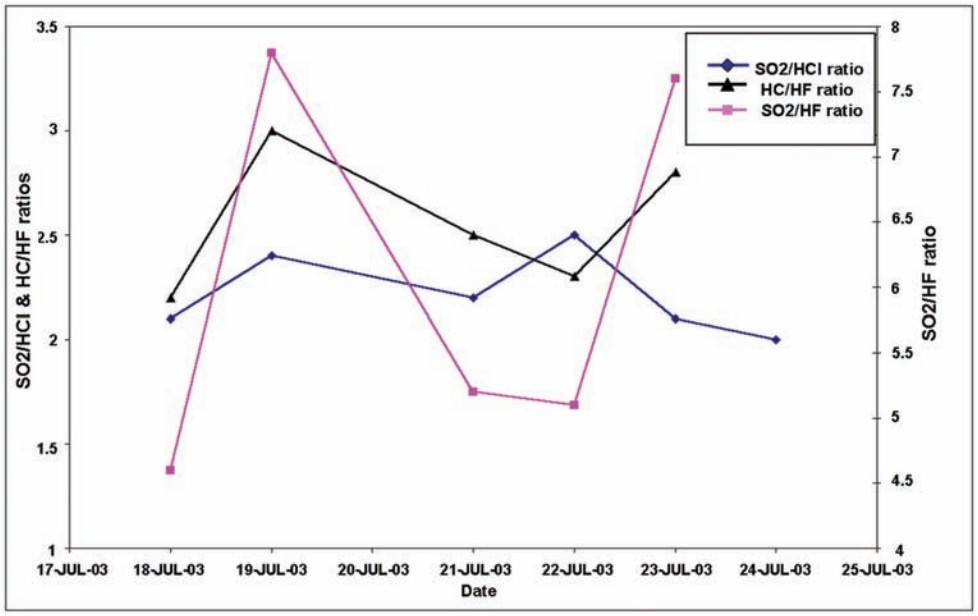

Figure 5.36 FTIR SO_2/HCl, SO_2/HF and HCl/HF ratio from Mt. Etna.
Figura 5.36 Monte Etna: rapporti SO_2/HCl, SO_2/HF e HCl/HF misurati con lo FTIR.

These revealed a relatively constant composition with a SO_2/HCl ratio between 2.0 and 2.5 and an SO_2/HF ratio between 4.6 and 7.8. (Table 5.22).

Date	Etna – FTIR	
	Number of Spectra	Site
18.07.2003	150	Zafferana
19.07.2003	400	Sapienza
21.07.2003	53	Ragalna
22.07.2003	61	Biancavilla
23.07.2003	61	Ragalna
24.07.2003	100	Fornazzo

Table 5.22 FTIR measurements at Mt Etna.
Tabella 5.22 Misure FTIR sul Monte Etna.

5.6.4 Volcanic plume measurement

A comparison of different volcanic plume measurement techniques was successfully performed during several days of testing between 17 and 27 July 2003 on Mt. Etna, Vulcano and Stromboli volcanoes. We used ground-based methods in order to provide ground-truth for airborne and spaceborne sensors. COSPEC and FTIR daily measurements revealed an average SO_2 flux from Etna of 1040 ± 470 t/d and SO_2/HCl and SO_2/HF ratios of 2.2 ± 0.2 and 6.0 ± 1.5 respectively. Flux measurements on Stromboli show an average value of 500 ± 275 t/d.

Acronyms

ASI (Agenzia Spaziale Italiana)
CNR-IROE (recently renamed CNR-IFAC) Istituto di Fisica Applicata "Nello Carrara"
ISS International Space Station
FASA Fire Airborne Spectral Analyser
MIR Middle infrared
TIR Thermal infrared
VIS Visible
FTIR Fourier Transform Infrared
MIROR Michelson Interferometer with Rotating Retroreflector
ABAS Advanced BIRD Airborne Simulator (ABAS)
BIRD (Bispectral Infrared Detection)

Acknowledgements

The 2003 Etna field campaign was funded by the Agenzia Spaziale Italiana (ASI) in the frame of two research projects: FASA (I/R/203/02) and HYPSEO (I/R/157/02).

We special thanks Dr. David Pieri and Micheal Abrams (NASA-JPL, ASTER Science Team) for the successfully acquisition and process of ASTER imagery during the field campaign.

We also thanks the Dr. Ruggero Casacchia (CNR) for his valuable work and help in reviewing this report.

Bibliography

Acharya P.K., Berk A., Bernstein L. S., Matthew M. W., Adler-Golden S. M., Robertson D. C., Anderson G. P., Chetwynd J. H., Kneizys F. X., Shettle E. P., Abreu L. W., Galery W. O., Selby J. E. A., Clough S. A. (1998): *Modtran User's Manual, Versions 3.7-4.0.* Air Force Research Laboratory, Space Vehicles Directorate, Air Force Materiel Command, Hanscom AFB, MA 01731-3010

Acocella, V., Behncke, B., Neri, M., D'Amico, S.(2003): *Link between major flank slip and eruptions at Mt. Etna (Italy).* Geophysical Research Letters, 30: DOI: 10.1029/2003-GLO 18642.

Acocella, V., Neri, M. (2003): *What makes flank eruptions? The 2001 Etna eruption and the possible triggering mechanisms.* Bulletin of Volcanology, 65, pp. 517-529, DOI: 10.1007/s00445-003-0280-3.

Allard, P. J., Carbonelle, N., Mètrich, H., Loyer P. & Zettwoog, P. (1994) : *Sulphur output and magma degassing budget of Stromboli volcano*. Nature, 368, pp. 326-330.

Allard, P. J., Jean-Baptiste P., D'Alessandro, W., Parello F., Parisi, B. & Flehoc C. (1997) : *Mantle-derived helium and carbon in groundwaters and gases of Mount Etna, Italy.* Earth and Planetary Science letters, 148, pp. 501-516.

Andres, R. J., Kyle P. R., Rose W.I., Stokes, J. B. (1987) : *SO_2 emissions during eruptive episode 48A, Kilauea Volcano, Hawaii.* IUGG XIX General Assembly : 407.

Andres, R. J., Kyle P. R., Stokes J. B., Rose W. I. (1989) : SO_2 *from episode 48A eruption, Hawaii : Sulfur dioxide emission from the episode 48A east rift zone eruption of Kilauea volcano, Hawaii.* Bull. Volcanol., 52, pp.113-117.

Andronico, D. et al., (2004): A multi-disciplinary study of the 2002-03 Etna eruption: insights for into a complex plumbing system. Bulletin of Volcanology, in print.

Armienti, P., Clocchiatti, R., D'Orazio, M., Innocenti, F., Petrini, R., Pompilio, M., Tonarini, S. (1994): *Etna petrography and chemical composition.* Acta Vulcanol., 6, pp. 3-5.

Badalamenti, B., Calderone, L., Liotta, M., Sansone, G., (1999): *Continuous monitoring. Volcanology and Chemistry of the Earth's interior – Italian Research Activity (1995-1998) report to IAVCEI.* Boll. Geol. Teor. Appl., 40-2 supplement: pp.214-216.

Barberi , F., Innocenti, F., Ferrara, G., Keller J., Villari, L. (1974): *Evolution of Aeolian Arc Volcanism (Southern Tyrrhenian Sea).* Earth Planet. Sc. Lett., 21, pp. 269-276.

Barberi, F., Neri, G., Valenza, M., Villari, L.,(1990*): Italian volcanic activity during 1987-1990. Volcanological research in Italy (1987-1990).* F. Barberi ed., Boll. Geof. Teor. Appl., Supplement vol. 32 , pp. 127-128, 427-445.

Barnaba F, and G. P. Gobbi, 2001: *Lidar estimation of tropospheric aerosol extinction, surface area and volume: Maritime and desert-dust cases.* J. Geophys. Res., 106 (D3), pp. 3005-3018.

Behncke, B, Neri, M. (2003b): *Cycles and trends in the recent eruptive behaviour of Mount Etna (Italy).* Canadian Journal of Earth Sciences 40, pp. 1405-1411, DOI: 10.1139/E03-052.

Behncke, B., Neri, M. (2003a): *The July-August 2001 eruption of Mt. Etna (Sicily).* Bulletin of Volcanology 65, pp. 461-476, DOI: 10.1007/s00445-003-0274-1.

Behncke, B., Neri, M., Carniel, R. (2003): *An exceptional case of lava dome growth spawning pyroclastic avalanches at Mt. Etna (Italy): the 1999 Bocca Nuova eruption.* Journal of Volcanology and Geothermal Research 124, pp. 115 - 128.

Behncke B., Berrino G., Velardita R. (2003) : *Ground deformation and gravity changes on the island of Pantelleria in the geodynamic framework of the Sicily channel.* (invited press). Abstract presented at the Annal Workshop 2003, Pantelleria, Italy (23-28 September 2003). on : Seismic Phenomena Associated with Volcanic Activity (view abstract).

Berrino, G., Corrado, G., Luongo, G. and Toro, B. (1984): *Ground deformation and gravity changes accompanying the 1982 Pozzuoli uplift.* Bull. Volcanol. 47 (2) , pp. 187-200.

Billi, A., Acocella, V., Funiciello, R., Giordano, G., Lanzafame, G., Neri, M. (2003): *Mechanisms for ground-surface fracturing and incipient slope failure associated to the July-August 2001 eruption of Mt. Etna, Italy: analysis of ephemeral field data.* Journal of Volcanology and Geothermal Research 122, pp. 281-294.

Bluth, G. J. S., Shnetzel, C. C., Kreuger, A. J., Walter, L. S. (1993) : *Annual volcanic emission of sulfur dioxide to the atmosphere.* Eos Transaction AGV, 74, p. 688.

Briess,K., Jahn H., lorenz, E., Oertel, D., Skrbek, W., Zuhkov, B. (2003) : *Fire recognition potential of the Bi-spectral InfraRed Detection (BIRD) satellite.* Intern. Journ. Remote Sensing, in press.

Bruno, N., Caltabiano, T., Romano, T. (1999) :

SO(sub2) emissions at Mount Etna with particular reference to the period 1993-1995. Bulletin of Volcanology. 7 (1) , pp. 27-34.

Burton, M. R., Oppenheimer, C., Horrocks, L. A., Francis, P. W. (2000) : *Remote sensing of CO2 and H2O emission rates from Masaya volcano, Nicaragua.* Geology, 28, pp. 915-918.

Burton, M. R., Murè, F., Sawyer, G., Allard, P., (2003) : *FTIR measurements of 2002/2003 flank eruption of Mt. Etna.* EGS-AGU-EUG joint Assembly, Nice.

Caltabiano, T., Romano, R., Buretta, G. (1994): *SO_2 flux measurements at Mount Etna.* J. Geophys. Res. 99 (D6) , pp. 809-819.

Carbonnelle, J., Dajlevic, D., Zettwoog P., Sabroux, J. C. (1982) : *Gas output measurements from an active volcano.* Bull. Volcanol., 45, pp. 267-268.

Casadevall T. J., Stokes, J. B., Greenland, L. P., Malinconico, L. L., Casadevall J. R., Furukawa, B. T.(1987) : *So2 and CO2 emission rates in Kilauea volcan. 1979-1984.* chap. 29 in : Decker, R. W., Wright, T.L. and Stauffer, P. H. eds., Volcanism in Hawaii : U.S. Geological Survey Professional Paper 1350: vol. 1, pp. 771-780.

Chartier, T. A., Rose, W. I., Stokes, J. B. (1998) : *Detailed record of SO_2 emissions from PUU Oo between episodes 33 and 34 of the 1983-1986 ERZ eruption, Kilauea, Hawaii.* Bull. Volcanol., 50, pp. 215-228.

Chiodini, G., Cioni, R., Guidi, M., Raco, B. and Marini, L., (1998): *Soil CO2 measurements in volcanic and geothermal areas.* Appl. Geochem. 13-5, pp. 543-552.

Chiodini, G., Cioni, R., Magro, G., Marini, I., Panichi, C., Raco, B. and Russo, M. (1997): *Chemical and isotopic variations of Bocca Grande Fumarole (Solfatara volcano, Phlegraean Fields).* Acta Vulcanologica, 8 (2) , pp. 228-232.

Corrado, G., Guerra, I., Lo Bascio, A., Luongo, G. and Rampoldi, R. (1976): *Inflation and microearthquake activity of Phlegrean Fields, Italy.* Bull. Volcanol., 40 (3) , pp. 169-188.

Cristofolini, R., Lentini, F., Patanè, G., Rasà, R., (1979): *Integrazione di dati geologici, geofisici e petroglifici per la stesura di un petroglifo crostale in corrispondenza dell'Etna.* Boll. Soc. Geol. It., 98, pp. 239-247.

De Gennaro, M., Franco, E. and Stanzione, D. (1980): *Le alterazioni ad opera di fluidi termali alla solfatara di Pozzuoli (Napoli).* Mineralogia e Geochimica. 49, pp. 5-22.

Diliberto, I.S., Gurrieri, S., Valenza, M. (2002): *Relationships between diffuse CO2 emissions and volcanic activity on the island of Vulcano (Aeolian Islands, Italy) during the period 1984-1994.* Bulletin of Volcanology, 64, pp. 219-228.

Di Vito, M., Lirer, L., Mastrolorenzo, G., Rolandi, G., and Scandone, R. (1985): *Volcanological map of Campi Flegrei.* Min. Prot. Civ. Univ. degli Studi di Napoli.

Di Vito, M., Lirer, L., Mastrolorenzo, G., and Rolandi, G. (1987): *The 1538 Monte Nuovo eruption (Campi Flegrei, Italy).* Bull. Volcanol., 49, pp. 608-615.

Di Vito, M.A., Isaia, R., Orsi, G., Southon, J., de Vita, S., D'Antonio, M., Pappalardo, L., and Piochi, M. (1999): *Volcanism and deformation in the past 12 ka at the Campi Flegrei caldera (Italy).* J. Volcanol. Geotherm. Res., 91, pp. 221-246

Dozier, J., 1981, *A method for satellite identification of surface temperature fields of subpixel resolution.* Remote Sensing of Environment, 11, pp. 221-229.

Elias, T., Sutton A. J., Tokes, J. B., Casadevall T. J. (1998): *Sulfur dioxide emission rates of Kilauea Volcano, Hawaii, 1979-1997.* U.S. Geological Survey Open-File Report 98-462.

Favara, R.., Francofonte, S., Madonia, P. and Valenza, M., (1997): *Modello idrogeologico dell'Isola di Vulcano e suo significato per la sorveglianza geochimica.* In: C.N.R./G.N.V., Convegno Annuale 1996, 3-5 Marzo 1997, Programma e Riassunti, pp. 162-163, Roma.

Francis, P., Maciejewski, A., Oppenheimer, C., Caltabiano, T. (1995): *SO_2: HCL ratios in the plumes from Mt. Etna and Vulcano determined by Fourier Transform Spectroscopy.* Geophysical Research Letters 22, pp. 1717-1720.

Francis, P., Burton, M. & Oppenheimer, C. (1998) : *Remote measurements of volcanic gas compositions by solar FTIR spectroscopy.* Nature, 396, pp. 567-570.

Gobbi, G. P. (1998): *Polarization lidar returns from aerosols and thin clouds: a framework for the analysis.* Appl. Opt., 37, pp. 5505–5508.

Gobbi, G. P., Barnaba, F., Giorgi R., Santacasa, A. (2000) : *Altitude-resolved properties of a Saharian-Dust event over the Mediterranean. Atmospheric Environment.* 32, pp. 5119-5127.

Gurrieri, S. and Valenza, M., (1988): *Gas transport in natural porous medium: a method for measuring CO2 flows from the ground in volcanic and geothermal areas.* Rendiconti della Societa' Italiana di Mineralogia e Petrologia, 43, pp. 1151-1158.

Haulet, R., Zettwoog, P., Sabroux, J. C. (1977) :

Sulfur dioxide discharge from Mount Etna. Nature, 268, pp. 715-717.

Hoff , R. M., Millan M. M. (1981): *Remote SO_2 mass flux measurements using COSPEC.* Air Pollut. Control Assoc., 31, pp. 381-384.

Jaeschke, W., H. Berresheim, and H. W. Georgii (1982): *Sulfur emission from Mount Etna.* J.Geophys. Res., 87 (C9) , pp. 7253-7261.

Keller, J. (1980): *The island of Vulcano.* Soc. Italiana Min. Petr.; 36: 368-413.

Krueger,A. J., S. J. Schaefer, N.Krotkov,G. Bluth, and S. Barker (2000): *Ultraviolet remote sensing of volcanic emissions.* In: Remote Sensing of Active Volcanism, edited by P. J.Mouginis-Mark, J.A. Crisp, and J. H. Fink, pp. 25-43,Geophysical Monograph 116, AGU,Washington,D.C.

Lanzafame, G., Neri, M., Acocella, V., Billi, A., Funiciello, R., Giordano, G. (2003): *Structural features of the July-August 2001 Mount Etna eruption: evidence for a complex magma supply system.* Journal of the Geological Society London 160, pp. 531-544.

Lenoble, J. (1993) : *Atmospheric Radiative Transfer.* (studies in Geophysical Optics and Remote Sensing). A. Deepak Pub. , May 1.

Lirer, L., Luongo, G. and Scandone, R. (1987): *On the volcanological evolution of Campi Flegrei, EOS, Trans.* Am. Geophys. Union, 68, pp. 226-234.

Lorenz, E:; Skrbek, W.(2001): *Calibration of a bi-spectral infrared push-broom imager.* Proc. SPIE: 4486, pp. 90-103

Lundgren, P., Berardino, M., Coltelli, M., Fornaro, G., Lanari, R., Puglisi, G., Sansosti, E., Tesauro, M. (2003) :*Volcanic sulphur dioxide fluxes from Etna, Vulcano and Stromboli measured with an automated scanning ultraviolet spectrometer.* J. Geoph. Res. :108, B9, 2455.

Malinconico, L. L. (1979): *Fluctuations in SO_2 emission during recent eruptions of Etna.* Nature, 278, pp. 43-45.

Malinconico, L. L. (1987): *On the variation of SO_2 emissions from volcanoes.* J. Volcanol. Geotherm. Res., 33, pp. 231-237.

Mercalli , G., Silvestri, O., Gblovitz, G., Clerici, V. (1891): *La eruzione dell'Isola di Vulcano.* Annali dell'Ufficio centrale di metereol., 10: pt. 4.

Millan, M. M. (1984): *The applications of Optical Correlation Techniques to the Remote Sensing of Air Pollution.* P. Camagni, S. Sandroni (eds.), Elsevier Pub. Co., New York, pp. 45-67.

Millan, M. M. (1978): *Remote sensing of SO_2, a data processing methodology.* Joint Conference on Sensing of Environmental Pollutants. 4th New Orelans, La. Nov. 6-11, 1977, Proceedings. (A79-15023 04-45) Washington, D.C., American Chemical Society, pp. 30-33.

Millan M. M., Hoff, R. M., (1977): *How to minimize the baseline drift in a COSPEC remote sensing.* Journal of Atmoshperic Environment vol. 11: n°9, pp. 857-860.

Moffat, A. J., Millan M. M. (1971): *The applications of optical correlation techniques to the remote sensing of SO_2 plume using sky light.* Atmos. Environn., 5, pp. 677-690.

Neri, M., Acocella V., Behncke, B. (2003): *The role of the Pernicana Fault System in the spreading of Mount Etna (Italy) during the 2002-2003 eruption.* Bulletin of Volcanology, DOI: 10. 1007/s00445-003-0322-x.

Newcomb, G. S., Millan, M.M. (1970): *Theory, applications, and results of long-line correlation spectrometer.* IEEE Trans. Geosci. Electron., GE 8, pp. 149-157.

Parkinson, K.J., (1981): *An improved method for measuring soil respiration on the field.* J. Appl. Ecol. 18, pp. 221-228.

Rittmann, A. (1958): *Sul meccanismo dell'attività vulcanica persistente.* Bollettino dell'Accademia Gioenia di Scienze Naturali di Catania, ser. IV, 4, pp. 352-360.

Rittmann, A. (1962): *On the mechanism of persistent volcanic activity.* Bulletin Volcanologique 24, pp. 301-313.

Romano, R., Vaccaro, C. (1986): *The recent eruptive activty on Mt. Etna. Sicily : 1981-1985.* Per. Mineral. 55, pp. 91-111.

Romano, R., (1982): Succession of the volcanic activity in the Etnean area. Mem. Soc. Geol. It., 23, pp. 27-48.

Rothman, L. S., Rinsland, C. P. ET AL. (1998): *The HITRAN Molecolar Spectroscopic Database and HAWKS (HITRAN Atmospheric Workstation).* 1996 Edition, Journal of Quantitative Spectroscopy and Radiative Transfer, 60, pp. 665-710.

Scandone, R., Bellucci, F., Lirer, L. and Rolandi, G. (1991): *The structure of the Campanian Plain and the activity of Neapolitan Volcanoes.* J. Volcanol. and Geoth. Res., 48 .

Skrbek, W., Lorenz, E. (1998): HSRS – *An infrared sensor for hot spot detection.* Proc. SPIE: 3437, pp. 167-176.

Stoiber,. Malinconico R.E.L.L, Williams, Jr S.N. (1983): *Use of correlation spectrometer at volcanoes.* In Forecasting Volcanic events, H. Tazieff & J-C Sabroux (eds) 425-44. Amsterdam Elsevier.

Sutton, A., Elias, T., Gerlach, T., and Stokes, J. (2001): *Implications for eruptive processes as*

indicated by sulfur dioxide emissions from Kilauea Volcano, Hawaii, 1979 – 1997. Journal of Volcanology and Geothermal Research, no. 108: pp. 283-302.

Sutton, J., Elias, T., Hendley, J. W. I., Stauffer, P. H. (1997): *Volcanic air pollution – a hazard in Hawaii.* U.S. Geological Survey fact Sheet: 169-97 (Reducing Rirsk from Volcano Hazards series), p. 2.

Tanguy, J. C.(1978): *Tholeitic basalt magmatism of Mount Etna and its relations with the alcaline series.* Contrib. Mineral. Petrol., 66, pp. 51-67.

Tonani, F. and Miele, G., (1991): *Methods for measuring flow of carbon dioxide through soils in the volcanic setting.* Proc. Int. Conf. Active Volcanoes and Risk Mitigation, 27 August-1 September, Napoli.

Valentino, G.M., cortecci, g., Franco, E. and Stanzione, D. (1999): *Chemical and isotopic compositions of minerals and waters from the Campi Flegrei volcanic system, Naples, Italy.* J. Volcanol. and Geoth. Res., 91, pp. 329-344.

W.M.O. (1984): *W.M.O. Manual.* on CodesW.M.O. vols 1 & 2: n° 306

M. Wooster, B. Zhukov and D. Oertell(2003): *Fire Radiative energy release for quantitative study of biomass burning: derivation from the BIRD experimental satellite and comparison to MODIS fire products.* Remote Sens. Environm., in press.

Zhukov, B., Briess, K., Eckehard, L., Skrbek, W.,Oertel, D. (2003): *Detection and Analysis of High-Temperature Events. in the BIRD Mission.* DLR, Berlin.

Istituto Nazionale di Geofisica e Vulcanologia
Via di Vigna Murata, 605 - 00143 Roma - Italy
www.ingv.it